PARAMETERS GOVERNING THE PIEZOELECTRIC PROPERTIES OF PVDF

by

Chloé MELIN

THESIS PRESENTED TO ECOLE DE TECHNOLOGIE SUPERIEURE AND INSA DE LYON IN PARTIAL FULFILLMENT FOR THE DEGREE OF DOCTOR OF PHYLOSOPHY
Ph.D.

MONTREAL, APRIL, 24TH, 2026

ÉCOLE DE TECHNOLOGIE SUPÉRIEURE
UNIVERSITÉ DU QUÉBEC

BOARD OF EXAMINERS

THIS THESIS HAS BEEN EVALUATED

BY THE FOLLOWING BOARD OF EXAMINERS

Mrs. Nicole Demarquette, Thesis Supervisor
Department of Mechanical Engineering at École de technologie supérieure

Mr. Jean-Marc Chenal, Thesis Supervisor
MATEIS at INSA Lyon

Mr. Ricardo Zednik, Thesis Co-supervisor
Department of Mechanical Engineering at École de technologie supérieure

Mr. Angelo Pommella, Thesis Co-supervisor
MATEIS at INSA Lyon

Mr. Jean Marie Raquez, External reviewer
Department of Chemical Engineering at Polytechnique

Mrs. Virginie Griseri, External reviewer
University of Toulouse

Mr. Ricardo Andrade, External examinator
Mackensie Presbyterian University

Mr. Jerome Castellon, External examinator
University of Montpellier

THIS THESIS WAS PRENSENTED AND DEFENDED

IN THE PRESENCE OF A BOARD OF EXAMINERS AND PUBLIC

ON MARCH, 23RD, 2026

AT INSA DE LYON

ACKNOWLEDGMENT

First and foremost, I would like to express my deepest gratitude to Professor Nicole Raymonde Demarquette for her humanity, sensitivity, empathy, and attentive listening, which allowed me to access the project I needed. I had many criteria, and she always let me express them freely, with constant understanding and kindness. I also thank her for all the help she provided in expressing and structuring my ideas, both during my doctoral exams and throughout the writing of this thesis.

I would also like to thank Professor Jean-Marc Chenal for agreeing to take an interest in my project without knowing me, after my initial contact. I am deeply grateful for his guidance, his brilliant ideas, and his enthusiasm, even in the face of disappointing results. Thank you for the long conversations, your availability, and your patience, especially with my numerous (and sometimes naïve) questions.

My thanks also go to Dr. Angelo Pommella, co-supervisor on the French side, of whom I had the privilege of being his first student. Thank you for your invaluable help with X-ray measurements, for your constant availability, and for your exemplary calm in all circumstances (the conference will be unforgettable with my last-minute corrections!).

I also thank Dr. Ricardo Zednik, co-supervisor on the Canadian side, who helped unblock certain reflections essential to piezoelectricity.

I am also grateful to the members of the jury Pr Jean Marie Raquez, Pr Virginie Griseri, Pr Jerome Castellon and Pr Ricardo Andrade for their time and willingness to evaluate this thesis.

I gratefully acknowledge the financial support of Ministère de l'Enseignement supérieur, de la Recherche et de l'Innovation and CRSNG which made this research possible.

I sincerely wish to thank all the members of the LGEF at INSA Lyon. Without the expertise of Dr. Jean-Fabien Capsal in piezoelectricity, this project would certainly not have had the same impact. Thanks also to Valérie, Fred, and Laurence for their help and welcome, which allowed me to find my place in a laboratory that was not originally mine.

I also thank all the fellow PhD students and post-doctoral researchers who shared this journey with me, with whom we could share our frustrations, doubts, but also our laughter. After all, it's good to complain a little, we are for most of us, after all, French! Thanks to Manon, Daria, Audrey, Naël, Thomas, Corentin, Elsa, Mathieu, and all the others for their camaraderie and support.

I would also like to thank my parents for their unwavering support since my birth and for always encouraging me to reach my full potential.

I would also like to extend my warmest thanks to my loved ones, particularly my partner Patricia Makhnin, who endured my long periods of absence with patience and love, I know it was not easy. Thanks also to her daughter, my stepdaughter, for her humor and lightheartedness, as well as to my brothers, who have watched me grow and flourish throughout this journey.

Finally, I wish to express my sincere gratitude to Dr. Piperno-Neumann and Dr. Valérie Dumaine, without whom this thesis could not have even begun.

.

PARAMETRES GOUVERNANT LES PROPRIETES PIEZOELECTRIQUES DU PVDF

Chloé MELIN

RESUME

Cette thèse étudie les effets du recuit thermique, de l'incorporation de PLA et de l'électrofilage sur la structure cristalline, la fraction de phase β et les propriétés piézoélectriques des matériaux à base de PVDF. L'étude montre que la haute performance piézoélectrique dépend non seulement de la fraction de phase β, mais aussi de la taille des cristallites, de l'orientation des chaînes et du champ électrique effectif lors du poling.

Des traitements de recuit ont été réalisés à des températures proches et éloignées du pic de cristallisation avant étirage et poling. La taille des cristallites, le degré de cristallinité et la fraction de phase β ont été caractérisés avant et après étirage, tandis que les propriétés piézoélectriques (d_{33}) ont été mesurées après poling. Le recuit a augmenté la taille des cristallites et le degré de cristallinité, avec un effet maximal pour les échantillons recuits à l'état fondu près de la température de cristallisation. Après étirage, les fractions de phase β étaient similaires pour les échantillons recuits et non recuits, mais les échantillons recuits conservaient des lamelles plus épaisses. Tous les échantillons ont montré des valeurs de d_{33} comparables, sauf celui recuit près du pic de cristallisation, dont le d_{33} a diminué de 23 à 30 % en raison de la taille cristalline plus grande et de l'orientation réduite des chaînes, limitant l'efficacité du poling.

Le PVDF a été mélangé par fusion avec 5 % et 40 % de PLA pour obtenir des morphologies perlées et co-continues. Le degré de cristallinité du PVDF est resté inchangé, tandis que la fraction de phase β a diminué fortement à 40 % de PLA. Après poling, l'échantillon perlé PVDF/PLA a présenté un d_{33} inférieur de 34 à 45 % par rapport au PVDF pur, dû à la différence de permittivité entre PVDF et PLA, réduisant le champ électrique effectif. Le mélange co-continu n'a montré aucune réponse piézoélectrique, la phase α étant majoritaire.

L'électrofilage du PVDF a favorisé une forte teneur en phase β et une meilleure orientation des chaînes grâce au fort étirement du procédé, conduisant à un d_{33} 30 % supérieur à celui du film étiré. Une étape de poling restait nécessaire. L'incorporation de 5% de PLA dans du PVDF électrofilé a complètement supprimé la piézoélectricité, probablement due à de très petits domaines PLA qui ont réduit le champ électrique local dans le PVDF, ont empêché l'orientation correcte des chaînes et lamelles PVDF lors de l'étirage, et ont fortement augmenté la surface interfaciale PVDF/PLA, favorisant des interactions qui ont entravé la rotation des chaînes lors du poling.

Ce travail montre que l'obtention de hautes performances piézoélectriques dans les systèmes PVDF nécessite non seulement une forte fraction de phase β, mais aussi un contrôle

précis de la taille cristalline, de l'orientation des chaînes et de la distribution du champ électrique lors du poling.

Mots clés: PVDF, Piezoelectricité, Recuit, PLA, Electrofilage

PARAMETERS GOVERNING THE PIEZOELECTRIC PROPERTIES OF PVDF

Chloé MELIN

ABSTRACT

This thesis investigates the effects of thermal annealing, PLA incorporation, and electrospinning on the crystalline structure, β-phase content, and piezoelectric properties of PVDF-based materials.

Thermal annealing treatments were performed at temperatures close to and further from the crystallization peak of PVDF prior to stretching and poling. The crystal size, degree of crystallinity, and β-phase content were characterized before and after stretching, while piezoelectric properties (d_{33}) were measured after poling. Annealing increased both crystal size and degree of crystallinity, with the strongest effect observed for samples melt-annealed near the crystallization temperature. After stretching, both annealed and non-annealed samples exhibited similar β-phase fractions, but the annealed samples retained thicker lamellae. All samples showed comparable d_{33} values except the one melt-annealed near the crystallization peak, whose d_{33} decreased by 23% to 30% depending on stretching conditions. This reduction was attributed to larger crystal size and lower chain alignment, which decreased poling efficiency and consequently the piezoelectric response.

PVDF was melt-blended with 5% and 40% PLA to obtain beaded and co-continuous morphologies, respectively. The degree of crystallinity remained unchanged upon PLA addition, while the β-phase fraction decreased significantly at 40% PLA content. After poling, the beaded PVDF/PLA sample exhibited a d_{33} value 34% to 45% lower than pure PVDF depending on the stretching conditions. This reduction was attributed to differences in permittivity between PVDF and PLA, which reduced the effective electric field in the PVDF phase during poling. The co-continuous blend exhibited no measurable piezoelectric response due to predominant α-phase formation.

Electrospinning of PVDF promoted a high β-phase content and enhanced chain orientation due to the large stretching ratio inherent to the process, leading to a d_{33} value 30% higher than that of the stretched film. However, an additional poling step was still required to activate piezoelectricity. Incorporation of 5% PLA into electrospun PVDF completely suppressed piezoelectricity, likely due to small PLA domains that reduced the local electric field in PVDF, prevented proper orientation of PVDF chains and lamellae during stretching, and dramatically increased PVDF/PLA interfacial area, promoting strong interactions and stiffening of the material that hindered chain rotation during poling.

Overall, this work demonstrates that achieving high piezoelectric performance in PVDF-based systems requires not only a high β-phase fraction, but also fine control of crystal size, chain orientation, and electric field distribution during poling.

Key words: PVDF, Piezoelectricity, Annealing, PLA, Electrospinning

X

TABLE OF CONTENTS

LIST OF TABLES

Page

LIST OF FIGURES

Page

LIST OF ABREVIATIONS

α-PVDF	Alpha phase of PVDF
β-PVDF	Beta phase of PVDF
γ-PVDF	Gamma phase of PVDF
DCM	Dichloromethane
DMA	Dynamic Mechanical Analysis
DMF	Dimethylformamide
DMAc	Dimethylacetamide
DMSO	Dimethyl sulfoxide
DSC	Differential Scanning Calorimetry
FTIR	Fourier-transform infrared spectroscopy
PDI	Polydispersity Index
PLA	Polylactic Acid
PVDF	Poly(vinylidene fluoride)
SEM	Scanning Electron Microscopy
SAXS	Small-Angle X-ray Scattering
WAXS	Wide-Angle X-ray Scattering
XRD	X-ray Diffraction

LIST OF SYMBOLS

D	Electric displacement vector (C/m^2 or m/V)
d	Piezoelectric coefficient matrix (C/N)
E	Electric field vector (V/m)
E	Young modulus (Pa)
ε	Dielectric permittivity
F(β)	β-phase fraction in the crystalline phase of PVDF
Mw	Weight-average molecular weight (g/mol)
q	Scattering vector ($Å^{-1}$)
R	Stretching ratio
$\mathbf{s}^{\mathbf{E}}$	Elastic compliance tensor (Pa)
T	Mechanical stress vector (Pa)
T	Temperature (°C)
Tg	Glass transition temperature (°C)
Tm	Melting temperature (°C)

INTRODUCTION

The growing global demand for sustainable and portable power sources has become a key issue in modern technology. Conventional electrochemical batteries, although widely used, face significant limitations such as finite lifespans, environmental hazards, and the inconvenience of regular recharging. These challenges have motivated the development of self-powered systems capable of harvesting energy from their surroundings.

Among the different energy-harvesting strategies, piezoelectric materials stand out because they can directly transform mechanical vibrations or stress into electrical energy. Conventional ceramic piezoelectrics, including lead zirconate titanate (PZT), display relatively high piezoelectric coefficients, with typical d_{33} values in the range of 200–600 pC/N (Gomez, 2010 ; Zhang et Zhao, 1999). However, their brittleness and the presence of toxic lead components limit their suitability for flexible or wearable applications.

To address these drawbacks, polymer-based piezoelectric materials such as poly(vinylidene fluoride) (PVDF) and its copolymers have gained growing attention. PVDF offers a unique combination of mechanical flexibility, low density, chemical resistance, and good piezoelectric response, making it a strong candidate for next-generation flexible energy harvesters and sensor devices.

PVDF is a semicrystalline polymer that can crystallize into three main crystalline forms, corresponding to different chain conformations known as α, β, and γ phases (Figure 0.1). The α phase is non-polar and, consequently, non-piezoelectric. In contrast, the β phase is polar and exhibits a strong dipole moment; when the dipoles are aligned through poling, it provides the highest piezoelectric response among the three crystalline forms. The γ phase possesses intermediate polarity and piezoelectric properties between those of the α and β phases. The α phase is thermodynamically stable and is typically obtained under conventional processing methods.

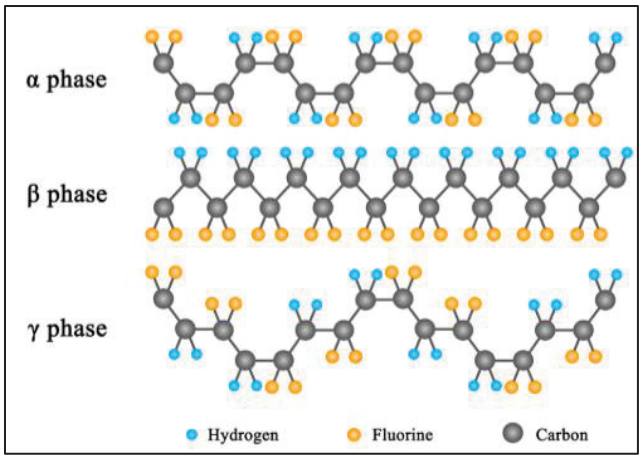

Figure 0.1 PVDF chain conformations (Lu *et al.*, 2020)

Therefore, considerable effort has been devoted to promoting and increasing the β-phase content in PVDF. Several approaches have been explored, including thermal annealing, blending PVDF with PLA, and electrospinning.

Despite extensive efforts to enhance the β-phase content in PVDF, several aspects remain poorly understood. The mechanisms by which thermal annealing promotes β-phase formation are not fully elucidated, and the combined effect of annealing and mechanical stretching on β-phase content and piezoelectric performance has not been systematically investigated. Similarly, while blending PVDF with PLA has been reported to increase the β-phase fraction through electrostatic interactions at polymer interfaces, its impact on piezoelectric properties has not been consistently characterized. Finally, although electrospinning is known to generate high β-phase content due to significant polymer chain stretching, the influence of PLA incorporation on electrospun PVDF fibers, and the resulting piezoelectric performance, has yet to be explored.

To address these gaps, the present study systematically investigates the effects of annealing followed by mechanical stretching, as well as PLA incorporation, on the β-phase content and piezoelectric properties of PVDF films and electrospun membranes. It is hypothesized that annealing will either directly increase β-phase content or promote crystal growth, thereby facilitating the α-to-β phase transformation during subsequent stretching. Stretching is expected to further enhance polymer chain orientation, improving poling efficiency and piezoelectric response. Incorporation of PLA is anticipated to further increase

β-phase formation and enhance piezoelectric performance, particularly in electrospun membranes, due to the high stretching ratios and synergistic effects of polymer blending.

Specifically, this study aims to identify the factors influencing the piezoelectric properties of PVDF. To achieve this, the work is organized around three sub-objectives:

1. Evaluate the effects of thermal annealing and stretching on crystal size, β-phase fraction, and piezoelectric properties of PVDF films.
2. Investigate the influence of PLA blending on the morphology, β-phase content, and piezoelectric performance of PVDF films.
3. Examine the piezoelectric properties of electrospun PVDF and PVDF/PLA membranes, focusing on the combined effects of high stretching ratios and PLA incorporation.

By systematically addressing these aspects, this work provides new insights into strategies for optimizing the piezoelectric performance of PVDF-based materials for flexible energy harvesting and sensor applications.

This work is organized into five chapters. Chapter 1 provides a comprehensive literature review covering the general properties of PVDF, its thermal annealing, PVDF/PLA blends, and electrospinning techniques. Chapter 2 presents the objectives of the study, along with the materials and methods employed. Chapters 3, 4, and 5 report the experimental results related to PVDF annealing, PVDF/PLA blends, and the electrospinning of PVDF and PVDF/PLA blends, respectively.

CHAPTER 1

LITERATURE REVIEW

This chapter is organized into four sections. The first section introduces general concepts related to piezoelectric PVDF, providing the background necessary to understand this research, along with the techniques commonly employed to promote its piezoelectric crystalline phase. The remaining three sections focus on specific approaches reported in the literature to increase the β-phase fraction and induce piezoelectricity in PVDF: Section 1.2 addresses the annealing of PVDF, Section 1.3 examines the effect of blending PVDF with PLA, and Section 1.4 discusses the electrospinning of PVDF.

1.1 Piezoelectricity in PVDF

1.1.1 Piezoelectricity Linear Constitutive Equations

A piezoelectric material is a material capable of converting mechanical energy into electrical energy and vice versa. When a piezoelectric material is mechanically stressed, it becomes electrically polarized, a phenomenon known as the direct piezoelectric effect. Conversely, when an electric field is applied to a piezoelectric material, it undergoes mechanical deformation, which is referred to as the converse piezoelectric effect (Figure 1.1).

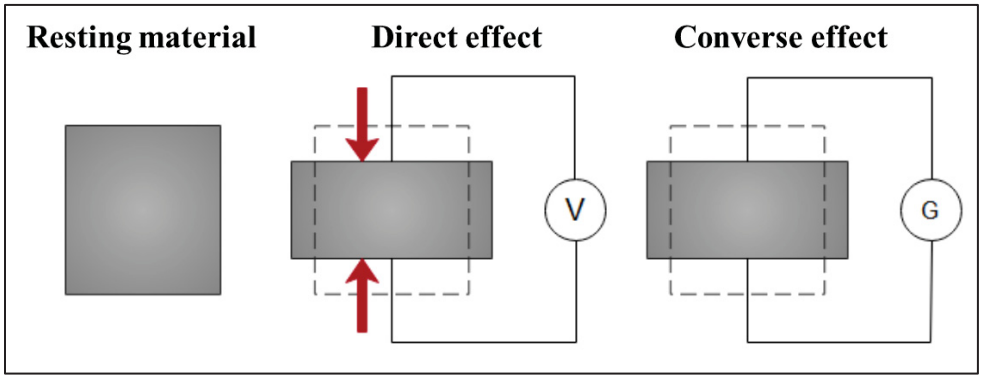

Figure 1.1 Direct and converse piezoelectric effects

Considering that the deformation of the material is in the elastic regime, the interactions between mechanical and electrical responses are described by the linear piezoelectric constitutive equations, which couple mechanical stress, mechanical strain, electric field, and electric displacement. These equations can be expressed as:

$$\boldsymbol{S} = \boldsymbol{s^E T} + \boldsymbol{d^t E} \qquad (1.1)$$
$$\boldsymbol{D} = \boldsymbol{dT} + \boldsymbol{\varepsilon^T E}$$

Where $\mathbf{s^E}$ is the elastic compliance tensor (6×6) at constant electric field, $\boldsymbol{\varepsilon^T}$ is the dielectric permittivity tensor (3×3) under constant stress, **d** is the piezoelectric charge coefficient matrix (3×6), and d^t denotes its transpose, **S** is the mechanical strain vector (6×1), **T** is the mechanical stress vector (6×1), **E** is the electric field vector (3×1), **D** is the electric displacement vector (3×1).

In practice, PVDF films are stretched in the 1 direction (see section 1.1.5) and poled (see Section 1.1.3) in the 3 direction (Figure 1.2).

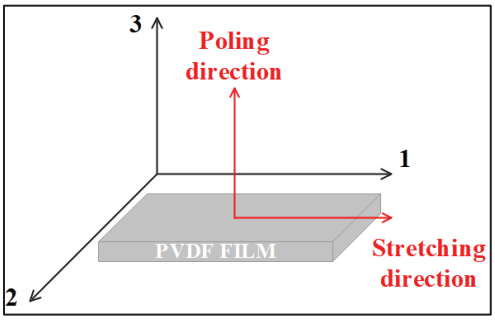

Figure 1.2 Stretching and poling directions in PVDF

Upon mechanical solicitation (direct effect), the resulting piezoelectric response is often characterized by piezoelectric coefficients d:

- d_{33}: the longitudinal piezoelectric coefficient, which represent the electric charge generated along the poling direction (3) per unit mechanical stress applied in the same direction (3)

- d_{31}: the transverse piezoelectric coefficient, which represents the charge generated along the poling direction (3) per unit mechanical stress applied perpendicular in the stretching direction (1)

With the piezoelectric phenomenon now clarified, the following section addresses the role of PVDF's crystalline structure in governing its piezoelectric response.

1.1.2 PVDF Crystal Structure

As discussed in the introduction, the chain conformation of PVDF plays a key role in determining its piezoelectric behavior. However, the way these chains are packed within the crystalline unit cell is equally critical.

For a crystal to exhibit piezoelectric properties, its unit cell must lack a center of symmetry. When a non-centrosymmetric unit cell is subjected to mechanical stress, a net polarization is induced in the crystal (Kasap, 2006).

Figure 1.1 presents the crystalline unit cells of β-PVDF (Form I), α-PVDF (Form II) and γ-PVDF (Sessler, 1981).

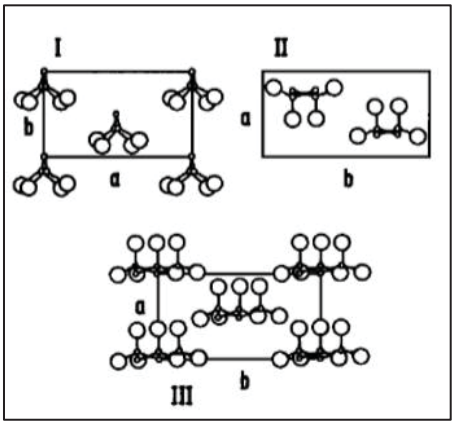

Figure 1.3 β-PVDF crystalline unit cells (Form I), α-PVDF crystalline unit cell (Form II) and γ-PVDF (Form III) projected in the a-b plane (Sessler, 1981)

The β-phase and γ-phase unit cells are non-centrosymmetric, as their dipoles are aligned in the same direction, resulting in a net dipole moment. Consequently, both β-PVDF and γ-PVDF crystals conformation can exhibit piezoelectricity, although the γ phase displays weaker piezoelectric behavior due to its lower dipole moment. When stress is applied along the b-axis, the polarization of these crystals is modified. In contrast, the α-PVDF unit cell is centrosymmetric, which results in a non-polar crystal without piezoelectric activity.

With the role of the PVDF crystalline structure now established, the following section discusses the necessity of poling the material.

1.1.3 Importance of Poling

Having PVDF crystallized in the β-phase is not sufficient to achieve strong piezoelectric properties, as the dipoles remain mostly randomly oriented (Figure 1.4a). To develop a net polarization, the dipoles must be aligned in a preferred direction, which is precisely the role of the poling process.

Poling consists of applying an external electric field that induces spontaneous polarization by reorienting dipoles along the field direction (Figure 1.4b). The mechanism of dipole reorientation has been described through combined experimental and theoretical studies. In β-phase PVDF, polarization proceeds through the nucleation and propagation of kinks, localized chain-segment rotations, that occur mainly at lamellar surfaces and domain boundaries, where the rotation energy is lower. These kinks enable the progressive reorientation of dipoles in successive 60° steps (Kepler et Anderson, 1992 ; Takahashi et Odajima, 1981 ; Furukawa, Date et Johnson, 1983).

Upon removal of the field, the dipoles partially relax and become locked in a quasi-aligned configuration. Maximizing this remanent polarization (P_r) is essential to achieving optimal piezoelectric performance in PVDF (Figure 1.4c) (Sukumaran *et al.*, 2021).

Indeed, unpoled β-phase PVDF exhibits poor piezoelectric properties. Poling is therefore indispensable to align the dipoles and render PVDF functional as a piezoelectric material (Lei *et al.*, 2015 ; Ruan *et al.*, 2018 ; Bodkhe *et al.*, 2018).

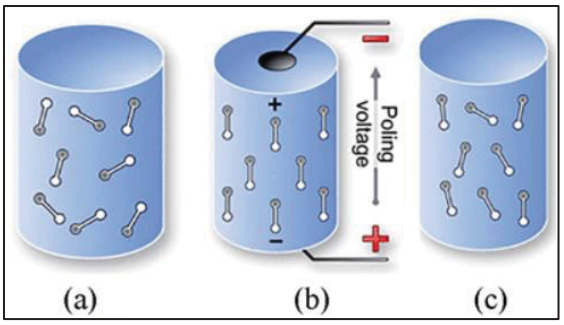

Figure 1.4 Poling of PVDF (Sukumaran *et al.*, 2021)

Having discussed the role of β-phase orientation, the following section examines the contribution of the amorphous phase to the piezoelectric response of PVDF.

1.1.4 Effect of the Amorphous Phase Compressibility on the PVDF Piezoelectric Response

In addition to the presence of poled β-phase crystals, another key factor contributes to the piezoelectricity of PVDF. A β-crystallized PVDF sample consists of both oriented β crystals, each possessing a net dipole moment, and an amorphous phase. The overall polarization P of the sample can be expressed as shown in Equation 1.2, where N denotes the number of polar molecules or polar crystals per unit volume, and p_0 is the dipole moment of each polar entity:

$$P = N \times p_0 \tag{1.2}$$

In PVDF, the piezoelectric response depends non only from the number and orientation of the β crystals but also on the mechanical properties of the amorphous phase. Indeed, under mechanical stress applied above T_g, the amorphous domains deform more readily than the rigid β-phase crystals, leading to a change in the effective density of dipoles per unit volume. This variation in dipole density modifies the net polarization of the material and gives rise to the measured piezoelectric response.

Thus, while the crystalline structure of PVDF is central to its piezoelectric response, the contrast in mechanical properties between the crystalline and amorphous phases also plays a crucial role in enabling piezoelectricity (Sessler, 1981).

Having reviewed all the requirements for obtaining a functional piezoelectric PVDF material, the next section focuses on the methods for producing and enhancing the piezoelectric β phase of PVDF.

1.1.5 β Phase Formation and Enhancement

As discussed in the previous sections, the presence of the β phase is essential for PVDF to exhibit strong piezoelectric properties. However, the β phase is metastable, and under typical processing conditions PVDF crystallizes preferentially into the thermodynamically stable α phase. The greater stability of the α phase compared to the β phase arises from a combination of steric hindrance and favorable electrostatic interactions, which make the all-trans conformation of β-PVDF less favorable energetically.

Indeed, the van der Waals radius of fluorine is 1.47 Å (Tredwell, 2012), which is roughly twice the distance separating two fluorine atoms in the α conformation (Figure 1.5). As a result, the closer packing of fluorine atoms in the β conformation is sterically unfavorable (Figure 1.5). In addition to steric hindrance, dipole–dipole repulsion further destabilizes the β arrangement, since adjacent fluorine atoms possess the same polarity and repel one another.

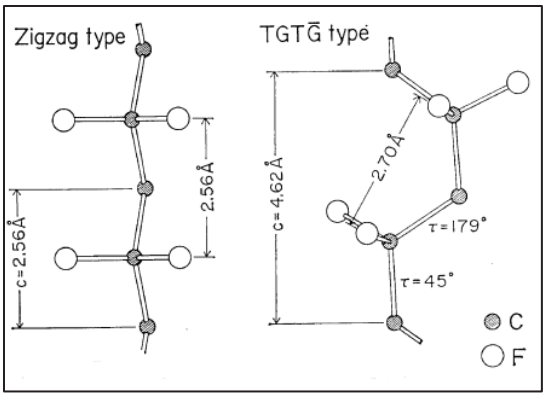

Figure 1.5 Distance between two consecutive fluorine atoms in the α phase (right) and in the β phase (left) (Hasegawa, Kobayashi et Tadokoro, 1972)

However, several strategies have been developed to enhance the β-phase fraction in PVDF, either by tailoring the material composition or by applying specific processing routes.

On the compositional side, approaches include copolymerization of PVDF (Zhang *et al.*, 2013), blending with miscible such as PMMA (De Neef *et al.*, 2018 ; Song, Decal et Feng, 1990 ; Bansal *et al.*, 1995) or immiscible polymers such as Nylon 11 or PLA (Gao et Scheinbeim, 2000 ; Zhong *et al.*, 2011), and the incorporation of functional particles, such as CNT or $BaTiO_3$, into the PVDF matrix (Yee *et al.*, 2012 ; Mendes *et al.*, 2012).

From a processing perspective, β-phase crystallization can be promoted through high-pressure crystallization (Matsushige, 1978 ; Doll et Lando, 1970) or ultrafast cooling (Oka, Murata et Koizumi, 1986 ; Yang et Chen, 1987) from the melt, solvent casting using polar solvents (Gregorio et Borges, 2008 ; Nishiyama *et al.*, 2017 ; Li *et al.*, 2019), annealing under suitable conditions (Satapathy *et al.*, 2011 ; Sharma, Madras et Bose, 2014), mechanical stretching of α-phase films (Sencadas *et al.*, 2012 ; Ruan *et al.*, 2018), or electrospinning (He *et al.*, 2021).

The most industrially relevant and straightforward method to increase the β-phase fraction in PVDF is mechanical stretching of α-phase films, followed by a poling step to induce piezoelectricity.

The efficiency of the α-to-β phase transformation during stretching primarily depends on two key parameters: the drawing ratio and the stretching temperature. Studies have consistently shown that optimal transformation occurs at stretching temperatures between 60

°C and 100 °C combined with drawing ratios between 3 and 5 (Gregorio et Ueno, 1999 ; Sencadas *et al.*, 2012 ; Ruan *et al.*, 2018). At a fixed temperature, increasing the drawing ratio enhances the β-phase content, whereas at a fixed stretching ratio, raising the stretching temperature reduces the β-phase fraction (Figure 1.6). When the stretching temperature exceeds 120 °C, only orientation of the α phase is observed, without conversion into the β phase (Gregorio et Ueno, 1999 ; Sencadas *et al.*, 2006 ; Gomes *et al.*, 2010).

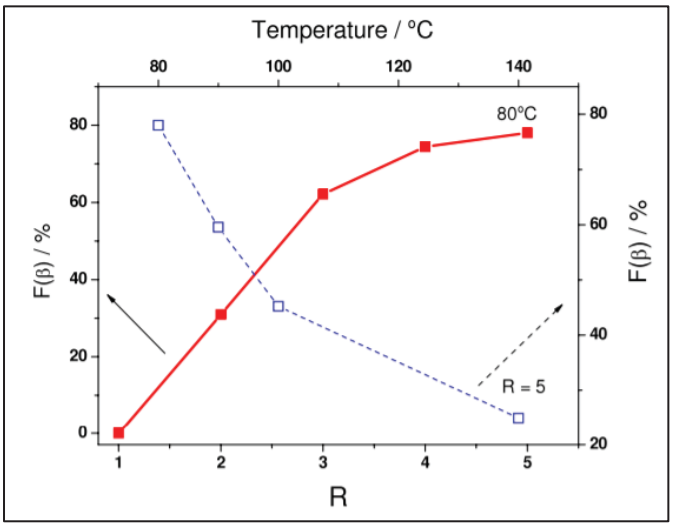

Figure 1.6 Influences of the stretching ratio R and stretching temperature on the β phase content F(β) (Gomes *et al.*, 2010)

The α-to-β phase transformation appears to be more efficient at lower stretching temperatures for two main reasons. First, the crystallization rate of the β phase is believed to be higher in the range of 60–80 °C, which promotes its formation during deformation. Second, at these lower temperatures, the viscosity of PVDF is higher, enabling more effective stress transfer from the amorphous regions to the crystalline domains during stretching. This enhanced stress transfer facilitates the conformational change of chains within the α phase, favoring their transformation into the β phase (Sajkiewicz, Wasiak et Gocl, 1999).

With the piezoelectricity of PVDF and the common methods for obtaining the β phase already discussed, the following section focuses on the effect of annealing on the β-phase fraction and the resulting piezoelectric properties

1.2 Annealing of PVDF

Table-A I-1 compiles the literature on the effect of thermal treatments, and specifically annealing, on the β-phase fraction before poling and the resulting piezoelectric properties of PVDF after poling. For clarity, a condensed version is presented here (Table 1.1). The "Fabrication" column specifies the sample preparation method, "Initial phase" indicates the predominant crystalline phase (α, β, γ) prior to annealing, "Annealing temperature" lists the temperature yielding the highest β-phase content (F(β)) along with the corresponding percentage when specified in the article, "Degree of crystallinity" reports the associated crystallinity index (X_c), and "Piezoelectric properties" details the values of the piezoelectric coefficient (d_{33}) or remanent polarization (P_r) obtained for the film with the highest β-phase content after the poling step.

Table 1.1 Literature summary on PVDF annealing for piezoelectric applications

Fabrication	Initial phase	Annealing temperature	Degree of crystallinity	Piezoelectric properties	Reference
Solvent casting with DMSO	γ	90°C		P_r = 4.9 μC/cm^2	(Satapathy *et al.*, 2011 ; Satapathy *et al.*, 2008)
Hot pressed	α	100°C F(β) = 60 %			(Sharma, Madras et Bose, 2014)
Solvent casting with DMF		110 °C F(β) = 66 %	Max at 110°C X_c = 54 %	d_{33} = 24 pC/N	(Jaglan et Uniyal, 2022)
Solvent casting with DMAc		140°C F(β) = 78 %	Max at 140°C Xc = 46 %		(Zhu *et al.*, 2016)
Spin coated with DMSO	γ	90°C Mixture of α and β		P_r = 6.6 μC/cm^2	(Hess, Rudolph et Reid, 2015)
Solvent casted with DMF		100°C		P_r = 0.39 μC/cm^2	(Kaur *et al.*, 2017)
Spin coated with DMF	β	100°C F(β) = 80%			(Shaik *et al.*, 2017)
Electrospinning with DMF/Acetone		100°C F(β) = 87 %	Max at 100°C Xc = 45 %	P_r = 0.42 μC/cm^2 d_{33} = 15 pC/N	(Satthiyaraju et Ramesh, 2019)

Most of the studies suggest that intermediate annealing temperatures, typically around 100°C, promote the transformation of the primary α or γ phases into the electroactive β phase, without stretching or the application of an electric field.

This phenomenon is attributed to the increased chain mobility at intermediate temperatures, which facilitates molecular reorganization into the metastable β phase conformation. At higher annealing temperatures, however, the formation of the more thermodynamically stable α phase is favored (Zhu *et al.*, 2016 ; Satapathy *et al.*, 2011). The enhanced β-phase formation at this temperature has also been attributed to its higher crystallization rate compared with the α phase under these conditions (Satapathy *et al.*, 2008).

The enhancement of piezoelectric properties is consistently associated with an increased β phase fraction and/or a higher degree of crystallinity (Satapathy *et al.*, 2011 ; Kaur *et al.*, 2017 ; Jaglan et Uniyal, 2022 ; Hess, Rudolph et Reid, 2015 ; Satthiyaraju et Ramesh, 2019).

The existing literature predominantly investigates the effects of annealing on PVDF films produced by solvent casting with polar solvents. It is well established that polar solvents, combined with controlled evaporation rates, promote the crystallization of PVDF into electroactive phases such as β or γ. Consequently, annealing in these studies was typically applied to films already containing a high proportion of electroactive phases. In contrast, the present study focuses on the effect of annealing on a melt-processed film primarily composed of α phase. Two annealing temperatures were selected: the first, 100°C, is believed to favor the formation of β phase, while the second, 140°C, aims to increase the crystal size as it is closer to the crystallization temperature of PVDF (Annex II).

Furthermore, most studies in the literature have evaluated piezoelectric properties without applying a post-treatment mechanical stretching step, yet reported relatively high values. This is unexpected, as significant d_{33} values generally require not only the presence of β phase but also its pre-orientation through stretching. Without this step, poling is largely inefficient, resulting in poor piezoelectric performance. Indeed, one study showed that the dielectric permittivity of solvent-cast PVDF with a high β-phase fraction differs depending on whether the phase is oriented, with oriented materials exhibiting the highest permittivity (Gregorio et Ueno, 1999). This indicates that oriented materials can be polarized more efficiently under an electric field, ultimately enhancing piezoelectric properties.

Stretching is also well-known to significantly increase the β-phase fraction in PVDF. However, in studies where stretching was applied after annealing (Sharma, Madras et Bose, 2014), the resulting piezoelectric properties were not reported, leaving a gap in understanding the synergistic effects of thermal and mechanical treatments.

Therefore, this study aims to investigate the effect of stretching on annealed films in terms of β-phase content. It is expected that stretching will further increase the β-phase fraction in films annealed at 100°C. Moreover, increasing the initial crystal size and thickness of the

amorphous lamellae prior to stretching (annealing at 140°C) is anticipated to enhance the α-to-β phase transformation.

The influence of annealing and stretching on crystal size, β-phase content, and the piezoelectric response of poled samples will be systematically examined.

The following section focuses on another approach to increase the β-phase fraction in PVDF: blending with PLA.

1.3 PVDF/PLA Blends

Table-A III-1 compiles the literature on the effect of PLA incorporation on the β phase fraction and piezoelectric properties of PVDF. For clarity, a condensed version is presented here. The “Fabrication” column specifies the sample preparation method, “Composition” indicates the weight ratio of PVDF/PLA used, with the composition of best β phase improvement in red, “Stretching Conditions” gives the stretching conditions that led to the highest β phase content, “F(β)” lists the highest β phase content obtained for both the pure PVDF and the blend before and after stretching, and “Piezoelectric properties” details the values obtained for the film with the highest β-phase content both in the blend and in the pure PVDF after stretching and poling.

Table 1.2 Literature summary on PVDF/PLA blends for piezoelectric applications

Fabrication	Composition	Stretching conditions	F(β)	Piezoelectric properties	Reference
Solvent casting with DMF	100/0 70/30 0/100	R = 4 T = 80°C (for pure PVDF) T = 100°C (for the blend)	Before stretching $F_{PVDF}(\beta)$ = 30 % $F_{blend}(\beta)$ = 20 % After stretching $F_{PVDF}(\beta)$ = 82 % $F_{blend}(\beta)$ = 50 %	P_{rPVDF} = 55 mC/m^2 d_{31PVDF} = 3.2 pC/N P_{rblend} = 110 mC/m^2 $d_{31blend}$ = 2.6 pC/N	(Mukri *et al.*, 2024)
Solvent casting with DMAc	100/0 30/70 50/50 70/30	R = 3 T = 80°C v = 4 mm/min	Before stretching $F_{PVDF}(\beta)$ = 45 % $F_{blend}(\beta)$ = 50 % After stretching $F_{blend}(\beta)$ = 70 % Value not indicated for pure PVDF but said to be less than blend		(Mishra *et al.*, 2021)
Melt	100/0 95/5 90/10 85/15 80/20	R = 4 T = 60°C v = 5mm/min	Before stretching F(β) = 0% for both the pure PVDF and the blend After stretching $F_{PVDF}(\beta)$ = 90 % $F_{blend}(\beta)$ = 95 %		(Xie *et al.*, 2013)
Solvent casting with DMF	100/0 70/30 50/50 30/70		F(β) increases upon PLA addition (just qualitative)		(Rasanani *et al.*, 2022)
Melt	0/100, 100/0 20/80, 80/20 40/60, 60/40	Not specified but probably stretching upon filament deposition	F(β) decreases upon PLA addition $F_{PVDF}(\beta)$ = 81 %		(de Oliveira *et al.*, 2023)

From Table 1.2, when PVDF/PLA blends are manufactured from the melt, no enhancement of the β phase content in PVDF is observed without any stretching step (Xie *et al.*, 2013 ; de Oliveira *et al.*, 2023). By contrast, when PVDF/PLA blends are prepared by solvent casting using polar solvents such as DMF or DMAc, most studies report an increase in the β phase fraction (Mishra *et al.*, 2021 ; Rasanani *et al.*, 2022). This increase has been attributed to electrostatic interactions occurring at the PVDF/PLA interfaces (Figure 1.7).

The different outcomes between melt-processed and solvent-cast blends may be explained by the fact that such interactions do not directly induce a conformational change in PVDF, but rather stabilize it once formed. During melt processing, PVDF crystallizes into its thermodynamically stable α phase, and PLA does not play a significant role. In solvent casting, however, PVDF chains can adopt the metastable β conformation, and the presence of PLA likely helps to stabilize this form during solvent evaporation, preventing more efficiently relaxation into the α phase near the polymer interfaces. As a result, the β phase content in the blends is slightly higher than in pure PVDF.

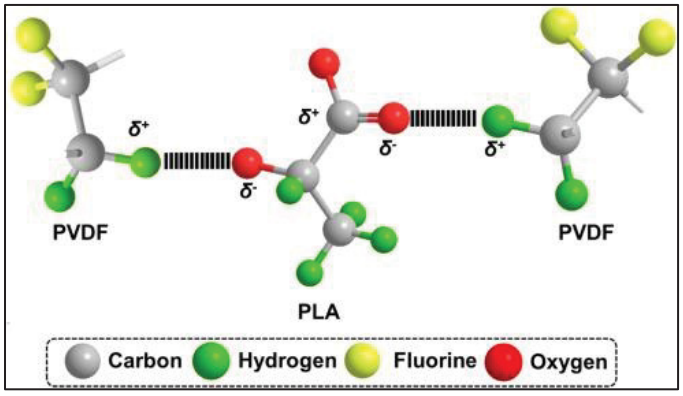

Figure 1.7 PVDF/PLA interaction (Mishra *et al.*, 2021)

In PVDF/PLA blends, the β-phase content obtained after stretching can surpass that of pure PVDF. In the PVDF/PLA beads-in-matrix blend, the lower storage modulus and viscosity of dispersed PLA beads promote their preferential deformation and rupture under stretching, generating cavities. This induces heterogeneous stress distribution, concentrating local stress in the PVDF matrix and facilitating necking that drives α-to-β phase transformation (Xie *et al.*, 2013).

The piezoelectric properties of PVDF in the presence of PLA have been reported only once. However, in that study, different stretching and poling conditions were applied to pure PVDF and to the blend, making a direct and meaningful comparison inappropriate.

This study aims to fabricate PVDF/PLA blends with two distinct morphologies (i.e., beaded and co-continuous), as the co-continuous morphology has not yet been investigated. The effect of PLA incorporation on both the β phase fraction before and after stretching as well as the piezoelectric properties will be reported in a consistent and comparable manner.

In the next section, the effect of electrospinning on the β phase fraction as well as on the piezoelectric properties of PVDF is discussed.

1.4 Electrospinning of PVDF

1.4.1 Typical Electrospinning Setup and Influencing Parameters

Figure 3.8 illustrates a typical electrospinning setup. A polymer solution (or melt) is loaded into a syringe and extruded through a spinneret (needle). A high-voltage electric field is applied between the spinneret and a conductive collector, which may be either planar or rotating to enable the deposition of aligned fibers. When the electrostatic force surpasses the surface tension of the solution, a jet is ejected from the needle tip and directed toward the collector. During its flight, the jet experiences bending instabilities induced by solvent evaporation and the solution’s conductivity, leading to the characteristic whipping motion.

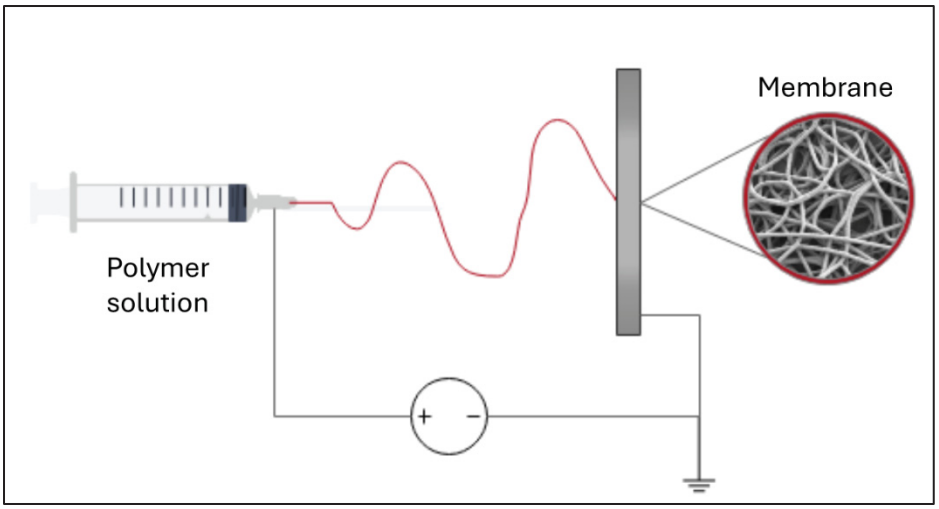

Figure 1.8 Typical electrospinning setup

The spinnability of the solution, the morphology of the resulting fibers, and the β-phase content in electrospun PVDF are strongly influenced by the electrospinning parameters. These parameters can be classified as follows:

- Solution parameters: viscosity (entanglement, Mw, concentration), electrical properties (conductivity, dielectric constant), surface tension
- Process parameters: flow rate of the solution, electric field (voltage, distance)
- Ambient parameters: Temperature, humidity

The influence of these parameters on fiber diameter and their effect on β-phase content are summarized in Table-A IV-1. This table is included in Annex IV since optimization of these parameters was not undertaken in this project. In brief, the literature indicates that tuning parameters to increase fiber stretching and reducing the fiber diameter generally results in a higher β-phase fraction.

1.4.2 Advantages of the Electrospinning Process Compared to Films and Resulting Piezoelectric Properties

Electrospinning has been reported to favor extensive β-phase formation, generally attributed to the very high stretching ratios involved (Azzaz et al., 2021). For example, electrospinning was found to increase the β-phase fraction to 55 %, compared to 0.5 % in a cast film prepared with the same DMF/acetone solvent system (Yu *et al.*, 2013), although this very small β-phase content is surprising, since the presence of DMF combined with slow solvent evaporation would normally be expected to favor higher β-phase formation (Li *et al.*, 2019). However, the β phase fraction reported in the studies summarized in Table 1.3 are not always higher than the one reported in Table-A II-1, but higher β phase amount in electrospinning could also come from facilitated crystallization of PVDF upon high stretching.

In addition, the literature suggests that the in-situ poling occurring during the process may reduce or even eliminate the need for a subsequent poling step, thereby enabling the straightforward fabrication of piezoelectric PVDF (Dani *et al.*, 2024 ; Mokhtari *et al.*, 2025 ; Szewczyk *et al.*, 2020 ; Joseph *et al.*, 2018 ; Gheibi *et al.*, 2014).

Table 1.3 summarizes a few studies reporting the electrospinning parameters used to produce PVDF membranes, along with the resulting fiber diameters, β-phase fractions, and piezoelectric properties. According to these studies, the piezoelectric properties were measured without any post-poling treatment, yet the materials still exhibited piezoelectric behavior. For instance, an electrospun PVDF membrane with a β-phase content of 83% achieved a d_{33} value of 15.2 pC/N, whereas a biaxially stretched film prepared at a stretching ratio of 3.5 at 100 °C contained only 53% β-phase and exhibited a lower d_{33} of 11.7 pC/N. (Wu et Chou, 2016).

This study investigates the effect of electrospinning on the β-phase fraction and d_{33} coefficient of PVDF, in comparison with stretched and poled films produced by melt processing. In addition, the influence of PLA incorporation into the membranes is examined.

Table 1.3 Review on electrospinning of PVDF

Solution	Electric field E (voltage V, distance d)	Flow rate q	Ambiant parameters (temperature T, humidity H)	Fiber diameter	F(β) (%)	Piezoelectric properties	Reference
24 wt.% in DMAc/Acetone 1/1 v/v	V = 15 kV d = 18 cm E = 0.8 kV/cm	q = 6 mL/h	T = 25°C H = 30-60 %	0.8 - 1.46 µm	50 - 74 %	1.6 – 5.6 pm/V (PFM measurement)	(Szewczyk *et al.*, 2020)
2g of PVDF dissolved in 6 mL of DMF and 4 mL of acetone	V = 15 kV d = 15 cm E = 1 kV/cm	q = 0.6 - 3 mL/h		150 – 300 nm	66.9 - 75.8 %	25 – 35 mV (peak-to-peak voltage upon hammer force)	(Singh, Lye et Miao, 2019)
16 – 20 – 26 wt.% PVDF dissolved in DMF/acetone (4/6 v/v)	V = 15 kV d = 15 cm E = 1 kV/cm	q = 1 mL/h	RT	0.2 – 0.8 µm	77.5 – 86 %	2 – 4 V (peak-to-peak determined with homemade testing platform applying force of 10N at 1 Hz)	(Shao *et al.*, 2015)
2.2 g PVDF in 6 mL DMF and 4 mL acetone	V = 20 kV d = 20 cm E = 1 kV/cm	q = 0.05 mL/h		Around 100 nm	83 %	d_{33} = 15.2 pC/N (method not provided)	(Wu et Chou, 2016)

CHAPTER 2

EXPERIMENTAL

2.1 Objectives and Resulting Experimental Plan

As outlined in the introduction, the primary objective of this thesis is to identify the factors influencing the piezoelectric properties of PVDF. To achieve this several approaches have been investigated:

- Annealing of PVDF, which is hypothesized to enhance piezoelectric properties either by directly increasing the β phase fraction or the degree of crystallinity, or by enlarging the crystalline domain size, thereby facilitating the α-to-β phase transformation during mechanical stretching
- Incorporation of PLA into the PVDF matrix, which is expected to enhance the β phase content after stretching thanks to storage modulus mismatch
- Electrospinning of PVDF and PVDF/PLA blends, which is anticipated to generate a high proportion of oriented β phase crystals, potentially eliminating the need for a post processing poling step

For each sub-objective, the corresponding experimental procedures, the parameters characterized at each stage, and the associated characterization techniques are summarized in Figures 2.1, 2.2, and 2.3. In these schematics, blue boxes represent the experimental steps, while white boxes indicate the parameters characterized together with the corresponding analytical methods. A detailed description of the experimental workflow and characterization techniques is provided in Sections 2.3 and 2.4.

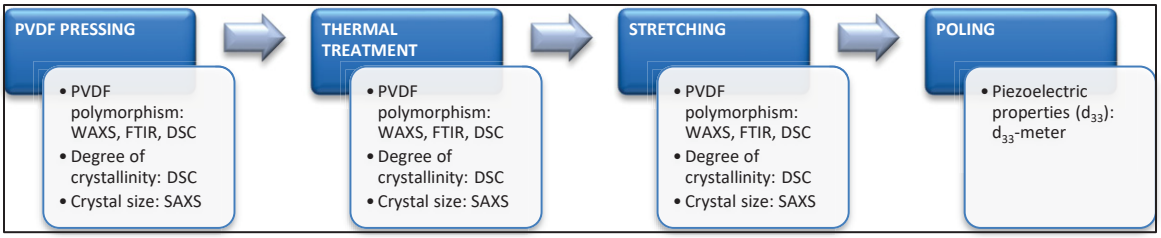

Figure 2.1 PVDF annealing steps (blue box), characterized parameters and their characterization techniques (white box)

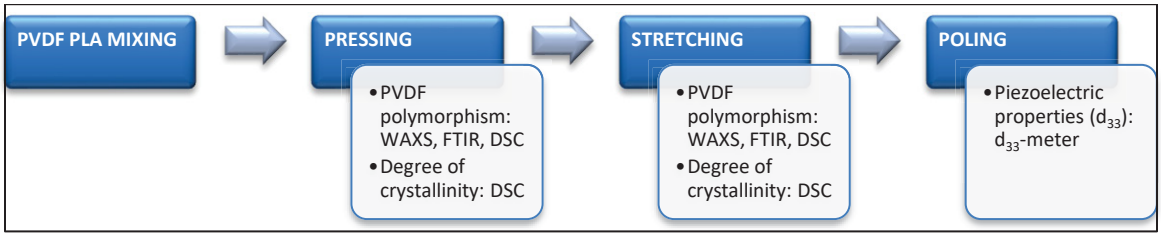

Figure 2.2 PVDF/PLA blend fabrication steps (blue box), characterized parameters and their characterization techniques (white box)

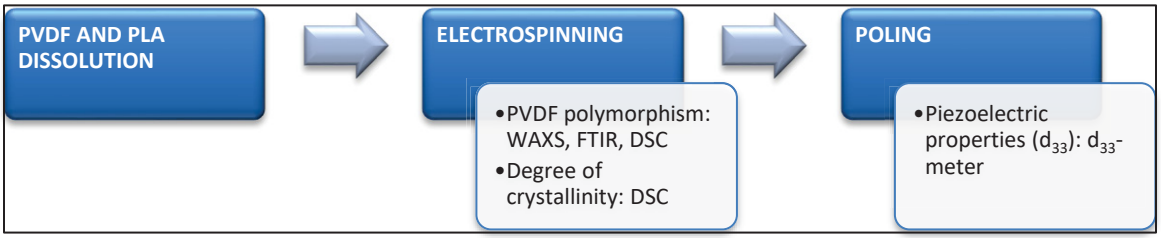

Figure 2.3 PVDF electrospinning steps (blue box), characterized parameters and their characterization techniques (white box)

2.2 Materials

PVDF Kynar 740 and 741, which correspond to the same grade in pellet and powder form respectively, were provided by Arkema. The pellet form (Kynar 740) was used for blending with PLA, whereas the powder form (Kynar 741) was employed for compression molding and solution-based processing, i.e. electrospinning.

Both PLA grades, 2500HP and 4060D, were supplied by NatureWorks. The 2500HP grade is semi-crystalline, while 4060D is predominantly amorphous. This selection enabled the investigation of the effect of PLA stereoregularity on the α-to-β phase transformation of PVDF during stretching, while maintaining a comparable molecular weight between the two grades.

The relevant properties of these three polymer grades are given in Table 2.1.

Table 2.1 Properties of the used polymers

	PVDF Kynar 740/741	**PLA 2500HP**	**PLA 4060D**
Density (g/cm^3)	1.78[a]	1.24[b]	1.24[c]
Weight average molecular weight Mw (g/mol)	410 000[d]	192 000[e]	188 000 - 191 000[f,g]
Polydispersity Index PDI			1.63 – 1.8[f,g]
Tg (°C)	-40[a]	55 – 60[b]	52 – 58[c]
Tm (°C)	168[a]	165 – 180[b]	
Processing Temperature (°C)		210[b]	210[c]

[a]PVDF Kynar 741 Datasheet, [b]PLA 2500 HP Datasheet, [c]PLA 4060D Datasheet, [d](Chen *et al.*, 2015), [e](Mohammadi *et al.*, 2023),[f](Liparoti *et al.*, 2024), [g](Litauszki *et al.*, 2023)

2.3 Processing

2.3.1 PVDF/PLA mixing

PVDF Kynar 740 and PLA 2500HP were melt-blended in a twin-screw Extruder Haake Rheomix OS from Thermo scientific, at 210 °C and 100 rpm, using PVDF/PLA weight ratios

of 95/05, 70/30, and 60/40. These different compositions were selected to obtain distinct blend morphologies, ranging from droplet-in-matrix (beaded) structures to co-continuous phases.

In parallel, PVDF Kynar 740 and PLA 4060D were blended under the same extrusion conditions at a 70/30 weight ratio to investigate the influence of PLA stereoregularity on the α-to-β phase transformation of PVDF during stretching.

For comparison purposes, pristine PVDF Kynar 740 was also extruded twice under the same processing conditions.

All compositions were extruded twice to ensure homogeneous mixing.

2.3.2 Pressing

Pristine PVDF Kynar 741 (powder form), extruded PVDF Kynar 740 (pellet form) and extruded PVDF/PLA blends were compression molded using a manual press Model 3856 25-12H from Carver at 210°C, respectively for a total of 9 minutes. Initially, the PVDF powder, or extruded PVDF pellets or blends were placed between the two heated plates without applying pressure for 4 minutes to allow uniform melting. Subsequently, a light "kiss" pressure of 40 kPa was applied for 2 minutes, followed by a final pressure of 100 kPa for 3 minutes. After pressing, the molten samples were rapidly transferred between two cold metal plates to ensure controlled cooling.

2.3.3 PVDF and PLA Dissolution

The solvent used for electrospinning must satisfy several key criteria:

- It must effectively dissolve the polymer
- It must possess sufficient volatility to allow solvent evaporation before the fiber reaches the collector
- It must exhibit adequate electrical conductivity and permittivity

To meet all these requirements, a binary solvent system composed of DMSO and acetone in the 60/40 volume ratio was selected. DMSO, the solubility parameter of which closely matches that of PVDF, i.e. 23.2 $MPa^{1/2}$ (Shaliutina-Kolešová, 2018), ensures good polymer dissolution. Although DMSO exhibits relatively low electrical conductivity, its high dielectric permittivity facilitates the electrospinning process. Moreover, DMSO was selected over DMF, that is commonly used, due to its significantly lower toxicity, making it a safer alternative for both handling and environmental considerations. Acetone, although it dissolves primarily the amorphous regions of PVDF, enhances the volatility of the solvent system, promoting efficient drying of the fibers during their travel from the needle to the collector. Acetone can also act as a solvent for PLA, which has a solubility parameter of 21.3 $MPa^{1/2}$ (Hsiao et Nagai, 2024), although only limited amounts of PLA are soluble in it.

The relevant physical properties of DMSO and acetone are summarized in Table 2.2.

Table 2.2 Physical properties of the used electrospinning solvents

(Ian M. Smallwood, 1996)	**DMSO**	**Acetone**
Solubility parameter ($MPa^{1/2}$)	26.6	20.5
Vapor pressure at 21°C (mmHg)	0.7	194
Boiling Point (°C)	189	56
Electrical conductivity (S/cm)	2E-7	5E-9
Permittivity at 20°C	46.6	20.6

The PVDF concentration in the solvent mixture was set to 9 wt.%, a value exceeding the entanglement concentration and thus enabling fiber formation. The entanglement concentration was determined from rheological measurements, and the corresponding viscosity–concentration curve is provided in Annex V.

In addition, after amorphizing crystalline PLA, it was possible to dissolve 1 wt.% PLA in the DMSO/acetone (60/40 v/v) solvent system by maintaining the mixture at reflux and

preventing solvent loss with a distillation setup. This procedure inhibited PLA recrystallization and enabled its dissolution.

As a result, a stable solution containing 9 wt.% PVDF with 5 wt.% PLA (PVDF/PLA 95/05 w/w), prepared with either crystalline or amorphous PLA, was successfully obtained and electrospun, along with the reference 9 wt.% pure PVDF solution.

2.3.4 Annealing

After the pressing of PVDF Kynar 741 (powder form), four different annealing procedures were carried out and are detailed in Figure 2.4.

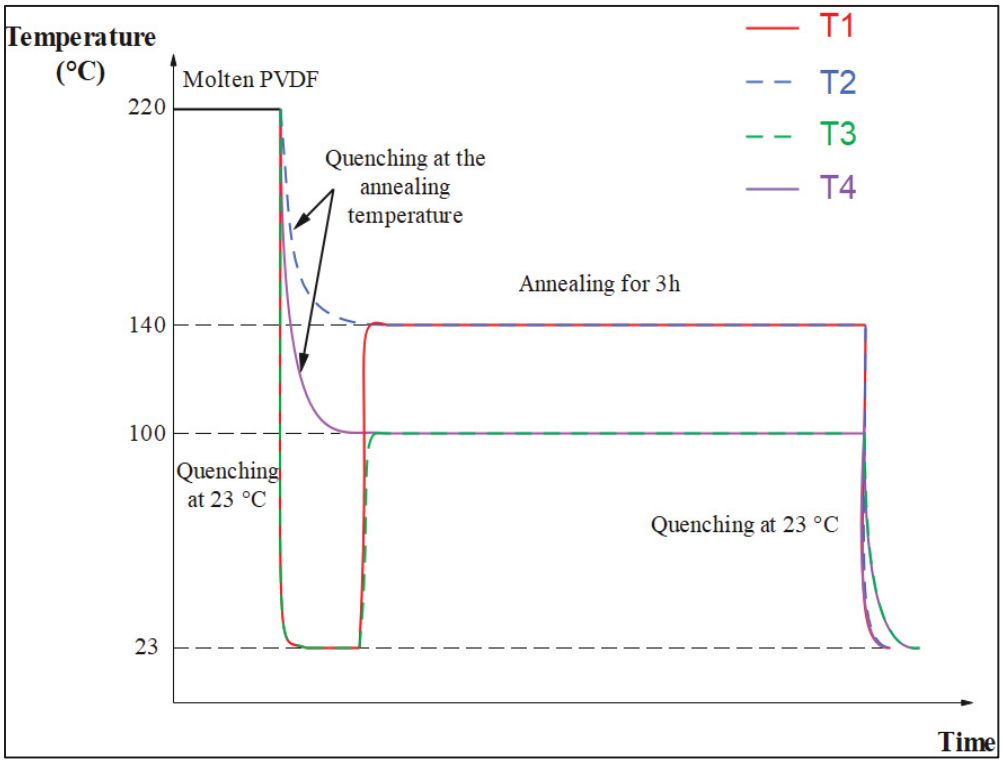

Figure 2.4 Annealing procedures

The annealing temperatures for T1 and T2 were selected based on the DSC results obtained for PVDF, which indicate that maximum crystallization occurs around 140 °C (Annex

II). It is assumed that increasing the thickness of the amorphous lamellae facilitates their deformation during stretching, thereby promoting the α-to-β phase transformation.

In contrast, the annealing temperatures for T3 and T4 were selected based on literature reports (Table 1.1) indicating that annealing at this temperature can enhance the β-phase content even in the absence of stretching. This choice also allows isolating the effect of temperature alone from that of stretching, as this temperature is typically employed during the stretching process.

2.3.5 Stretching

Pressed PVDF, pressed and annealed PVDF, and pressed PVDF/PLA blends were all subjected to uniaxial stretching using a universal testing machine AGS-X from Shimadzu at a stretching ratio (R) of 3 and at temperatures (T) of 60 °C (T60), 80 °C (T80), and 100 °C (T100). For certain samples, stretching was not feasible at specific temperatures due to material limitations. The stretching conditions under which each sample could or could not be stretched are summarized in Table 2.3, with detailed explanations regarding the feasibility of stretching provided in Annex VI.

Table 2.3 Obtained Stretched Samples

	R3T60	**R3T80**	**R3T100**
PVDF	Yes	Yes	Yes
PVDF-T1	Yes	Yes	Yes
PVDF-T2	Yes	Yes	Yes
PVDF-T3	Yes	Yes	Yes
PVDFPLA9505	No	Yes	Yes
PVDFPLA7030	Yes	No	No
PVDFPLA6040	Yes	No	No
PVDFPLAam7030	Yes	Yes	Yes

2.3.6 Electrospinning

Electrospinning was performed using a semi-industrial L-100 electrospinning machine from Bionicia (Figure 2.5), equipped with a multineedle head comprising 20 needles. A rotating collector was employed, not to induce fiber alignment, since the rotation speed was relatively low, but primarily to enable the fabrication of larger membrane areas compared to a stationary planar collector.

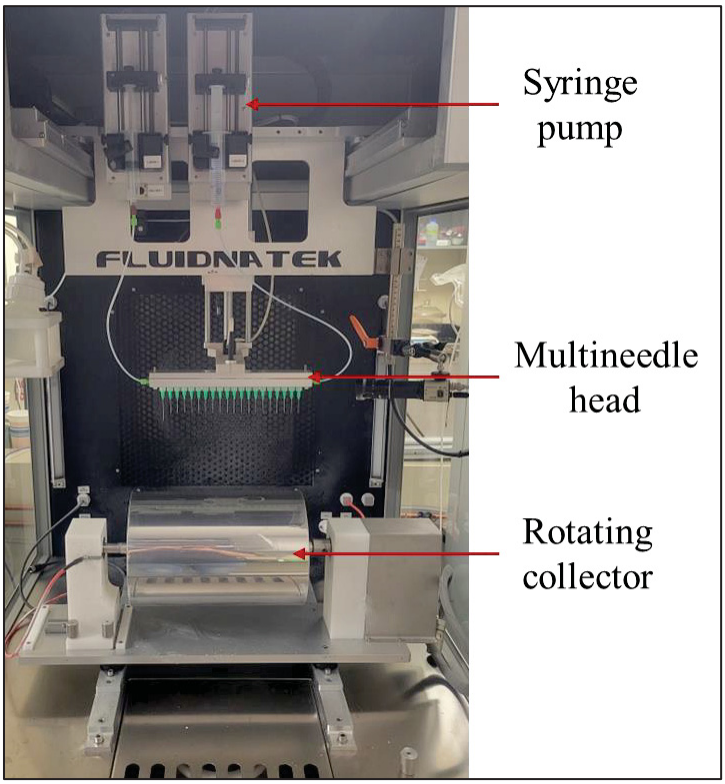

Figure 2.5 Electrospinning machine L-100

The electrospinning parameters used to fabricate the membranes of PVDF and PVDF/PLA blends are summarized in Table 2.4. It is important to note that these parameters were selected to predominantly produce fibrous structures. The objective of this study was not to optimize membrane morphology or investigate the influence of electrospinning conditions,

but rather to assess the effect of the electrospinning process on the β-phase content and the resulting piezoelectric properties of PVDF.

Table 2.4 Electrospinning parameters

Parameter	Value
Electric field (kV/cm)	1.9
Needles potential (kV)	30
Collector potential (kV)	-10
Distance (cm)	21
Flow rate/needle (µL/h)	500
Collector rotating speed (rpm)	200

2.3.7 Poling

DC poling of all stretched samples and electrospun membranes was carried out in dielectric oil to prevent flashover or electrical breakdown. The poling was performed at an electric field of 100 V/µm for 1 h at 23 °C using a high-voltage power supply SL60P300 from Spellman. A gold electrode of 8 mm diameter was deposited on both sides of the samples prior to the poling.

2.4 Characterizations

2.4.1 Morphology

2.4.1.1 Appearance

Scanning Electron Microscopy (SEM) was used to characterize the morphology of both the PVDF/PLA blends and the electrospun membranes. For the blends, 1 mm-thick disks were prepared by compression molding and subsequently fractured in liquid nitrogen. Selective

dissolution of PLA was then carried out using dichloromethane (DCM) to reveal the phase morphology.

Both the fractured surfaces of the blends and the surfaces of the electrospun membranes were sputter-coated with gold using a Cressington sputter coater operated at 60 mA for 60 seconds.

Morphological observations were carried out using a TM3000 scanning electron microscope from Hitachi at an accelerating voltage of 15 kV for the PVDF/PLA films.

2.4.1.2 Crystal Size

The crystal morphology of PVDF samples pressed, annealed or not and stretched at 100 °C, was characterized by Small-Angle X-ray Scattering (SAXS). Samples stretched at lower temperatures could not be properly analyzed due to cavitation-induced air pockets formed during stretching, being the air signal covering completely the crystallite signal due to the higher electronic difference air-PVDF matrix compared to PVDF crystallite-matrix. Electrospun PVDF membranes were also analysed by SAXS.

SAXS measurements were performed using the XEUSS 3.0 HR X-ray scattering setup from Xenocs equipped with a Copper source (wavelenght 1.54 Å), with a sample-to-detector distance of 0.37 m and 0.9 m allowing one to cover a range of scattering vector q from 1×10^{-2} $Å^{-1}$ to 8×10^{-1} $Å^{-1}$, and an exposure time of 300 seconds.

An autocorrelation function was applied to the scattering data to extract the long period (L_p), the crystalline lamella thickness (L_c), and the amorphous domain thickness (L_a).

The analysis to determine these three parameters is performed with the following steps:

- Extrapolation of the scattering curve to q = 0 and q = ∞

For q = 0 Equation 2.1 is used where A and B are constant to determine and q is the scattering vector

$$I(q) = Ae^{Bq^2} \tag{2.1}$$

For q = ∞ Equation 2.2 is used where C and D are constant to determine

$$I(q) = \frac{C}{q^4} + \frac{D}{q^2} \tag{2.2}$$

- Fourier transform of the extrapolated data to obtain the correlation function (Equation 2.3)

$$\Gamma_{1D}(R) = \frac{1}{Q^*} \int_0^\infty I(q) q^2 \cos(qR)\, dq \tag{2.3}$$

Where I is the intensity of the signal, R is the radial distance from the center of mass of the crystal and Q* is the scattering invariant calculated with Equation 2.4

$$Q^* = \int_0^\infty I(q) q^2 dq \tag{2.4}$$

- Graphical determination of L_p and L_c determined with the 1D correlation function (Figure 2.6). L_a is determined by substraction.

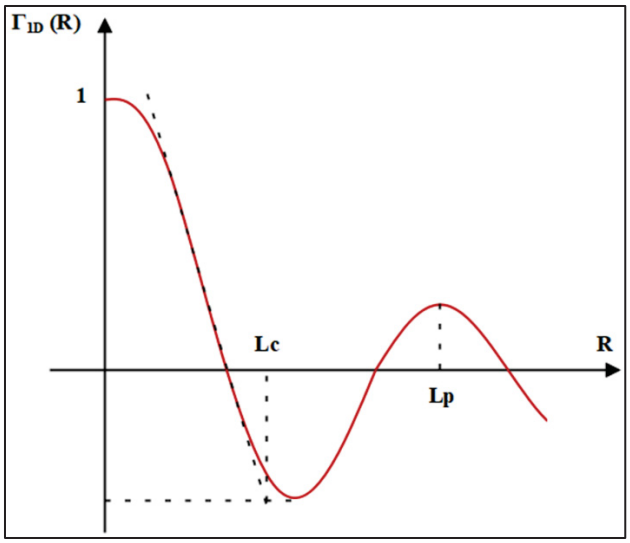

Figure 2.6 Graphical determination of Lp and Lc

2.4.2 Degree of Crystallinity

DSC measurements for all samples were performed using a DSC 8000 from PerkinElmer over a temperature range from 25 °C to 210 °C, with a heating rate of 10 °C/min.

For the PVDF/PLA samples, the melting peaks of PVDF and PLA were deconvoluted when necessary. The degree of crystallinity (X_c) of PVDF and PLA, when applicable, was calculated using Equation 2.5. In this equation, ΔH_m is the measured melting enthalpy of the polymer (PVDF or PLA), and ΔH^0_m is the melting enthalpy of the 100% crystalline polymer, taken as 105 J/g for PVDF (Cheng *et al.*, 2011) and 93 J/g for PLA (Zhang *et al.*, 2018).

$$X_c = \frac{\Delta H_m}{\Delta H_m^0} \tag{2.5}$$

2.4.3 PVDF Polymorphism

WAXS was used as a qualitative tool to confirm the phase composition and was performed using the XEUSS 3.0 HR X-ray scattering setup from Xenocs equipped with a

Copper source (wavelenght 1.54 Å), with a sample-to-detector distance of 54 mm, and an exposure time of 120 seconds.

Quantitative analysis was not performed due to the significant overlap of diffraction peaks, as illustrated in Table 2.5, which makes peak deconvolution unreliable.

Table 2.5 PVDF crystalline phase diffraction angles and planes (Martins, Lopes et Lanceros-Mendez, 2014)

	2θ	**Crystal Plane**
α	17.66	(1 0 0)
	18.30	(0 2 0)
	19.90	(1 1 0)
	26.56	(0 2 1)
β	20.26	(1 1 0) (2 0 0)
γ	18.50	(0 2 0)
	19.20	(0 0 2)
	20.04	(1 1 0)

Fourier Transform Infrared Spectroscopy (FTIR) was used to identify the three main crystalline phases of PVDF: α, β, and γ. Measurements were performed using a Nicolet iS50 FTIR spectrometer from ThermoFisher Scientific in attenuated total reflectance (ATR) mode. The spectra were recorded over the range from 4000 to 500 cm^{-1} with a resolution of 4 cm^{-1}. The absorption bands of each phase are given in Table 2.3.

Table 2.6 FTIR absorption bands of the three main crystalline phases of PVDF(Martins, Lopes et Lanceros-Mendez, 2014)

	α	β	γ
Wavenumber (cm-1)	408	510	431
	532	840	512
	614	1279	776
	766		812
	795		833
	855		840
	976		1234

As shown in Table 2.3, certain absorption bands are shared among multiple crystalline phases of PVDF, while others are specific to a single phase. For instance, the band at 1234 cm^{-1} is characteristic of the γ phase and can therefore be used as an indicator of its presence However, it cannot be reliably quantified, as it can overlaps with neighboring peaks in this spectral region. Moreover, the Beer–Lambert law cannot be applied since the extinction coefficient of this band is not known. The presence of the γ phase can also be confirmed by DSC thermograms, as it melts at a higher temperature (~180 °C) than the α and β phases (160–172 °C). However, this method does not allow for its quantification.

To estimate the electroactive phase fraction, F(EA), Equation 2.6 is used. This equation is based on the absorbance at 763 cm^{-1}, which is attributed exclusively to the α phase, and at 840 cm^{-1}, which corresponds to both the β and γ phases.

$$F(EA) = \frac{X_{\beta+\gamma}}{X_\alpha + X_{\beta+\gamma}} = \frac{A_{\beta+\gamma}}{\frac{K_\alpha}{K_{\beta+\gamma}} A_\alpha + A_{\beta+\gamma}} = \frac{A_{\beta+\gamma}}{1.26A_\alpha + A_{\beta+\gamma}} \quad (2.6)$$

Where X_α is the degree of crystallinity of α and $X_{\beta+\gamma}$ the degree of crystallinity of β+γ, K_α and $K_{\beta+\gamma}$ are 6.1 x 104 and 7.7 x 104 $cm^2.mol^{-1}$ respectively and A_α and $A_{\beta+\gamma}$ are intensities of the α and β bands at 763 cm-1 and 840 cm-1 respectively.

The fractions of the β and γ phases were determined using the peak-to-valley height ratio (P2VHR) method, as proposed by Cai et al. (Cai *et al.*, 2017), by comparing the peaks at 1279 cm^{-1} and 1234 cm^{-1} with their nearest valleys, as described by Equations 2.7 and 2.8, respectively.

$$F(\beta) = F(EA) \times \frac{\Delta h_\beta}{\Delta h_\beta + \Delta h_\gamma} \tag{2.7}$$

$$F(\gamma) = F(EA) \times \frac{\Delta h_\gamma}{\Delta h_\beta + \Delta h_\gamma} \tag{2.8}$$

Here, Δh_β and Δh_γ represent the absorbance differences between the peak around 1279 cm^{-1} and its nearest valley at around 1260 cm^{-1}, and the peak around 1234 cm^{-1} and its nearest valley at around 1225 cm^{-1}, respectively.

The overall β phase content (X_β) and overall γ phase content (X_γ) take into account the degree of crystallinity of the material and are calculated with Equation 2.9 and Equation 2.10, respectively.

$$X_\beta = F(\beta) \times X_C \tag{2.9}$$

$$X_\gamma = F(\gamma) \times X_C \tag{2.10}$$

2.4.4 Piezoelectric Properties

The piezoelectric properties, specifically the d_{33} coefficient, were measured using a d_{33} -meter PM-300 from PiezoTest. Measurements were conducted at room temperature with a dynamic force amplitude of 10 N and a frequency of 110 Hz. The d_{33} coefficient was measured on ten samples prepared under identical processing conditions, and both the mean value and the standard deviation were determined.

For the films, the force-applying head used during measurement was smaller than the deposited electrodes, and therefore no correction was applied to the measured d_{33}.

For the membranes, however, the small force head could not be used because it generated excessive localized stress, damaging the membrane and preventing measurement. Instead, a flat force head with a diameter larger than that of the electrode was employed (1 cm vs. 8 mm). Increasing the electrode diameter was avoided, as it would have raised the risk of dielectric breakdown during poling, which was already challenging.

Consequently, a correction factor was applied to approximate the d_{33} of the membranes. Assuming that the stress is homogeneously distributed over the contact area, which is reasonable given the relatively small mismatch between the force head and electrode diameters, the corrected d_{33} can be estimated using Equation 2.11.

$$d_{33,membrane} = \frac{S_{force\ head}}{S_{electrode}} \times d_{33,measured} \approx 1.56 \times d_{33,measured} \tag{2.11}$$

Where $d_{33,membrane}$ represents the approximated piezoelectric coefficient of the membrane, $S_{forcehead}$ is the contact area of the force-applying head, $S_{electrode}$ is the area of the gold electrode deposited on the membrane, and $d_{33,measured}$ is the value provided directly by the d_{33}-meter.

2.5 Electrostatic Modeling (COMSOL)

Finite element simulations were performed using COMSOL Multiphysics® to investigate the local redistribution of the electric field in PVDF/PLA blends during electrical poling. A two-dimensional electrostatic model was employed, based on a representative volume element (RVE) approach.

The geometry consisted of a square PVDF domain with an area of 1 μm², within which a circular PLA inclusion (equivalent sphere projection) was embedded. The radius of the PLA inclusion was calculated to match the experimental PLA volume fraction of the PVDF/PLA 95/05 (w/w) blend, assuming an equivalent spherical PLA domain. In addition, an elliptical air

region surrounding the PLA inclusion was introduced to represent cavitation voids generated during stretching.

The materials were modeled as linear, homogeneous, and isotropic dielectrics, with relative permittivities of $\varepsilon_r = 10.8$ for PVDF and $\varepsilon_r = 2.7$ for PLA and $\varepsilon_r = 1$ for air.

Electrostatic boundary conditions were applied by imposing a constant electric potential of 100 V on the top edge of the PVDF domain, while the bottom edge was set to ground. The lateral edges were defined as electrically insulating. Simulations were performed under steady-state conditions.

The spatial distribution of the electric field was computed throughout the domain, and average electric field values were extracted separately within the PVDF matrix and within the PLA inclusion. These values were used to quantify the effective electric field experienced by each phase during poling.

2.6 Synthesis and Transition Toward Results

The experimental methodology developed in this work was designed to systematically investigate the influence of processing conditions and material formulation on the piezoelectric properties of PVDF. Three main approaches were considered: annealing, blending with PLA, and eletrospinning.

These approaches were implemented through a combination of controlled processing steps, including melt blending, compression molding, annealing, stretching, electrospinning, and electrical poling. Each processing step was designed to control key structural parameters of PVDF, including crystallinity, phase composition, and lamellar structure, which may influence its piezoelectric properties.

A comprehensive set of characterization techniques was employed to establish clear structure–property relationships. Morphological analyses (SEM, SAXS), thermal characterization (DSC), phase identification (WAXS, FTIR), and direct piezoelectric measurements (d_{33}) were combined to provide a multi-scale understanding of the material behavior.

This integrated experimental framework enables the evaluation of how composition and processing parameters contribute to the development of electroactive phases and ultimately affect the piezoelectric performance of PVDF-based systems. The results obtained from this methodology are presented and discussed in the following chapter.

CHAPTER 3

PIEZOELECTRIC PROPERTIES OF ANNEALED PVDF

3.1 Results and Discussion

3.1.1 Effect of Annealing on the Crystal Size

SAXS curves of all pressed, annealed (annealing protocols T1, T2, T3, T4) and stretched samples at 100°C (R3T100) are presented in Figure 3.1. For the stretched samples, the data were integrated on the axis perpendicular to the stretching direction (Figure 3.1b) and perpendicular to the stretching direction (Figure 3.1c).

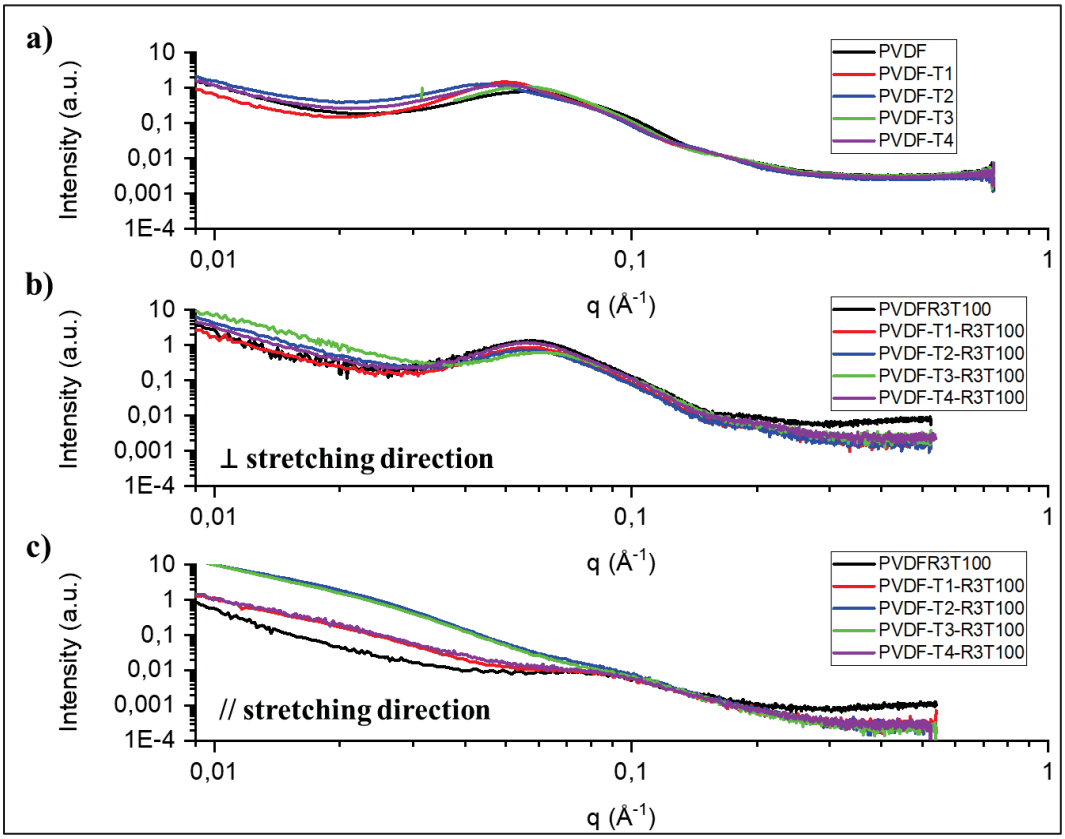

Figure 3.1 SAXS measurement of pressed (a), stretched samples in the direction perpendicular to stretching (b) and in the direction parallel to stretching (c)

According to Figure 3.1a, annealing of the just pressed samples results in an increase in the long period, as evidenced by the shift of the main SAXS peaks toward smaller q values (Table 3.1). This suggests that the thickness of the crystalline lamellae, the amorphous layers, or both have increased. Another small peak appears around q = 0.2 $Å^{-1}$, suggesting the presence of a second population of crystals with a smaller long period.

Upon stretching (Figure 3.1b), the non-annealed PVDF sample exhibits a shift of the main long-period peak toward lower q values (Table 3.1), indicating an increase in the long period after deformation. Considering that the pure PVDF was quenched between two cold metallic plates, it is plausible that very small crystallites were initially intercalated between larger ones. Stretching could induce the melting of these smaller crystallites, thereby increasing the long period observed in the stretched sample. Conversely, in the annealed samples, such small crystallites likely disappeared during the annealing process. Consequently, these samples display a shift of the long-period peak toward higher q values (Table 3.1), indicating a reduction in the long period. This behavior is consistent with crystallite fragmentation and compression of the amorphous layers in the direction perpendicular to the deformation axis, as a result of molecular chain alignment.

As shown in Figure 3.1c, the main long-period peak nearly disappears in all samples. When still observable, it shifts toward smaller q values (around 0.02 $Å^{-1}$), indicating an increase in the long period along the stretching direction. Similarly, the secondary peak previously observed around q = 0.2 $Å^{-1}$ also shifts to approximately 0.1 $Å^{-1}$, confirming an increase in the corresponding long period upon deformation.

The parameters L_p, L_c and L_a extracted from the main long period peak in SAXS data (Figure 3.1a and 3.1b) and are given in Table 3.1.

Table 3.1 Determination of q in $Å^{-1}$ from the SAXS spectrum and calculation of Lp, Lc and La in Å.

	Pressed				R3T100			
	q[a]	**Lp[b]**	**Lc[b]**	**La[b]**	**q[a]**	**Lp[b]**	**Lc[b]**	**La[b]**
Non-annealed	0.057	88	38	50	0.056	94	38	56
Solid-state annealing 140°C (T1)	0.051	103	41	62	0.057	94	39	55
Melt-annealing 140°C (T2)	0.044	112	47	65	0.058	97	42	55
Solid-state annealing 100°C (T3)	0.056	94	40	54	0.058	91	39	52
Melt-annealing 140°C (T4)	0.050	103	44	59	0.057	94	40	54

[a]Determined graphically as the abscissa corresponding to the maximum intensity of the SAXS spectrum.

[b]Determined using the autocorrelation function described in Section 2.4.1.2 from the data in Figure 3.1b.

The annealing treatments T1 and T3 led to a slight (5-8%) increase in crystalline domain size, whereas the melt treatments T2 and T4 resulted in a more significant (16-24%) increase. These results can be interpreted in terms of chain mobility. Indeed, in T1 and T3 the samples were cooled down to room temperature after melting and then heated to the annealing temperature whereas, in T2 and T4 the samples were cooled down directly to the annealing temperature after melting. It can be supposed that the sample chain mobility at the beginning of annealing is higher in T2 and T4 compared to T1 and T3. Consequently, the crystal growth, and especially that of bigger crystals, should be enhanced in T2 and T4 thus leading to a more significant increase of the average crystal size. The increase is particularly pronounced for T2, as the crystallization temperature is closer to the temperature of maximum crystallization rate, favoring the formation of larger crystals. This is in good agreement with the literature, which

also reports that crystallization from the melt typically results in larger crystalline domains compared to those formed through cold crystallization (Yin *et al.*, 2022).

Upon stretching, a reduction in crystal size, consistent with a mechanical fragmentation of the crystalline lamellae, was observed for all samples except the not-annealed one. Furthermore, all stretched samples exhibited comparable crystal sizes, except for sample T2, which retained a crystalline lamella approximately 10% larger than that of the untreated stretched sample. This observation supports the hypothesis that stretching initially larger crystals results in proportionally larger crystalline fragments, whereas smaller initial crystals yield smaller fragments.

The effects of annealing and stretching on L_p, L_c and L_a are summarized in the scheme presented in Figure 3.2.

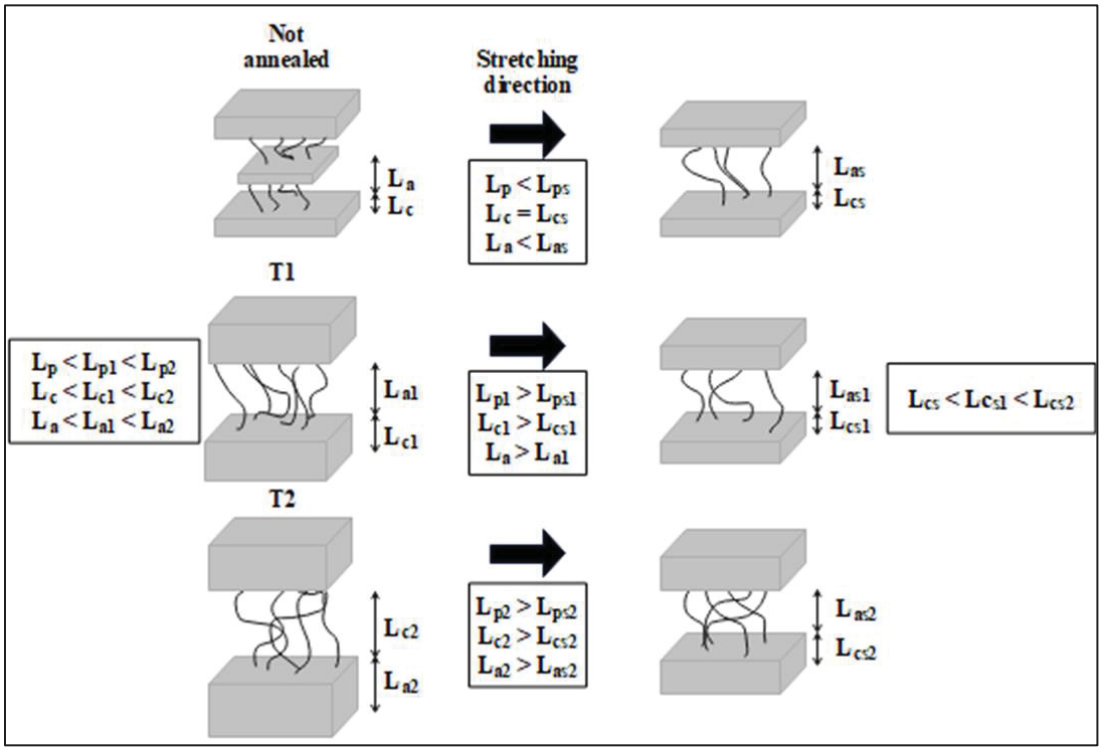

Figure 3.2 Effect of annealing and stretching on Lp, Lc and La

3.1.2 Effect of annealing on the Degree of Crystallinity

The first heating ramp of the DSC thermograms for untreated PVDF and annealed samples, both in pressed and stretched conditions, are presented in Figure 3.3.

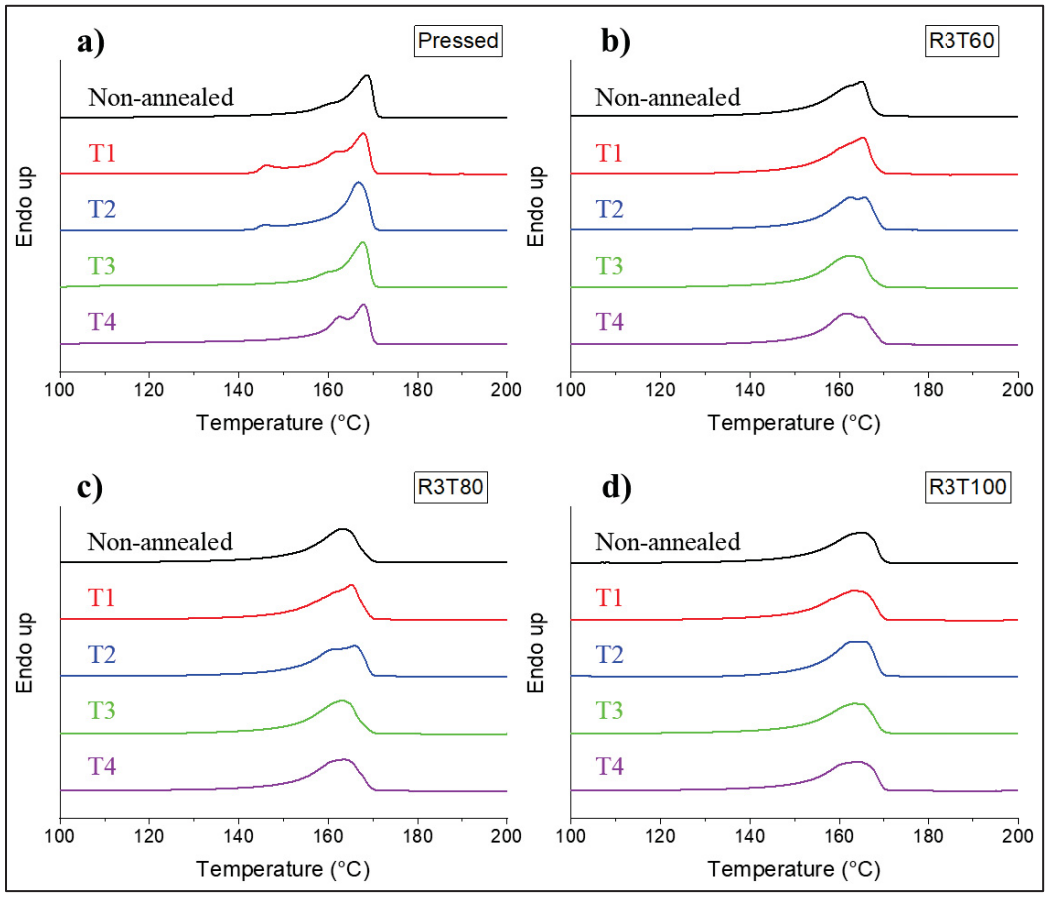

Figure 3.3 First heating ramp of pressed and stretched PVDF (non-annealed, black), PVDF annealed T1 (red), PVDF annealed T2 (blue), PVDF annealed T3 (green) and PVDF annealed T4 (purple). The stretching is carried out at ratio R=3 at different temperatures, i.e. 60°C (T60), 80°C (T80), 100°C (T100)

The degree of crystallinity for each sample was determined from the corresponding DSC thermograms and is reported in Table 3.2.

Table 3.2 Degree of crystallinity (%) of untreated and treated PVDF both pressed and stretched

	PVDF	PVDF-T1	PVDF-T2	PVDF-T3	PVDF-T4
Pressed	41	45	45	45	45
R3T60	41	43	44	42	40
R3T80	43	43	44	43	43
R3T100	43	43	41	43	43

Annealing induced an increase of around 10 % in the degree of crystallinity of the pressed samples independently of the annealing temperature (140°C or 100°C) or the cooling down to room temperature before annealing.

Stretching the non-annealed samples induces a modest increase in crystallinity (≈5%) at the highest stretching temperatures (80 °C and 100 °C). In contrast, stretching the annealed samples reduces the crystallinity gain initially provided by annealing, with the effect becoming more pronounced at higher stretching temperatures. From 80 °C onward, the additional crystallinity induced by annealing is completely erased. It should be emphasized, however, that although the total crystallinity of annealed and non-annealed samples becomes comparable after stretching, differences remain in terms of average crystal size, as shown in Figure 3.1. Specifically, annealed samples exhibit slightly larger crystals (2.5–15% increase), with the most pronounced effect observed for annealing treatments T2 and T4.

3.1.3 Effect of Annealing on Polymorphism

The WAXS results of PVDF pressed, pressed and annealed (T1 and T2) both before and after stretching at 100°C are shown in Figure 3.4. For all the pressed samples, the dominant crystalline phase appears to be the α phase, as indicated by the presence of three characteristic diffraction peaks located at approximately 18.5°, 20.1°, and 26.9°. Upon stretching, the diffraction peak at 20.1° shifts toward 20.9°, which is characteristic of the β phase. Additionally, the relative intensity of the peak at 26.9° decreases compared to the other peaks. These changes suggest that stretching promotes the transformation from the α phase to the β phase.

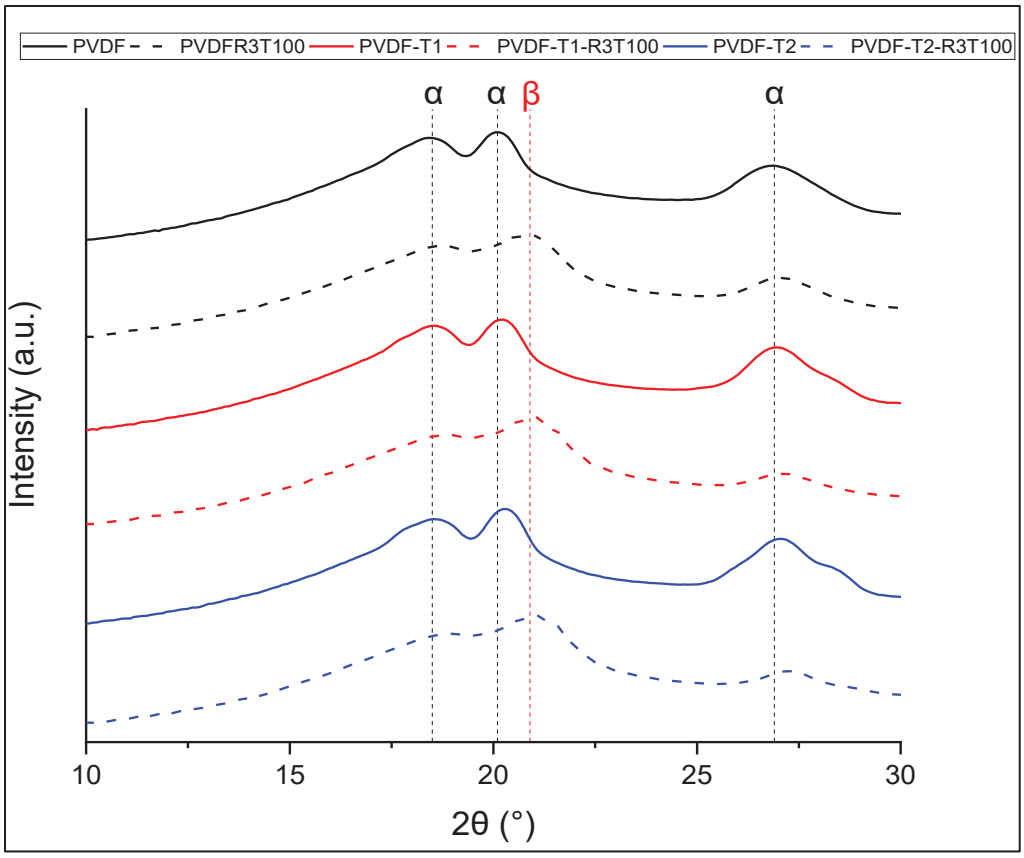

Figure 3.4 WAXS spectra of pressed (continuous line) and stretched (dashed line) PVDF (not annealed, black), PVDF annealed T1 (red) and PVDF annealed T2 (blue). The stretching is carried out at ratio R=3 at 100°C.

Figure 3.5 presents the FTIR spectra of pressed and stretched PVDF samples, both untreated and annealed T1 and T2.

The annealing applied to the pressed PVDF (Figure 3.5a) does not appear to induce any significant changes in its crystalline phase composition, as revealed by the FTIR spectra of the pressed samples. It can be concluded that when PVDF is stretched at 100 °C, the α-to-β phase transformation is induced solely by the mechanical stretching and not by the temperature at which the process is carried out.

Upon uniaxial stretching, regardless of the stretching temperature, a noticeable increase in the β phase is observed. This is evidenced by an increased absorbance of the CF_2 stretching band at 840 cm^{-1}, associated with the β and γ phases, as well as a decrease in the

CF_2 wagging band at 763 cm^{-1}, characteristic of the α phase. Those observations confirm the previous XRD results.

Although the bands at 840 cm^{-1} and 763 cm^{-1} were previously discussed in relation to phase transformation induced by stretching, Figure 3.4 also provides insight into the effect of stretching temperature. In particular, the relative intensity of the 840 cm^{-1} band (β and γ phases) with respect to the 763 cm^{-1} band (α phase) decreases as the stretching temperature increases, suggesting a reduced formation of electroactive phases at higher temperatures. This trend is consistent with findings reported in the literature (Gregorio et Ueno, 1999 ; Sencadas *et al.*, 2006 ; Gomes *et al.*, 2010).

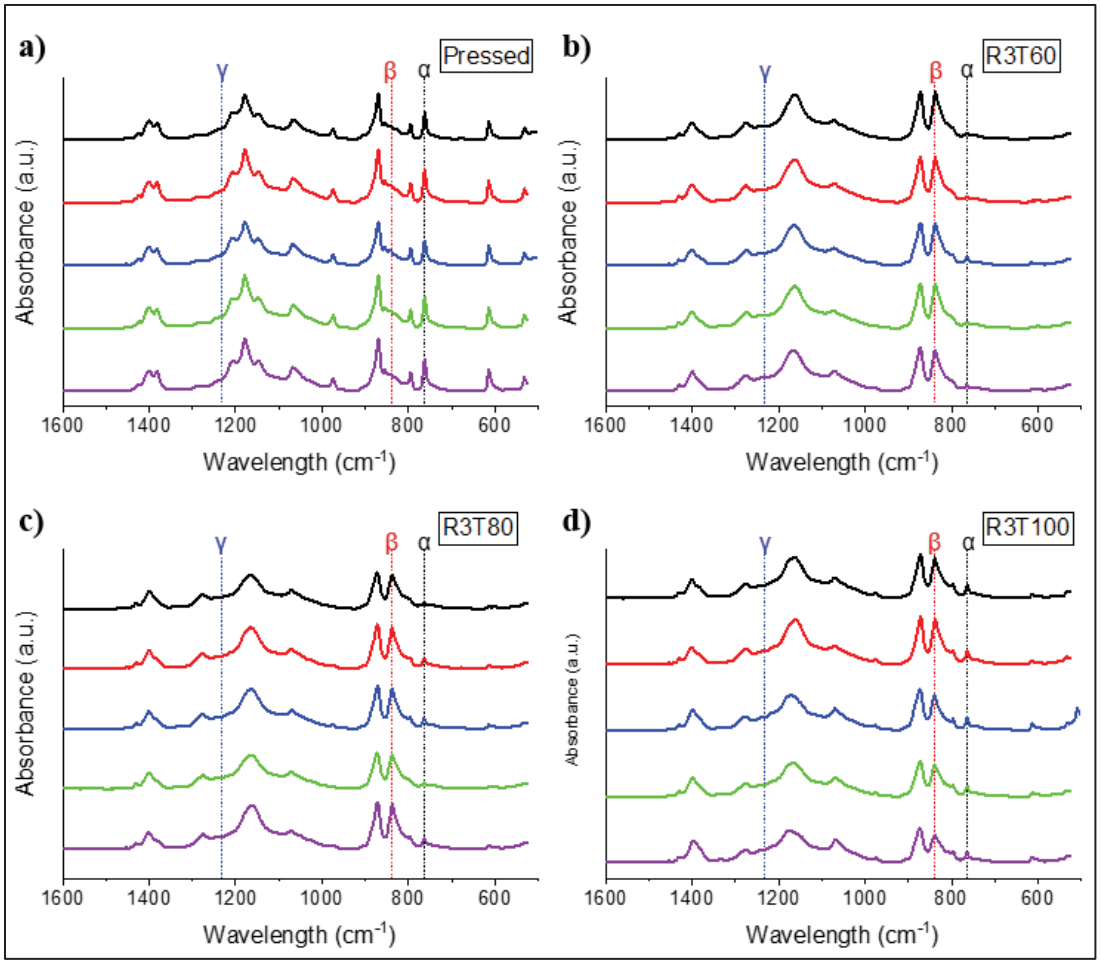

Figure 3.5 FTIR Spectra of pressed and stretched PVDF (non-annealed, black), PVDF annealed T1 (red), PVDF annealed T2 (blue), PVDF annealed T3 (green) and PVDF

annealed T4 (purple). The stretching is carried out at ratio R=3 at different temperatures, i.e. 60°C (T60), 80°C (T80), 100°C (T100)

Moreover, on Figure 3.5, no distinct absorption band attributable to the CF_2 wagging mode of the γ-phase is detected at 1234 cm^{-1}. The potential presence of the γ-phase can also be examined through Differential Scanning Calorimetry (DSC) analysis.

The thermograms in Figure 3.3 support the FTIR findings by confirming the absence of the γ phase, as no distinct endothermic peak is observed around its typical melting temperature, at 180°C. As a result, the β phase fraction F(β) can be directly determined from Equation 2.3, with F(β) = F(EA). The calculated values of the β phase fraction in the crystalline phase, along with the absolute content of β phase in the entire material (crystalline + amorphous phase), accounting for the degree of crystallinity determined in Section 3.1.2, are reported in Table 3.3.

Table 3.3 β phase fraction and overall β phase content (X_β) in the samples

	F(β) (%)			
	Pressed	**R3T60**	**R3T80**	**R3T100**
Untreated	30	86	82	71
T1	27	86	76	73
T2	32	81	76	69
T3	30	86	82	71
T4	30	85	77	69
	X_β (%)			
	Pressed	**R3T60**	**R3T80**	**R3T100**
Untreated	12	35	35	31
T1	12	37	33	31
T2	14	36	33	30
T3	14	36	35	31
T4	14	34	33	30

According to Table 3.3, none of the thermal treatments had a significant impact on PVDF polymorphism. The results obtained for sample T3 contradict existing literature, which generally reports that annealing at 100 °C promotes an increase in β-phase content. This could be due to the difference in the present initial phase before annealing. Indeed, in this study the initial phase is α while in the literature it was mostly β or γ. The increase in the β phase fraction in the literature might come either from an increase in the β crystal size or from a γ to β transformation more than from an α-to-β transformation, that would require overpassing a larger energy barrier.

In contrast, the results for sample T1 are consistent with the literature, as annealing at elevated temperatures such as 140 °C tends to favor the formation of the thermodynamically stable α-phase

Additionally, the annealing T2 and T4 were not expected to alter the crystalline phase composition of PVDF, given that under standard pressure and cooling conditions, PVDF predominantly crystallizes into the α-phase from the melt (Matsushige et Takemura, 1978 ; Yang et Chen, 1987 ; Oka et Koizumi, 1985).

Upon stretching, all samples demonstrated comparable β-phase fractions under identical stretching conditions, suggesting that annealing did not yield any measurable enhancement in the formation of the piezoelectric β-phase. Therefore, the initial hypothesis that annealing and increasing crystal size would facilitate a higher β-phase fraction was not validated in this study.

3.1.4 Effect of Thermal Treatment on the Piezoelectric Properties

Figure 3.6 presents the results of the d_{33} measurements for both annealed and untreated PVDF samples, correlated with the total β-phase content in the material. The data are shown for each set of applied stretching parameters.

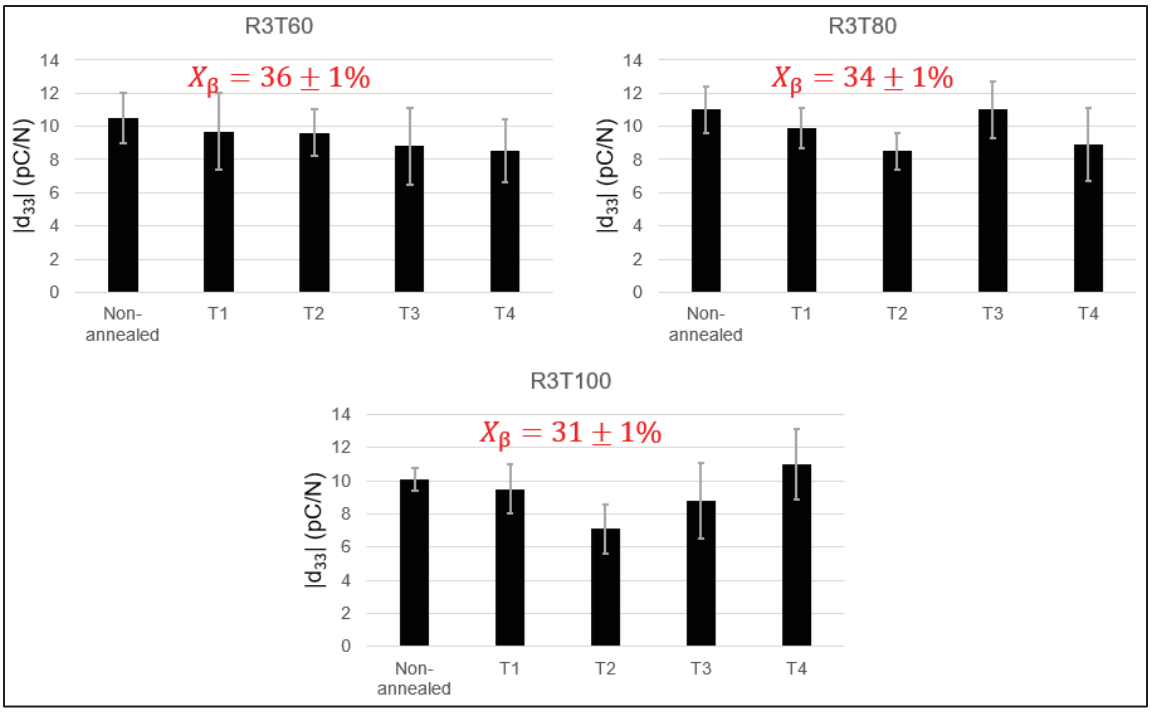

Figure 3.6 Overall β phase fraction (X_β) and d_{33} of stretched PVDF non-annealed and annealed after DC poling at 100 V/µm for 1h at 23 °C. The stretching was carried out at ratio R=3 at different temperatures, i.e. 60°C (T60), 80°C (T80), 100°C (T100)

It appears that none of the thermal treatments had a significant effect on either the β-phase content or the piezoelectric properties of the material, except for the T2 annealing. In this case, a notable decrease in piezoelectric performance was observed for the samples stretched at 80 °C and 100 °C, despite their β-phase fraction being nearly identical to that of the untreated samples.

To determine whether this decrease in the d_{33} coefficient was related to kinetic effects, d_{33} was measured as a function of the applied electric field for both untreated PVDF and PVDF-T2-R3T80 samples. In each case, the electric field was applied for 1 hour. Afterwards, the samples were short-circuited to eliminate any residual surface charges prior to d_{33} measurement. The results are presented in Figure 3.6.

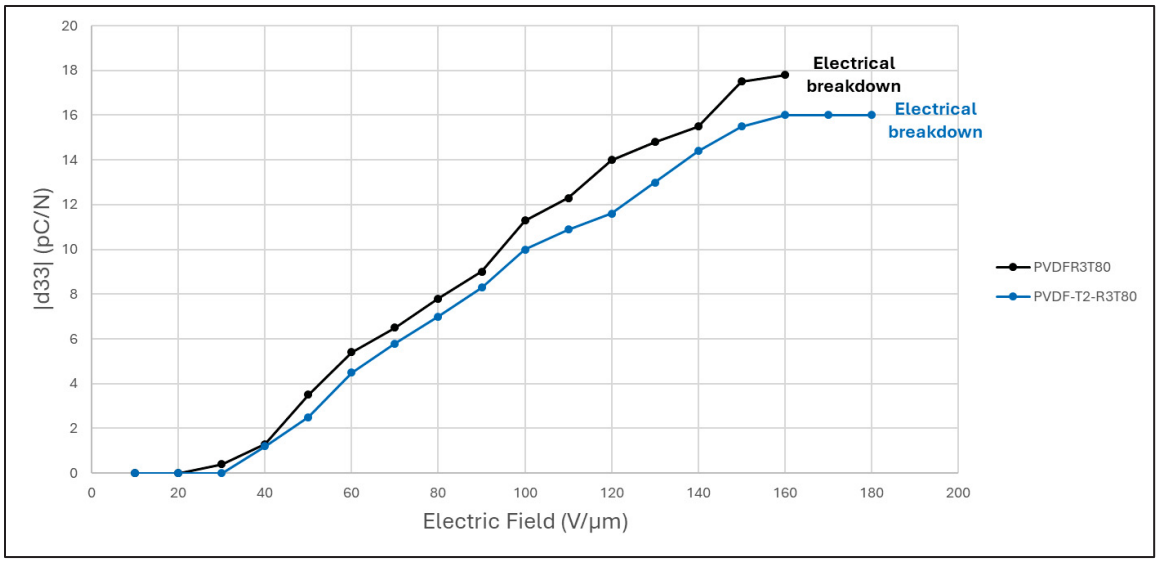

Figure 3.7 Evolution of d_{33} with poling field

Figure 3.6 shows that although the untreated PVDF sample experiences electrical breakdown at a higher field than the treated one, the T2 sample reaches saturation and its d_{33} value consistently remains below that of the untreated PVDF. This indicates that the reduced piezoelectric response in PVDF-T2 is not due to kinetic limitations during poling but rather stems from intrinsic material properties. Comparison of the WAXS patterns of the non-annealed sample and PVDF-T2 after stretching reveals that the polymer chains are more oriented along the stretching direction in the non-annealed film (Figure 3.8).

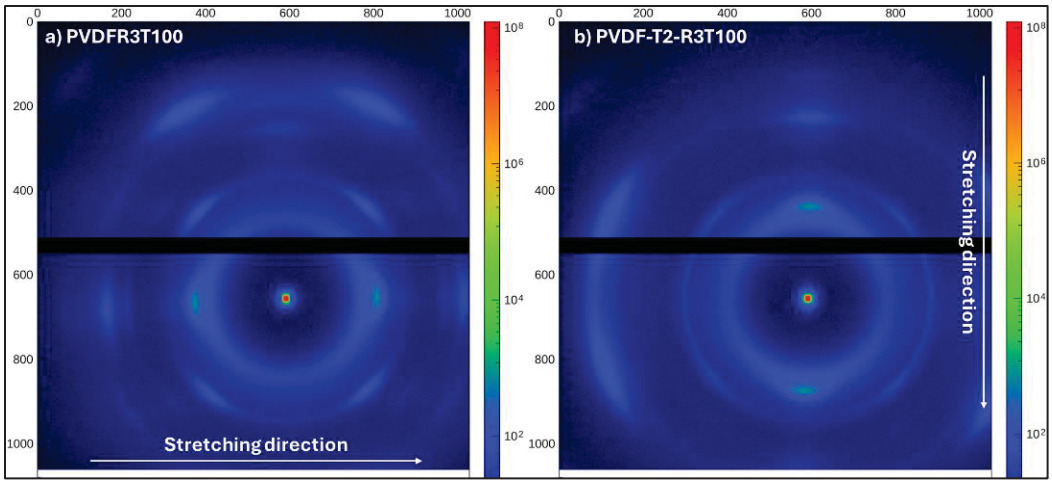

Figure 3.8 WAXS diffraction pattern of the a) non-annealed film and b) annealed T2 both stretched at stretching ratio (R) of 3 and temperature (T) of 100C

This lower of orientation must be responsible for the decrease in the piezoelectric properties. Indeed, even if the chains rotated upon poling to align with the field, if they are not perfectly aligned in the stretching direction, the vertical component of their dipole moment (p) is reduced compared to the more aligned chains, resulting in poorer polarization in the poling direction (Figure 3.9).

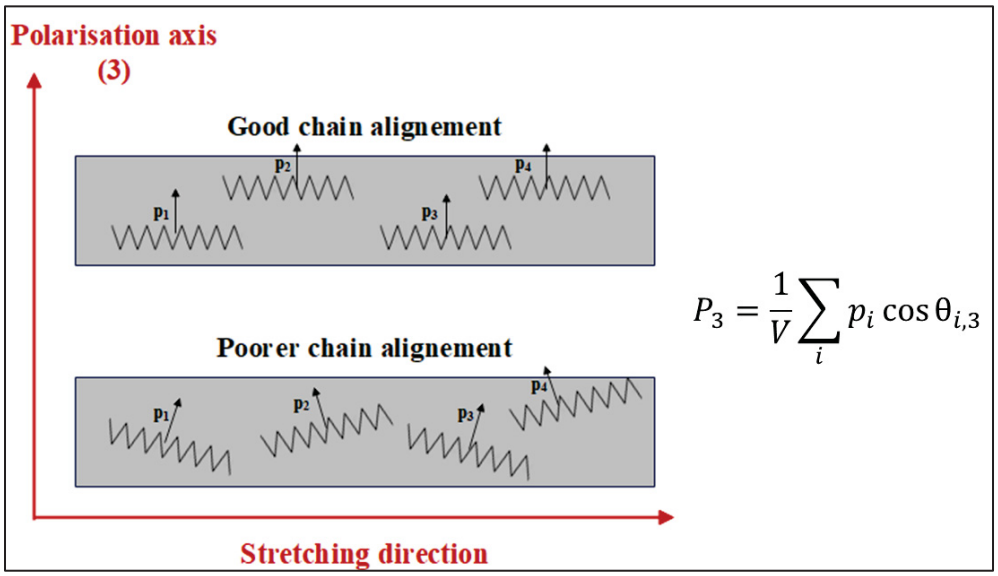

Figure 3.9 Polarization of a PVDF film in direction 3 with perfect chain alignment and poorer chain alignment. θ is the angle between the dipole moment and the polarization axis.

Moreover, at the applied poling field, which is below the saturation field, the reduced piezoelectric performance observed for the sample crystallized at 140 °C can also be attributed to the increased average crystallite size (Table 3.1). Larger crystals are generally more difficult to pole, resulting in lower polarization efficiency. This diminished ability to align dipoles in larger crystallites has been previously reported in the literature (Zhao et al., 2021; Han et al., 2012). (Zhao *et al.*, 2021 ; Han *et al.*, 2012).

Therefore, this study highlights that optimizing the piezoelectric properties of PVDF requires not only maximizing the β-phase content but also ensuring proper chain alignment prior to poling and controlling crystallite size to facilitate efficient dipole orientation during poling.

3.2 Conclusion

Annealing of PVDF obtained from the melt was carried out at two different temperatures. The first temperature (100 °C) was selected based on literature reports indicating an enhancement of the β-phase content in PVDF, either through an increase in β-phase fraction or in overall crystallinity. The second temperature was chosen close to the crystallization peak of PVDF to promote crystal growth. The rationale was that increasing the long period, particularly the thickness of the amorphous layers, would facilitate the α-to-β phase transformation by enabling greater stretchability of the amorphous regions and more efficient stress transfer to the crystalline domains, thus enhancing the transformation. Moreover, annealing was conducted both from the melt and from the solid state to assess the effect of chain mobility on the changes in PVDF crystal size, degree of crystallinity and polymorphism before and after stretching.

All annealing procedures led to an increase in the long period due to growth in both crystalline and amorphous lamellae. Melt annealing produced a more pronounced increase in crystal size owing to higher chain mobility, with the treatment at 140 °C having the greatest effect. Upon stretching the annealed samples, crystal fragmentation consistently occurred, and the crystals that were larger before stretching remained larger afterward.

A slight increase in the PVDF degree of crystallinity (~10%) was also observed. However, after stretching, this increase was lost, and both annealed and non-annealed samples exhibited nearly the same crystallinity.

The non-annealed and annealed samples exhibited comparable β-phase fractions before and after stretching when subjected to the same conditions.

Although the β-phase content was similar in all samples stretched under identical conditions, the piezoelectric properties (d_{33}) of the melt-annealed sample at 140 °C, after stretching and poling, were significantly lower. This decrease in d_{33} was attributed to both the larger crystal size, which hindered efficient poling, and the poorer chain orientation prior to poling.

This chapter demonstrates that the piezoelectric properties of PVDF depend not only on the β-phase content but also on maintaining small crystallite sizes to facilitate efficient poling and achieving good chain alignment during stretching, prior to poling, in order to maximize piezoelectric performance.

CHAPTER 4

PIEZOELECTRIC PROPERTIES OF PVDF/PLA BLENDS

4.1 Results and Discussion

4.1.1 Choice of PLA: Crystalline or Amorphous

The first step was to investigate whether crystalline or amorphous PLA better promotes the α-to-β phase transformation in PVDF, both in the pressed and stretched blend states. Figure 4.1 presents the FTIR spectra of PVDF blended with 30 wt.% crystalline and amorphous PLA, respectively, before and after uniaxial stretching.

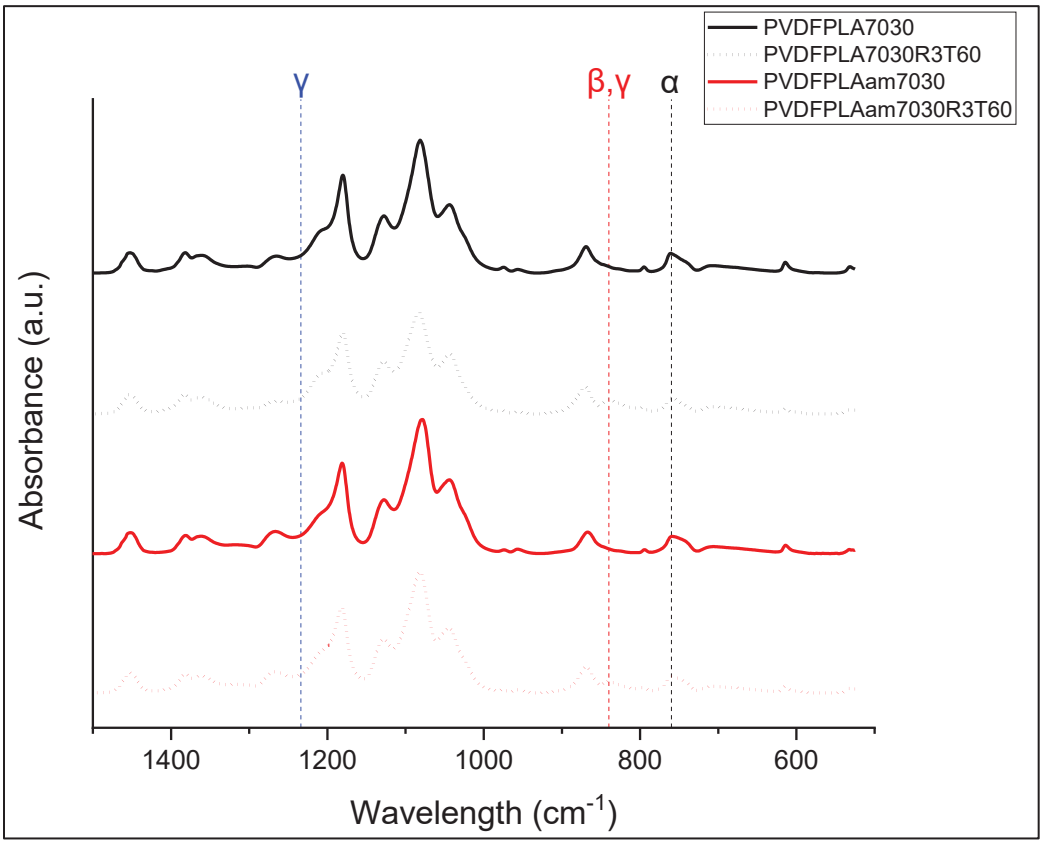

Figure 4.1 FTIR spectra of PVDFPLA7030 and PVDFPLAam7030 before (continuous line) and after (dashed line) stretching

Figure 4.1 shows that the FTIR spectra of the pressed PVDF/PLA blend samples exhibit no absorption bands around 840 cm^{-1} or 1234 cm^{-1}, indicating the absence of both β and γ crystalline phases. This confirms that the pressed samples are composed entirely of the non-polar α phase.

Upon stretching, a distinct CF_2 stretching band emerges at 840 cm^{-1}, characteristic of the electroactive β phase, while no detectable band appears at 1234 cm^{-1}, associated with the γ phase. These results suggest that stretching induces a partial α-to-β phase transformation in the blends, with no formation of γ phase. The calculated β phase fractions for each blend are presented in Table 4.1.

Table 4.1 β phase fraction (%) of the PVDFPLA7030 and PVDFPLAam7030 before and after stretching calculated with te FTIR results

	Pressed	**R3T60**
PVDFPLA7030	0	43
PVDFPLAam7030	0	36

Crystalline PLA was found to be more effective than amorphous PLA in promoting the α-to-β phase transformation.

It is well established that PLA crystallizes very slowly. As shown in Figure 4.2, pristine PLA cooled at 10 °C min^{-1} during DSC analysis does not exhibit crystallization. However, when PLA is blended with PVDF, the earlier crystallization of PVDF, due to its higher crystallization temperature, acts as a nucleating agent for PLA, enabling crystallization under the same cooling conditions. This indicates that in the PVDF/PLA 70/30 blend, the PLA phase is already partially crystalline after the pressing step, prior to stretching. The degree of crystallinity of PLA in the PVDFPLA7030 sample was determined to be 12 %.

Consequently, crystalline PLA was chosen for all subsequent experiments presented in this chapter.

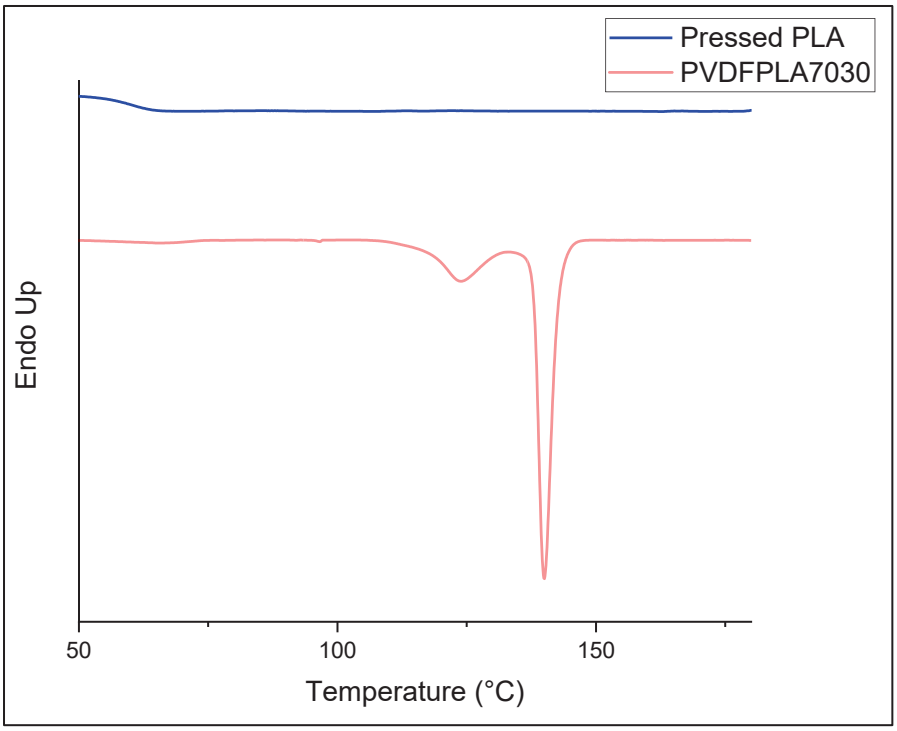

Figure 4.2 Crystallization DSC curve of pure PLA and PVDFPLA7030 obtained at a cooling rate of 10°C/min

Consequently, the PLA phase in PVDFPLA7030 exhibits a higher Young's modulus than in PVDFPLAam7030, where PLA remains amorphous. Due to its greater stiffness, crystalline PLA deforms less during stretching, transferring more of the applied strain to the PVDF phase and thereby enhancing the efficiency of the α-to-β phase transformation.

4.1.2 Blends Morphologies

PVDF/PLA blends were obtained at composition ratios of 95/05 w/w and 60/40 w/w and exhibited beaded and co-continuous morphologies, respectively. The corresponding microstructures of these blends are shown in Figure 4.3.

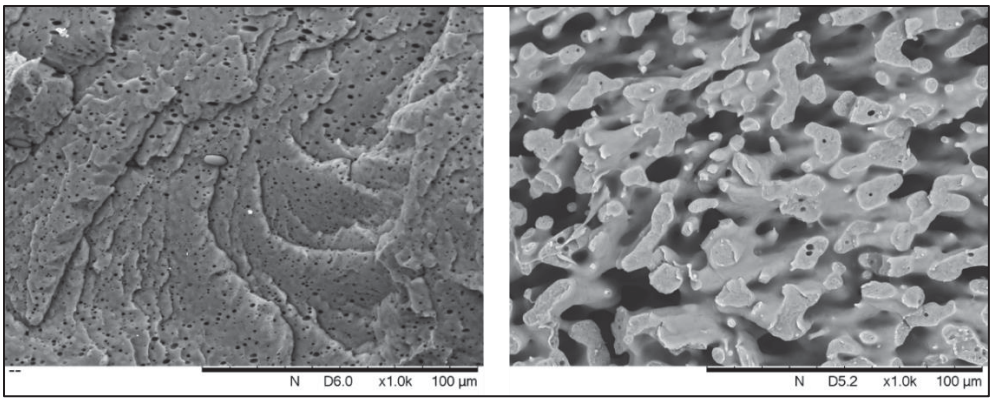

Figure 4.3 SEM micrographs of the fractured surface of PVDFPLA9505 (left) and PVDFPLA6040 (right) after the pressing step and dissolution of the PLA phase in DCM

4.1.3 PVDF/PLA Interaction in Beaded and Co-continuous Blends

To investigate potential interactions between PVDF and PLA, the FTIR spectra of the blends were compared with that of pressed PLA, focusing on the region around the PLA carbonyl (C=O) stretching band (Figure 4.4).

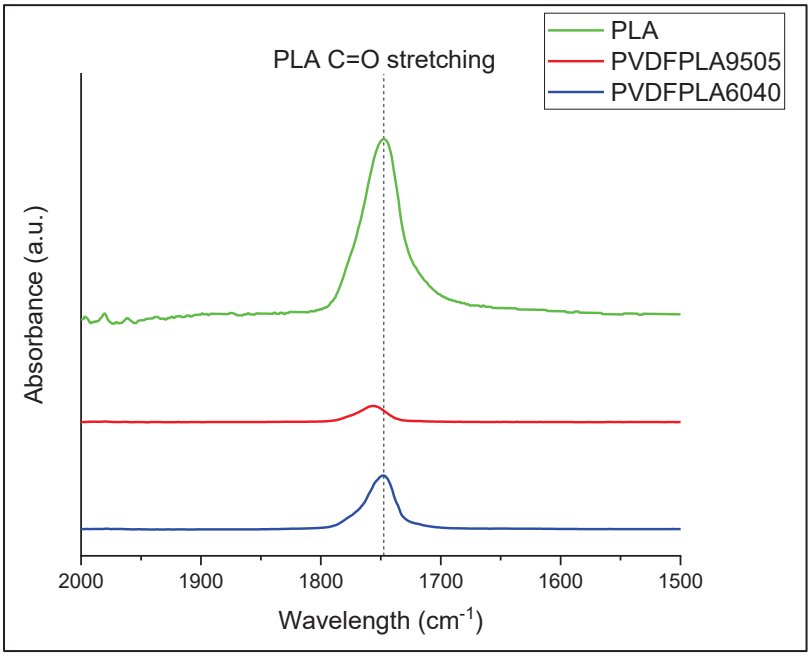

Figure 4.4 FTIR spectra of PLA, PVDFPLA9505 and PVDFPLA6040 in the C=O stretching band region

The C=O stretching band of pristine pressed PLA appears at 1748 cm^{-1}. In the PVDFPLA9505 blend, this band is significantly shifted, indicating an interaction between PVDF and PLA. This interaction is likely electrostatic in nature, involving the polar C=O groups of PLA and the C-H bonds of PVDF. In contrast, the shift is much less pronounced in the PVDFPLA6040 co-continuous blend. However, this does not necessarily imply the absence of interaction. As shown in the micrographs, the beaded morphology in the 95/05 blend results in a much higher interfacial area between PLA and PVDF due to the small PLA domains dispersed in the PVDF matrix. Conversely, the coarser morphology of the 60/40 blend leads to more PLA volume isolated from PVDF, reducing the apparent shift in the FTIR spectrum. This observation was corroborated by measuring the surface-to-volume ratio of the PLA phase using ImageJ for both morphologies (Annex VII). In the beaded morphology, the surface-to-volume ratio of PLA was 7 μm^{-1}, whereas it was 0.2 μm^{-1} for the cocontinuous morphology.

Section 4.1.5 investigates whether this interaction is sufficient to alter the PVDF chain conformation at the interfaces and promote the formation of the β phase.

4.1.4 Influence of Blend Composition and Morphology on the Crystallization of PVDF and PLA

The DSC thermographs of the first heating ramps of pressed and stretched samples are given in Figure 4.5.

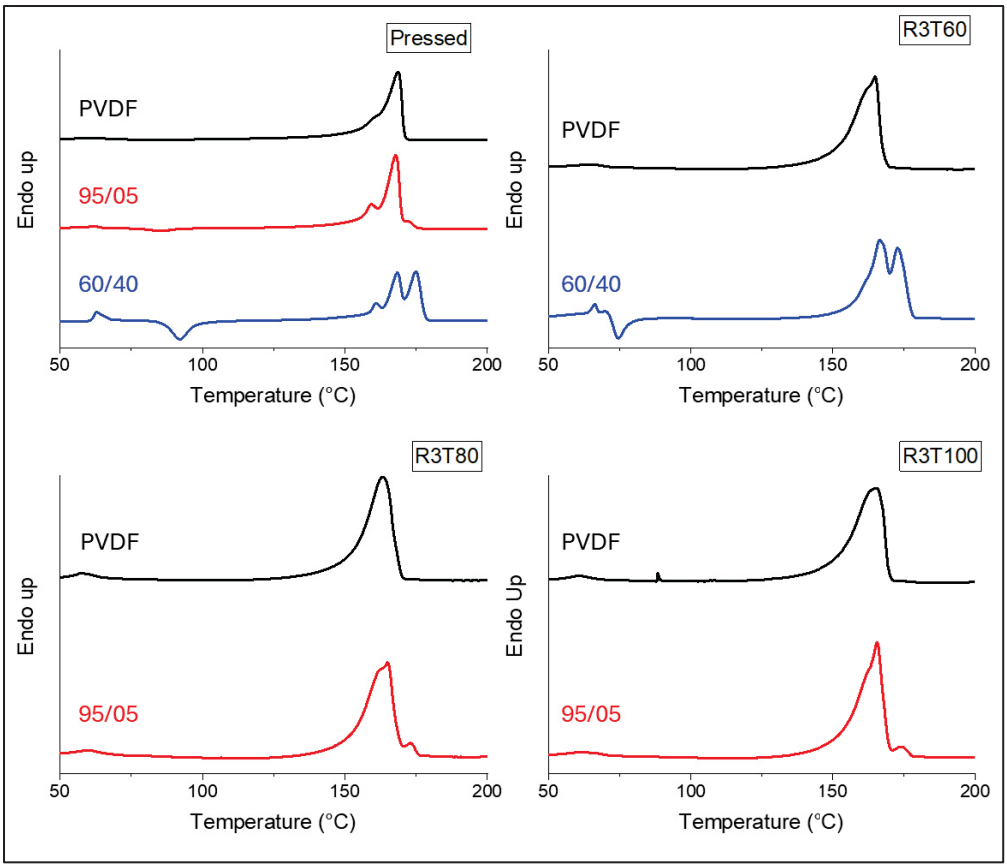

Figure 4.5 DSC thermographs of the first heating ramps of PVDF (black), PVDFPLA9505 (red) and PVDFPLA6040 (blue) before and after stretching at stretching ratio of R = 3 and 60°C (T60), 80°C (T80) and 100°C (T100)

Upon the addition of PLA, a new melting peak appears at approximately 173 °C, confirming the presence of the PLA. In the DSC thermograms of the pressed blends, a cold crystallization peak is observed between 85 °C and 92 °C, indicating that PLA did not reach its maximum possible crystallinity after pressing. This cold crystallization peak is also present in the stretched PVDFPLA6040 blend stretched near the Tg of PLA, whereas it appears to be absent in the PVDF/PLA9505 blend stretched at a temperature closer to the PLA crystallization temperature, determined to be approximately 125 °C (Figure 4.2).

The degrees of crystallinity for both PVDF and PLA, calculated from the thermograms, are reported in Table 4.2.

Table 4.2 Degree of crystallinity (%) of pure PVDF and PVDFPLA blends before and after stretching

	Pressed	R3T60	R3T80	R3T100
	PVDF			
PVDF	41	41	43	43
PVDFPLA9505	43		41	44
PVDFPLA6040	42	43		
	PLA			
PVDFPLA9505	15		33	33
PVDFPLA6040	14	27		

The incorporation of PLA did not influence the crystallization behavior of PVDF in either the pressed or stretched samples. Conversely, as discussed in Section 4.1.1, PVDF crystals act as nucleation sites for PLA, promoting its crystallization. When stretching is performed at temperatures near or above the glass transition temperature of PLA, a significant increase in PLA crystallinity is observed, which is consistent with the expected behavior of semicrystalline polymers under such conditions.

4.1.5 Effect of Blend Composition and Morphology on the PVDF Polymorphism before and after Stretching

Figure 4.6 shows the WAXS patterns of all pressed and stretched samples. For the pressed samples (Figure 4.6 a), the addition of 5% or 40% PLA does not appear to induce any phase transition in PVDF, as only the α phase is detected, with characteristic peaks at 17.6°, 18.5°, 20.1°, and 26.9°. In the case of PVDFPLA6040, an additional peak at 16.6° indicates the presence of crystalline PLA. This peak is absent in the PVDFPLA9505 sample; however, this does not necessarily imply that PLA is amorphous, but rather that its low concentration may have prevented its detection.

Upon stretching PVDF and PVDFPLA9505 (Figures 4.6c and 4.6d), the characteristic β-phase reflection at 20.9° emerges, accompanied by a reduction in the intensity of the α-phase

peaks, indicating an α-to-β phase transformation. In addition, the crystalline peak of PLA becomes visible, suggesting that stretching may promote PLA crystallization. By contrast, in PVDFPLA6040 (Figure 4.6b), this transformation appears to be significantly less efficient or even suppressed.

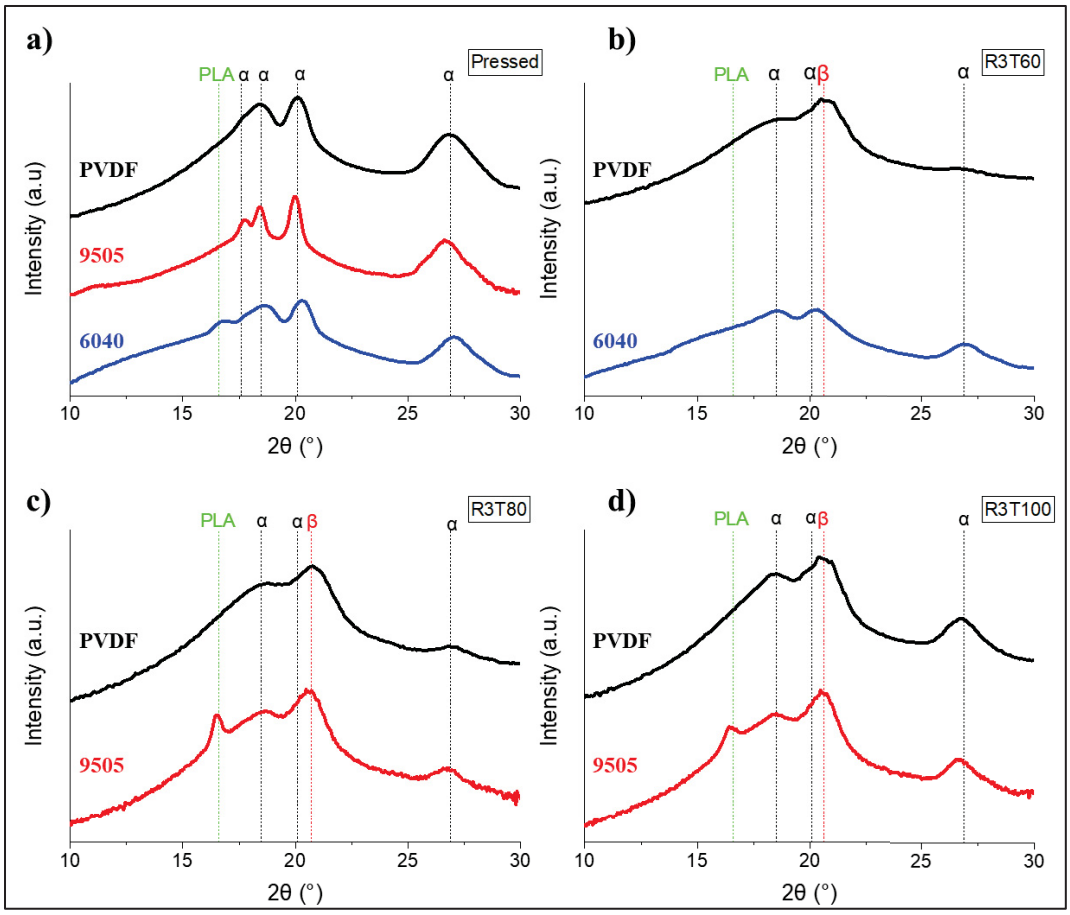

Figure 4.6 WAXS spectra of PVDF (black), PVDFPLA9505 (red) and PVDFPLA6040 (blue) before and after stretching at a stretching ratio of R = 3 and 60°C (T60), 80°C (T80) and 100°C (T100)

As the WAXS results remain qualitative, Figure 4.7 presents the FTIR spectra of neat PVDF and PVDF/PLA blends, both in the pressed and stretched states to confirm quantitatively the previous observations. The addition of 5% PLA to PVDF does not significantly affect the intensity ratio between the band at 840 cm^{-1} (assigned to the electroactive β phase) and the band at 763 cm^{-1} (assigned to the α phase). In contrast,

incorporation of 40% PLA results in a noticeable reduction of this ratio, indicating a suppression of β-phase formation. Upon stretching, this ratio increases in all cases, confirming the occurrence of the α-to-β phase transformation. However, under identical stretching conditions, the presence of 5% PLA does not appear to alter the electroactive phase content compared to neat PVDF, whereas 40% PLA significantly decreases the efficiency of the α-to-β transformation. In addition, no γ phase is detected in the samples, as evidenced by the absence of the characteristic FTIR band near 1234 cm^{-1}. This observation is further supported by DSC analysis (Figure 4.5), where no endothermic peak is observed around 180 °C, the melting temperature of the γ phase.

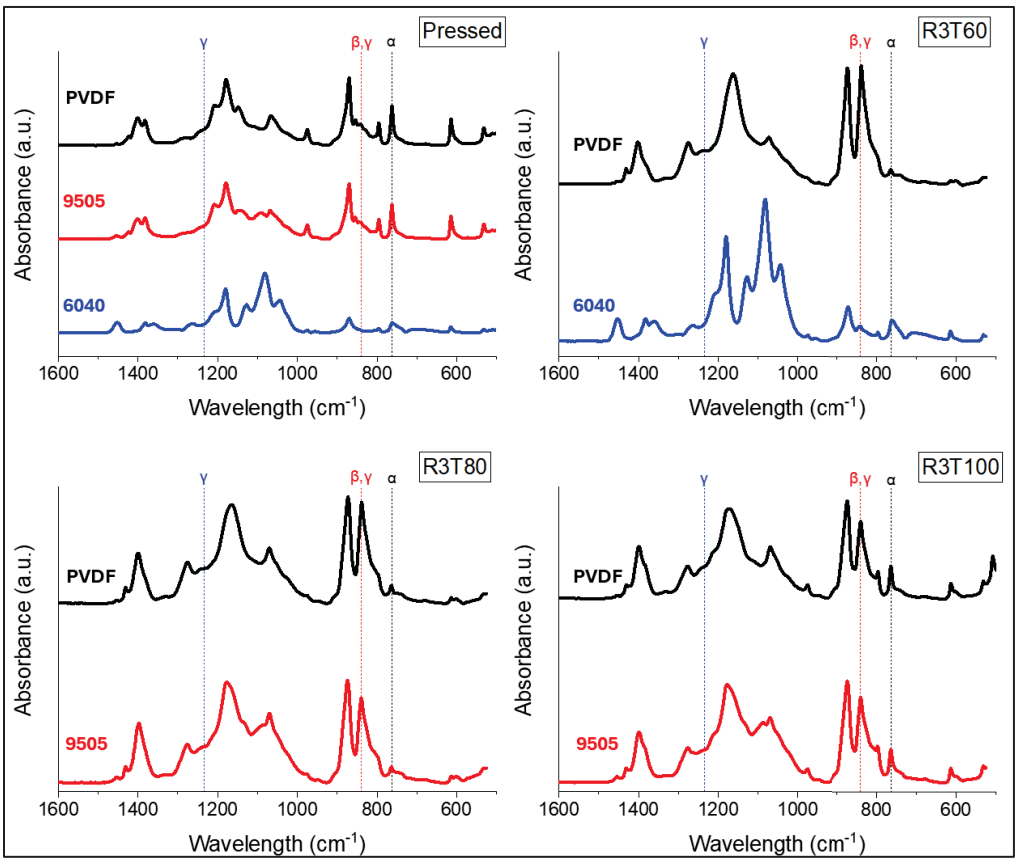

Figure 4.7 FTIR spectra of PVDF (black), PVDFPLA9505 (red) and PVDFPLA6040 (blue) before and after stretching at a stretching ratio of R = 3 and 60°C (T60), 80°C (T80) and 100°C (T100)

To validate these qualitative observations, the β-phase fraction was quantified from the FTIR spectra using Equation 2.3, since no γ phase was detected in the samples. The calculated values are summarized in Table 4.3. In addition, the overall β-phase content in the PVDF was determined by combining the FTIR-derived β fraction with the degree of crystallinity obtained from DSC analysis.

Table 4.3 β phase fraction and overall PVDF β phase content in the pressed and stretched samples

	F(β) (%)			
	Pressed	**R3T60**	**R3T80**	**R3T100**
PVDF	30	86	82	71
PVDFPLA9505	28	x	81	72
PVDFPLA6040	0	36	x	x
	Total amount of β phase in PVDF (%)			
	Pressed	**R3T60**	**R3T80**	**R3T100**
PVDF	12	35	35	31
PVDFPLA9505	12	x	33	32
PVDFPLA6040	0	15	x	x

The incorporation of PLA into the pressed samples appears to reduce the β-phase content as the PLA fraction increases. Similar trends have been reported in the literature for melt-processed blends, where either only the α-phase was observed regardless of PLA addition (Xie *et al.*, 2013), or the β-phase content decreased with increasing PLA concentration (de Oliveira *et al.*, 2023). These results suggest that the interaction between PVDF and PLA is insufficient to induce a conformational change in PVDF during melt processing.

Upon stretching, given the beaded morphology and the dispersion of crystallized PLA domains within the softer amorphous PVDF matrix, it was anticipated that the amorphous PVDF phase would accommodate most of the applied deformation. This deformation was expected to transmit higher stress to the PVDF crystals, thereby facilitating a more efficient α-to-β phase transformation (Figure 4.8).

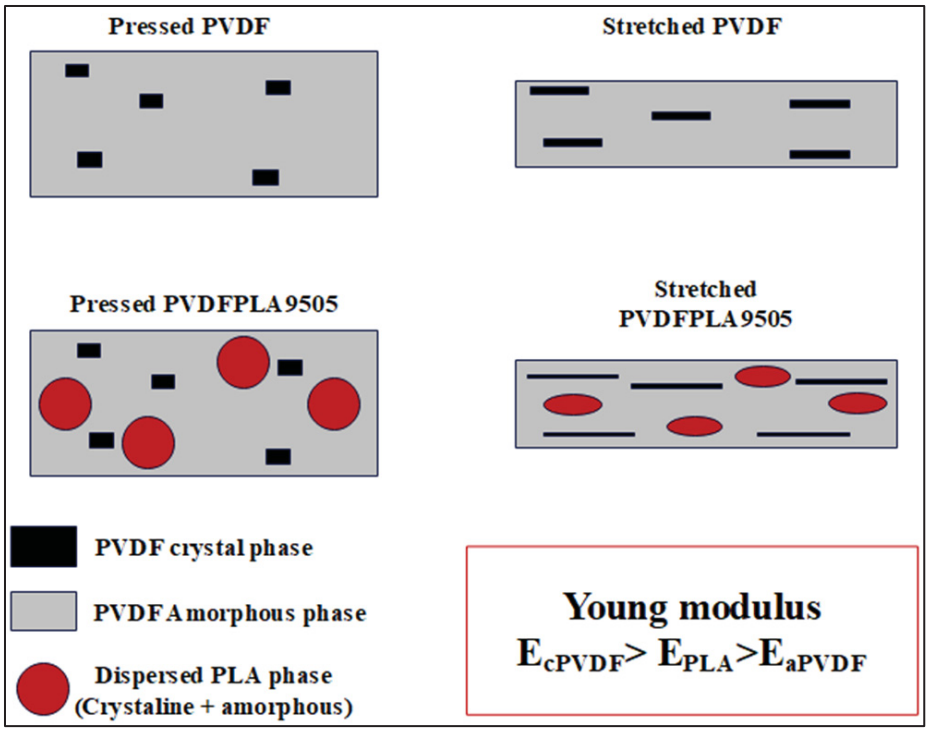

Figure 4.8 PVDF phase transformation upon stretching with and without dispersed PLA

However, none of these expectations were confirmed. This is likely due to cavitation at the interfaces between the two polymers, as evidenced by the morphology of PVDFPLA9505 after stretching (Figure 4.9).

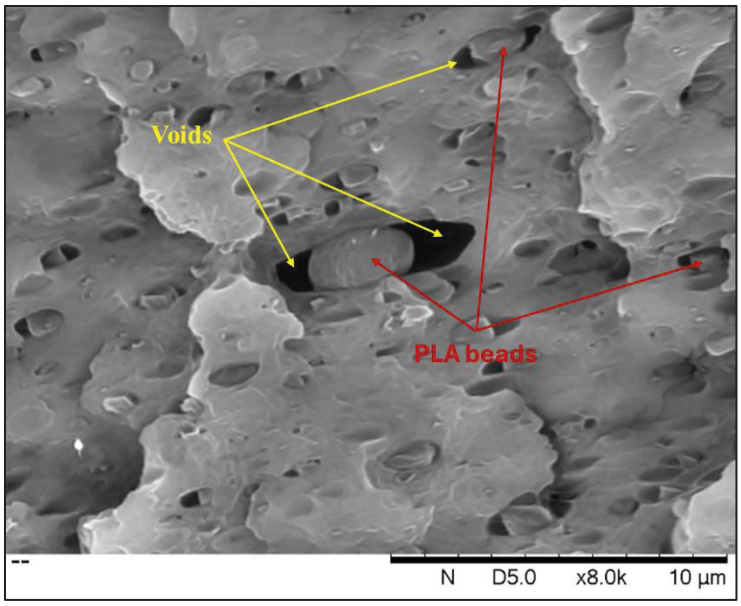

Figure 4.9 Morphology of stretched PVDFPLA9505R3T80

As a result, in the beaded sample, with PVDF as the matrix, the PVDF phase experiences stresses similar to those in neat PVDF during stretching. This observation contrasts with the reports in the literature, where the α-to-β phase transformation was enhanced by the addition of PLA upon stretching (Xie *et al.*, 2013 ; Mishra *et al.*, 2021). In these studies, the stretching rate was significantly lower than in the present work, which may have minimized cavitation and allowed a better deformation of the PVDF phase. Nevertheless, even in those cases, the increase in β-phase fraction compared to neat PVDF was relatively modest, typically ranging from 2.5 % to 7 % when reported.

In the co-continuous blend, both phases experience the same deformation, but the applied stress is distributed between them. Consequently, the stress acting on the PVDF phase is lower than in pure PVDF, resulting in a less efficient α-to-β phase transformation.

4.1.6 Resulting Piezoelectric Properties

Figures 4.10a and 4.10b present the overall β-phase content and d33, respectively, for the stretched and poled PVDF and PVDF/PLA blends.

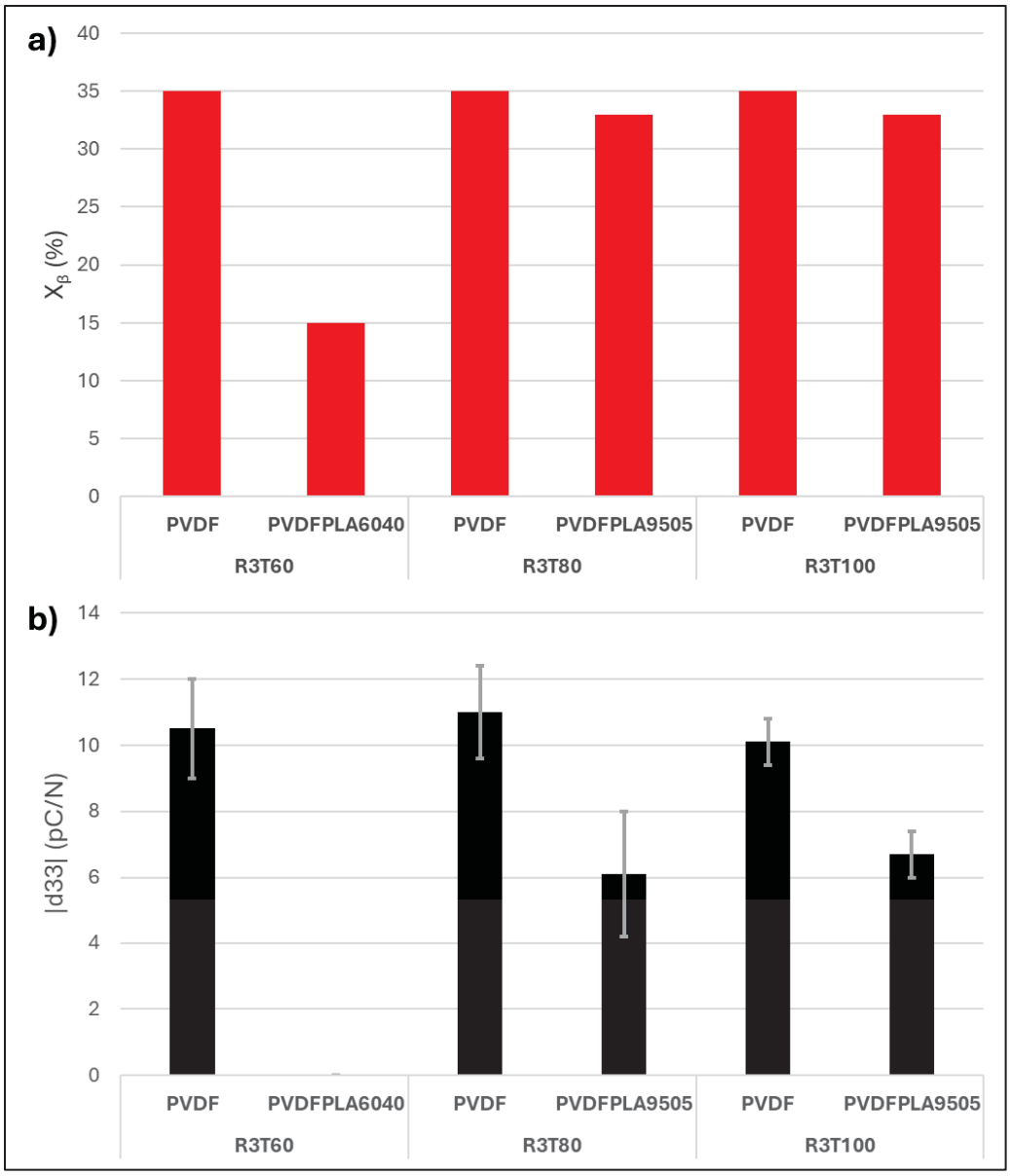

Figure 4.10 (a) Overall β phase content (X_β) and (b) d33 of PVDF and PVDF/PLA stretched at a stretching ratio (R) of 3 and temperature of 60°C (T60), 80°C (T80) and 100°C (T100) and poled at 100 V/µm for 1h at room temperature

As the PVDFPLA6040 sample was composed of mainly α phase even after stretching, its resulting d_{33} was 0 pC/N.

Figure 4.10 shows that although neat PVDF and the PVDFPLA9505 blend exhibit similar β-phase content under identical stretching conditions, the d_{33} value is significantly reduced in the presence of PLA. This decrease cannot be explained solely by the reduced PVDF

content (95 %), as the reduction is disproportionately large. A more plausible explanation lies in the dielectric mismatch between the two polymers: the relative permittivity of PVDF and PLA are 10.8 and 2.7, respectively, for the grades used in this study. Due to this contrast, during the poling step the electric field is preferentially concentrated within the PLA domains, thereby reducing the effective field experienced by the surrounding PVDF matrix.

To substantiate this hypothesis, a simplified COMSOL simulation was carried out (Section 2.5). As demonstrated by SEM picture on Figure 4.8, cavitation at the PVDF/PLA interfaces occurred under stretching, since no compatibilizer was used and crystalline PLA undergoes limited deformation.

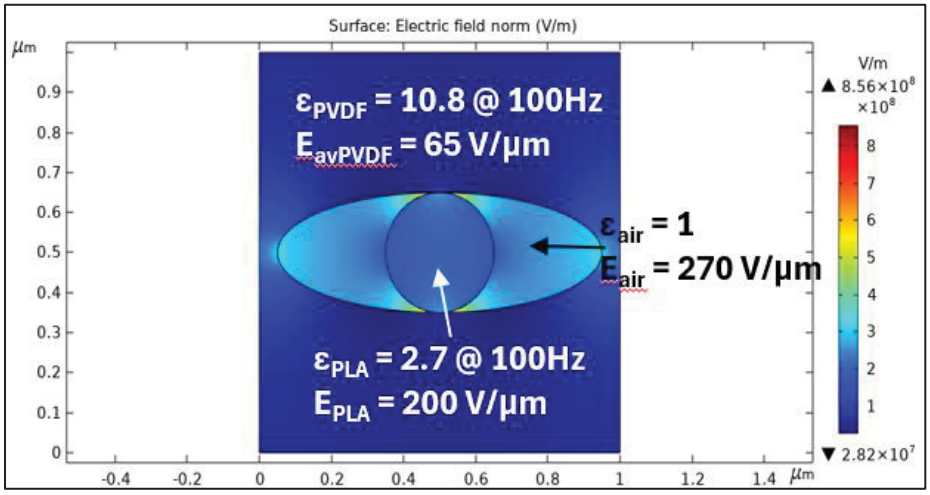

Figure 4.11 COMSOL simulation of the distribution of the electric field in the different material phases

Figure 4.11 demonstrates that the incorporation of PLA and interfacial voids, both having significantly lower permittivity than PVDF, leads to a reduction of approximately 35% in the effective electric field within the PVDF phase. To estimate the expected piezoelectric response under such reduced field conditions, the evolution of d_{33} was measured for a neat PVDF film with the same β-phase content as the PVDFPLA9505 blend, as a function of the applied electric field (Figure 4.12). From this dataset, the corresponding d_{33} value at an effective poling field of 65 V/μm was determined for comparison.

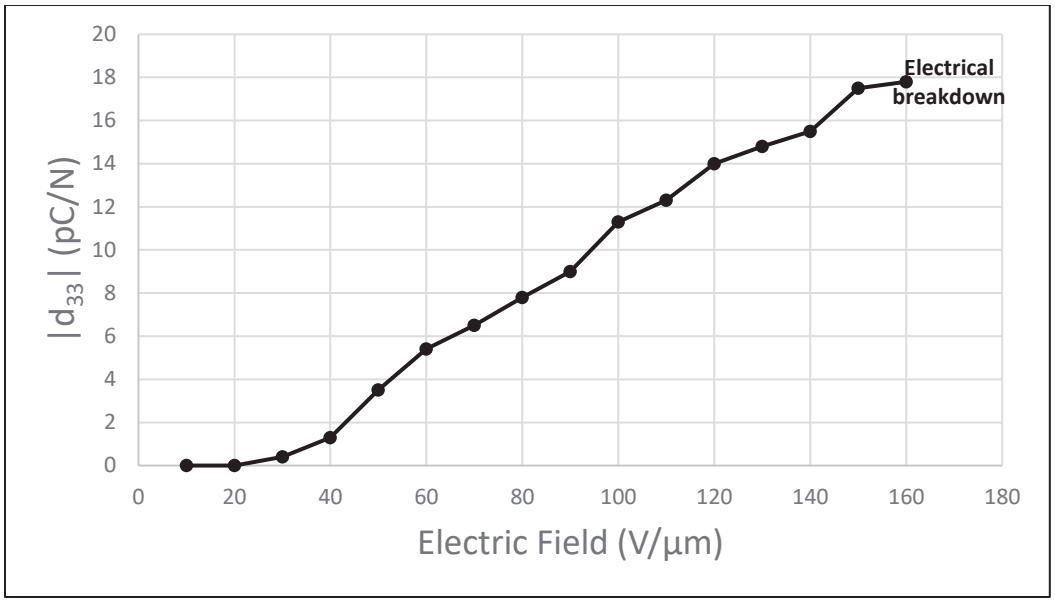

Figure 4.12 Evolution of the d33 as a function of the applied electric field in a PVDF films stretched at a stretching ratio R = 3 and a temperature of 80°C

By applying a linear regression between the data points at 60 V/µm and 70 V/µm, the d_{33} value expected at 65 V/µm was estimated to be approximately 6 pC/N. This matches the experimentally measured d_{33} for the PVDFPLA9505 blend, confirming that the reduction in piezoelectric performance originates from the decrease in effective electric field experienced by the PVDF during poling.

This result further highlights that a high β-phase content alone is not sufficient to ensure optimal piezoelectric properties; the dielectric environment and field distribution within the material during poling play equally critical roles.

4.2 Conclusion

PLA incorporation into PVDF has been reported to enhance the β-phase content of PVDF through electrostatic interactions between the C=O groups of PLA and the C–H bonds of PVDF at the polymer–polymer interfaces. In addition, previous studies indicate that PLA can facilitate the α-to-β phase transformation during stretching due to the mismatch in

mechanical properties, which locally increases the stress within the PVDF phase and at the PVDF/PLA interfaces.

In this study, PVDF was melt-blended with 5% and 40% PLA to obtain beaded and co-continuous morphologies, respectively. The degree of crystallinity, β-phase content, and piezoelectric coefficient (d_{33}) were characterized for pure PVDF and for the corresponding blends, both after film pressing and after stretching (and poling for piezoelectric measurements). The degree of crystallinity of PVDF remained unchanged upon PLA incorporation, both before and after stretching, and was approximately 42%.

At 5% PLA content, the β-phase fraction was nearly identical to that of pure PVDF, whereas at 40% PLA, the β-phase fraction decreased from 30% to 0%. These results indicate that in melt-processed PVDF/PLA blends, electrostatic interactions between the two polymers are insufficient to alter the PVDF chain conformation or enhance the β-phase content. Furthermore, excessive PLA content promotes PVDF crystallization exclusively in the α-phase form.

Upon stretching the PVDF/PLA 5% blend, the β-phase fraction, which might have been expected to increase, remained similar to that of pure PVDF. This lack of enhancement was attributed to cavitation at the PVDF/PLA interfaces. In the co-continuous PVDF/PLA 60/40 blend, the β-phase fraction was significantly lower than in pure PVDF stretched under the same conditions (36% vs. 86%). This reduction is explained by the distribution of stress between the PVDF and PLA phases, which lowers the stress experienced by PVDF and leads to a less efficient α-to-β phase transformation.

After poling, the PVDF/PLA 95/05 blend exhibited piezoelectric properties (d_{33}) that were 34–45% lower than those of pure PVDF stretched under the same conditions. This reduction was attributed to the concentration of the electric field in the PLA and in the voids created by cavitation, which decreased the effective electric field experienced by the PVDF phase during poling.

This chapter demonstrates that achieving good piezoelectric properties depends not only on the β-phase fraction but also on the distribution of the electric field during poling. When blending PVDF with another polymer, it is recommended that the added polymer have

a higher permittivity than PVDF at the poling temperature, so that the electric field is concentrated in the PVDF phase, thereby enhancing the piezoelectric response.

CHAPTER 5
PIEZOELECTRIC PROPERTIES OF ELECTROSPUN PVDF AND PVDF/PLA BLENDS

5.1 Results and Discussion

5.1.1 Membrane Morphology

SEM micrographs of the electrospun membranes are presented in Figure 5.1. All membranes exhibit comparable morphologies, consisting of fibers interspersed with beads and polymer agglomerates. Although the overall fiber quality is not optimal, the primary objective of electrospinning in this study was to get some fibers and achieve a high β-phase content and subsequently compare the piezoelectric properties with those of films. The fiber diameters range from approximately 10 nm to 110 nm.

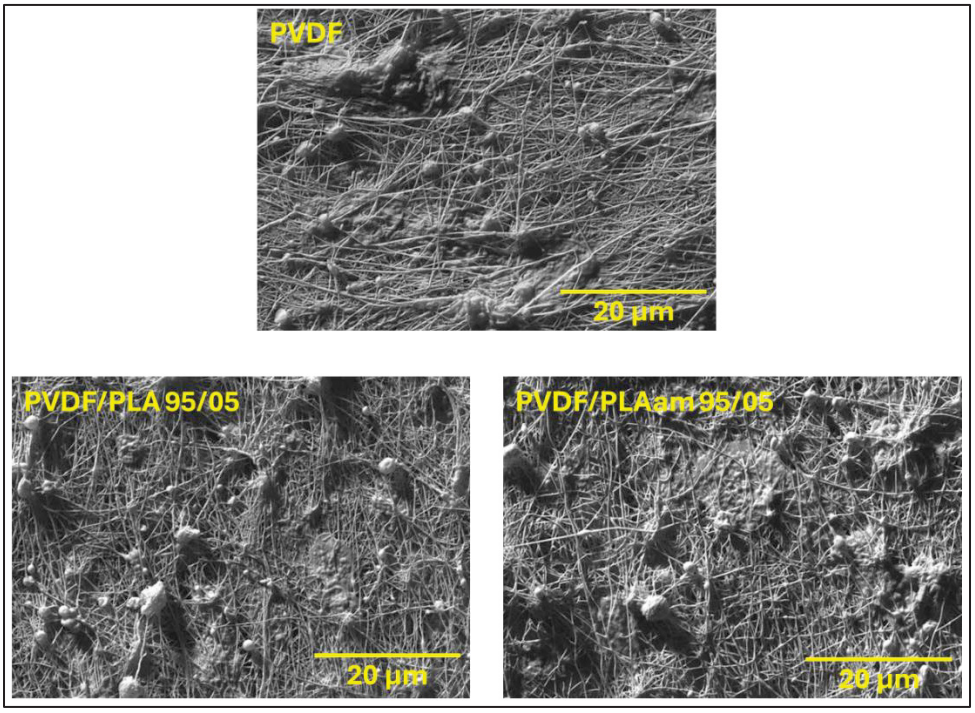

Figure 5.1 Microstructures of the membranes

5.1.2 Degree of crystallinity

The DSC thermographs corresponding to the first heating ramp of all electrospun membranes are shown in Figure 5.2. For the PVDF/PLA 95/05 sample, the additional transition slightly above the glass transition temperature does not correspond to a genuine thermal event but is instead attributed to PLA aging, as this membrane had been electrospun some time prior to the DSC measurement. Moreover, in the PVDF/PLA 95/05 sample, no PLA cold crystallization was observed, indicating that PLA had already reached its maximum crystallinity under the given processing conditions. This behavior can be explained by the confinement of PLA chains within the small fibers, which likely hinders further crystallization upon heating.

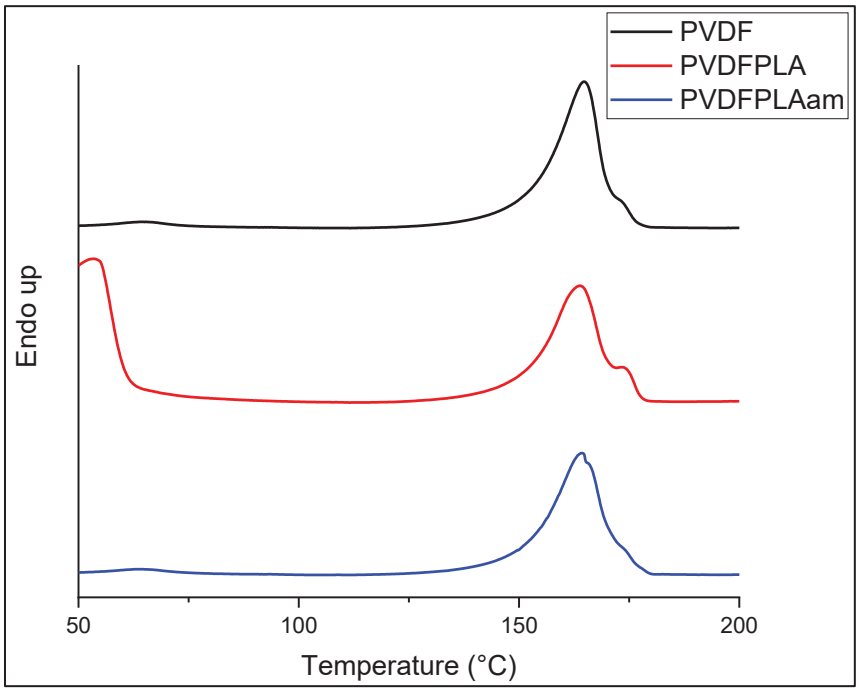

Figure 5.2 DSC thermographs of the first heating ramp of the membranes

The degrees of crystallinity of PVDF and PLA when present are calculated and reported in Table 5.1.

Table 5.1 Calculated degree of crystallinity of PVDF and PLA in the membranes

	PVDF	**PLA**
PVDF	52	
PVDFPLA9505	48	19
PVDFPLAam9505	,49	

A slight decrease in PVDF crystallinity is observed when 5% PLA, whether crystalline or amorphous, is incorporated into the sample. This reduction may result from the interaction between PVDF and PLA that slightly hinders the PVDF crystallization.

It can be observed that PVDF crystallinity is significantly higher in the electrospun samples compared to the stretched films (Table 4.2), with an increase of approximately 17–25%. This enhancement is likely related to the strong crystallization tendency of PVDF combined with the very high stretching ratios.

On the other hand, the degree of crystallinity of PLA in the electrospun membrane is 42–74% lower than in the stretched film. Although the high stretching ratio could promote PLA crystallization, its intrinsically slow crystallization kinetics, combined with rapid solvent evaporation and chain confinement within the small fiber diameter, likely limited further crystallization.

5.1.3 Effect of Electrospinning on the PVDF Polymorphism with and without PLA

The WAXS curves of the electrospun samples are given in Figure 5.3.

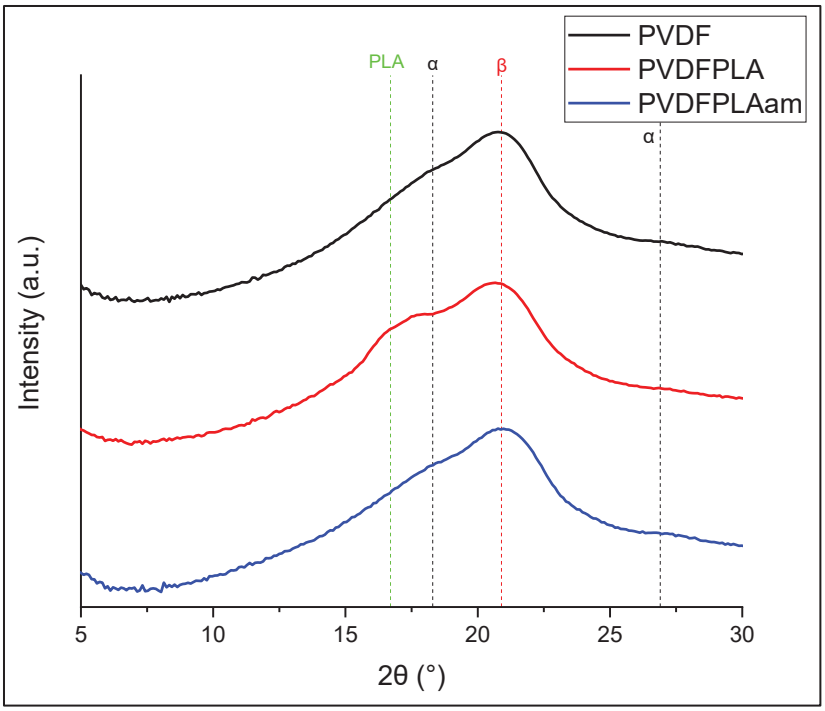

Figure 5.3 WAXS spectra of the membranes

The main diffraction peak observed in the PVDF and PVDFPLAam 95/05 samples appears at 20.9°, corresponding to the β phase. Two additional, smaller peaks are detected at 18.3° and 26.9°, which are characteristic of the α phase. In the PVDF/PLA sample, the same peaks are present along with an additional peak at 16.7°, confirming the presence of crystallized PLA within the membrane. Overall, Figure 5.3 indicates that the β phase is the dominant PVDF crystalline phase in all membranes.

The polymorphism of PVDF was investigated further with FTIR. The FTIR curves are given in Figure 5.4.

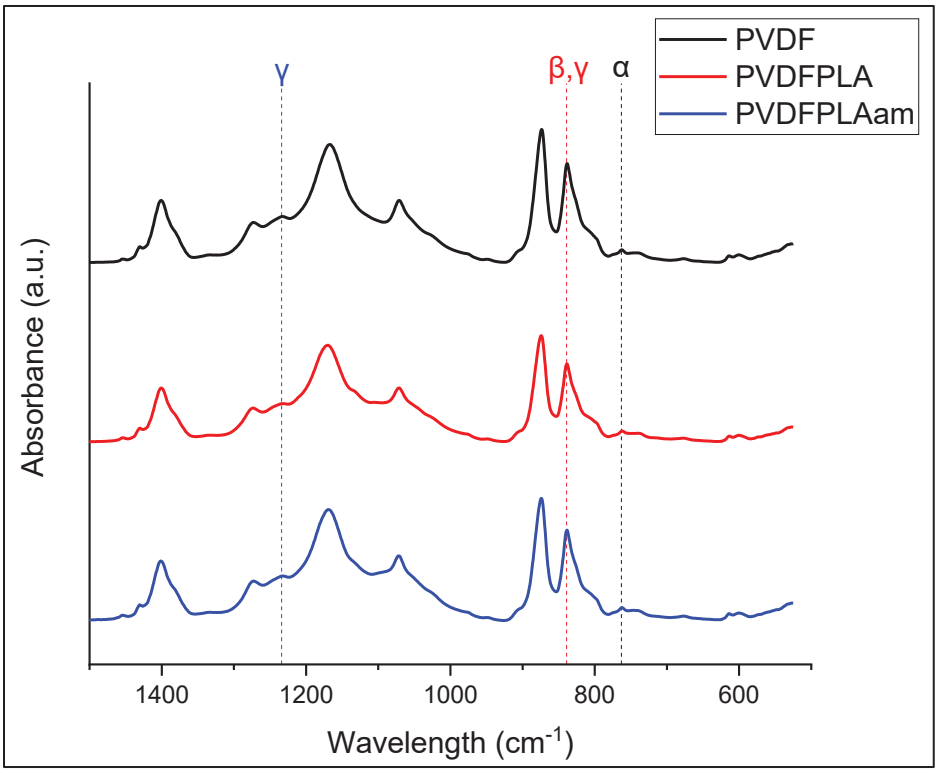

Figure 5.4 FTIR spectra of the membranes

The FTIR spectra confirm that the membranes are predominantly composed of electroactive phases, as evidenced by the strong absorption band at 840 cm^{-1}, characteristic of both β and γ phases, which is much more intense than the band at 763 cm^{-1}, assigned to the α phase. A small peak at 1234 cm^{-1} suggests the possible presence of γ phase. The γ phase content of the membranes was calculated using Equation 2. The electroactive phase fraction, β phase fraction and γ phase fraction of the membranes are provided in Table 5.2.

Table 5.2 Electroactive phase fraction (F(EA)), β phase fraction (F(β)) and γ phase fraction (F(γ)) of electrospun membranes

	F(EA)	**F(β)**	**F(γ)**
ES-PVDF	87	58	29
ES-PVDFPLA9505	85	57	28
ES-PVDFPLAam9505	85	57	28

The electroactive phase fraction and its distribution in electrospun membranes, with or without PLA, are very similar. This observation is consistent with that made for cast films, where the incorporation of 5 wt.% PLA did not significantly affect PVDF polymorphism.
In contrast to stretched samples, electrospun membranes exhibit a significant γ-phase content, whereas the latter is negligible in mechanically stretched samples. In stretched materials, the relatively slow deformation in the solid state allows PVDF chains sufficient time to align and adopt the all-trans β-phase conformation.

In solution-based processing, literature reports that PVDF may initially adopt the β phase in high-dipole-moment solvents due to favorable dipolar interactions. However, the final crystalline phase depends strongly on the solvent evaporation kinetics: slow evaporation favors retention of the β phase, intermediate rates promote a β-to-γ transition, and fast evaporation tends to favor the thermodynamically stable α phase (Nishiyama *et al.*, 2017 ; Gregorio et Ueno, 1999 ; Li *et al.*, 2019).

During electrospinning, the combination of high extensional strain and very rapid solvent evaporation likely prevents full relaxation of the polymer chains toward the non-polar α phase. As a result, the chains partially evolve from an initial β-like conformation toward the intermediate γ phase, while a fraction of the β phase is retained.

5.1.4 Effect of Poling on the Piezoelectric Properties of Electrospun PVDF and PVDF/PLA Blend

Before poling, none of the membranes exhibited piezoelectricity. This demonstrates that an additional poling step is necessary to induce piezoelectric response, since the electric field applied during electrospinning was not sufficient to orient the dipoles perpendicular to the membrane thickness. This observation contrasts with reports in the literature, which suggested that electrospinning could eliminate the need for a supplementary poling step (Dani *et al.*, 2024 ; Mokhtari *et al.*, 2025 ; Szewczyk *et al.*, 2020 ; Joseph *et al.*, 2018 ; Gheibi *et al.*, 2014). Notably, the electric field used in this study was nearly twice as high as those reported in the studies summarized in Table 1.3, yet it still failed to produce measurable piezoelectricity.

The overall β- and γ-phase contents, taking into account the degree of crystallinity as well as the d33 values of the membranes, are presented in Figures 5.5a and 5.5b, respectively. For comparison, a PVDF pressed film stretched at 60 °C and poled under identical conditions was used, as it exhibited a similar electroactive-phase fraction to that of the membranes. However, its degree of crystallinity was approximately 10% lower, resulting in a lower overall electroactive-phase content compared with the membranes.

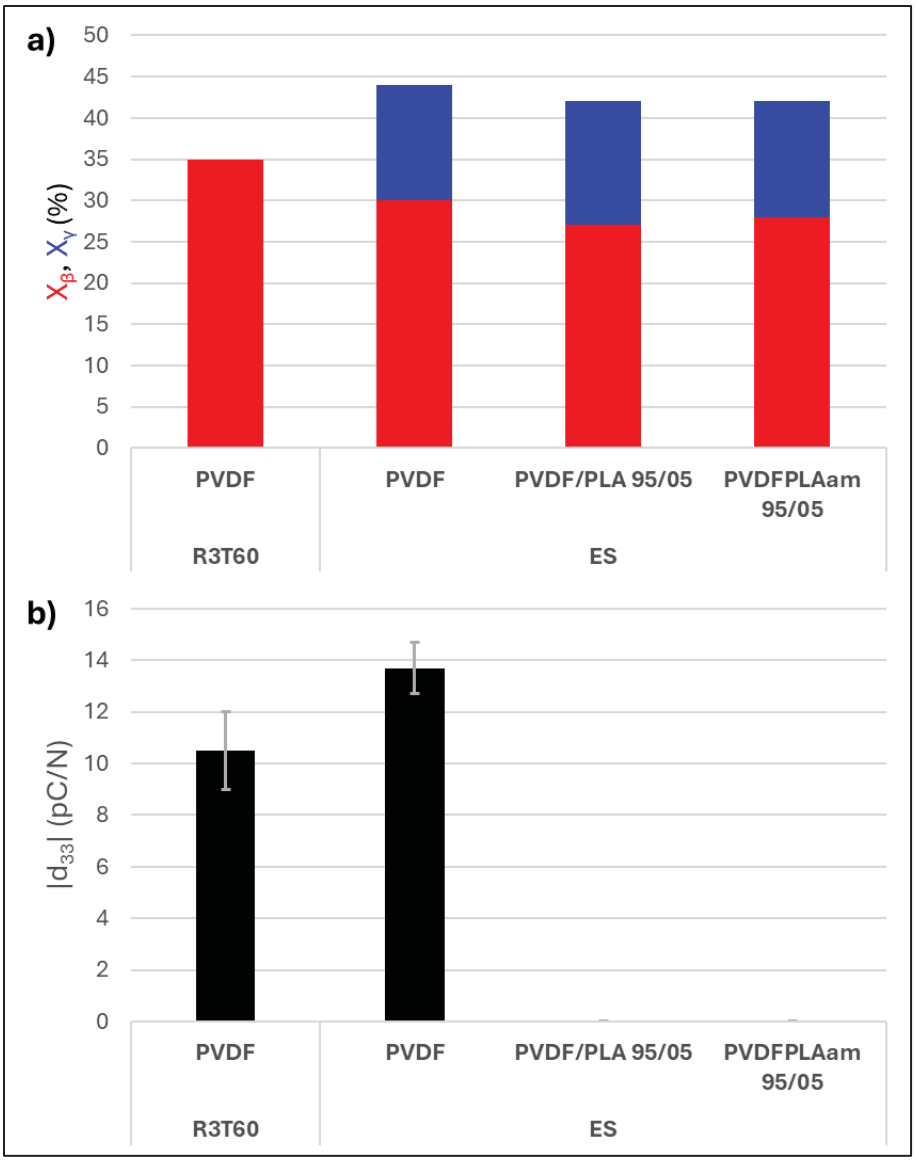

Figure 5.5 (a) Overall β phase content (Xβ), γ phase content (Xγ) and (b) d_{33} of a PVDF film stretched at stretching ratio (R) of 3 and temperature (T) of 60°C and electrospun membranes (ES)

The d_{33} of the PVDF membrane is approximately 30% higher than that of the stretched PVDF film (Figure 5.5). The main explanation is the higher electroactive phase content (29% higher) in the membrane compared to the film, due to higher degree of crystallinity along with better orientation of the chains in electrospinning due to high stretching ratio (Figure 3.9), facilitating the poling.

Finally, the presence of dielectric oil within the membrane pores may also play a role. Since the dielectric constant of the oil is higher than that of PVDF, selected to reduce the risk of electrical breakdown, the applied electric field may have been preferentially concentrated within the PVDF phase, resulting in a higher effective poling field, stronger polarization, and consequently an enhanced d_{33}. The effect of permittivity mismatch on polarization during poling was previously discussed in Chapter 4.

For the PVDF/PLAam sample, electrical breakdown consistently occurred before completion of the poling process, whereas the application of lower electric fields did not result in any measurable d_{33}.

Chapter 4 showed that incorporating 5% of semi-crystalline PLA into a PVDF film reduced the d_{33} by about 40%, due to the poling field being concentrated in the PLA phase. Nevertheless, a measurable d_{33} was still obtained after poling. In contrast, incorporating the same PLA into the electrospun membrane resulted in a null d_{33}. While the exact reason remains unclear, several additional factors beyond the focused field in the PLA phase could further explain the reduction in d_{33}.

The dissolution of both polymers in a common solvent system prior to electrospinning, combined with the high stretching ratio inherent to the electrospinning process and the reduced fiber diameter, likely promoted the formation of highly elongated and finely dispersed PLA domains within the PVDF fibers. These PLA domains could have hindered the proper orientation of PVDF lamellae and chains during stretching. As illustrated in Figure 3.9, low chain orientation results in low polarization in the thickness direction.

Moreover, this morphology significantly increases the interfacial area between the two polymers. Even though PLA domains are not located within the PVDF crystalline lamellae, they are situated in their immediate vicinity at the crystal–amorphous interfaces, which are known initiation sites for dipole switching. In this configuration, the PLA-rich regions may hinder PVDF chain rotation during poling by locally stiffening the material, since PLA has a higher modulus than PVDF at the poling temperature, or through interfacial interactions between the two polymers. Consequently, the propagation of the conformational kinks required for effective poling may be impeded. Attempts to increase the poling temperature

systematically led to electrical breakdown of the membranes, whereas reducing the electric field prevented any effective dipole alignment and resulted in a null piezoelectric response.

5.2 Conclusion

Pure PVDF and PVDF blended with 5% crystalline PLA or 5% amorphous PLA were successfully electrospun from a 9 wt.% solution using a DMSO/acetone (60/40 v/v) solvent system. The resulting membranes exhibited similar morphologies, consisting predominantly of fibers with some defects, as the electrospinning parameters were not fully optimized. The objective of this work was to maximize the β-phase content rather than to produce defect-free membranes.

The degree of crystallinity of the membranes slightly decreased upon PLA addition, likely due to interactions between PVDF and PLA that hindered PVDF crystallization. Compared to the stretched films, the electrospun membranes exhibited a higher degree of crystallinity, which can be attributed to the high stretching ratio inherent to the electrospinning process, promoting chain alignment and enhanced crystallization.

The electroactive phase fraction within the crystalline phase was nearly identical in the pure PVDF and blended membranes and remained relatively high (~86%). This high electroactive phase content was attributed to the high stretching ratio and rapid solvent evaporation during electrospinning, which limited chain relaxation. Notably, this electroactive phase fraction was comparable to that of the pure PVDF film stretched at 60 °C. However, some γ phase was present in the electrospun samples due to the presence of solvent and high evaporation rate combined with high stretching ratio.

The piezoelectric coefficient (d_{33}) of the PVDF membrane was approximately 30% higher than that of the film exhibiting the same β-phase fraction within the crystalline phase. This enhancement was attributed to the higher overall degree of crystallinity, which increased the total β-phase content in the material, as well as to the greater chain orientation in the electrospun fibers, which promoted higher polarization along the 3-direction.

Blending PVDF with 5% crystalline PLA resulted in a null d_{33} (0 pC/N), due to three synergistic effects: reduced electric field in the PVDF phase, lack of crystalline domain

orientation blocked by PLA domains, and dramatically increased PVDF/PLA interfacial area promoting strong interfacial interactions and stiffening of the material that hinder chain rotation during poling.

Finally, poling of the PVDF blended with 5% amorphous PLA was not possible at the same poling field used for the crystalline blend, as electrical breakdown systematically occurred. This behavior was attributed to the lower permittivity of amorphous PLA, which caused a stronger concentration of the electric field within the PLA phase. When the applied field was reduced to avoid breakdown, no measurable piezoelectric response was detected.

This chapter once again demonstrates that, under similar β-phase fractions and identical processing conditions, the material composition can drastically influence the piezoelectric properties. Moreover, even at the same composition and with a higher β-phase content, the PVDF/PLA 95/5 electrospun membrane exhibited no piezoelectric response, whereas the stretched film with a lower β-phase content retained some piezoelectric activity.

GENERAL CONCLUSION

This thesis investigated the influence of thermal annealing, mechanical stretching, PLA incorporation, and electrospinning on the β-phase content, crystal structure, and piezoelectric properties of PVDF-based materials.

The results demonstrate that achieving high piezoelectric performance in PVDF is governed by a combination of structural and processing factors. While the β-phase content is a necessary condition, it is not sufficient on its own; crystal size, chain orientation, and the distribution of the electric field during poling all play critical roles in determining the final piezoelectric response.

Thermal annealing was found to increase crystallite dimensions, while stretching annealed PVDF reduced chain alignment, which together decreased poling efficiency and consequently lowered the piezoelectric response.

Incorporation of PLA into PVDF films reduced the effective electric field experienced by the PVDF phase during poling, leading to lower piezoelectric properties even when the β-phase fraction was comparable.

Electrospinning of PVDF enhanced electroactive phase content and promoted chain orientation due to large stretching ratios, resulting in higher crystallinity and improved piezoelectric performance compared to PVDF films. Nevertheless, an additional poling step remained necessary despite the electric field applied during electrospinning. When PLA was incorporated into electrospun membranes, the piezoelectric response dropped to zero, likely due to the presence of small and elongated PLA domains, which both reduced the effective electric field in PVDF, prevented PVDF chain orientation, and hindered chain rotation during poling.

These findings highlight that the efficiency of poling and the resulting piezoelectric properties arise from the interplay between crystallite size, chain orientation, material composition, and processing conditions.

Overall, this work provides a comprehensive understanding of how processing and material design affect the piezoelectric performance of PVDF-based systems. The insights gained can guide the development of flexible PVDF-based energy-harvesting devices and

sensors and lay the groundwork for future studies focused on optimizing processing strategies and material compositions.

RECOMMENDATIONS

This thesis demonstrated that the piezoelectric properties of PVDF depend not only on the β-phase fraction but also on:

- Crystal size and chain/lamellae orientation: Smaller crystals reduce the poling field required to rotate the chains and allow better chain alignment upon stretching, leading to improved piezoelectric properties.
- Distribution of the electric field during poling: Incorporating high-permittivity elements helps focus the electric field within the PVDF, thereby reducing the field required for efficient poling.
- Interactions between blend components: Strong interactions between PVDF and added polymers or fillers, particularly with large interfacial areas, can hinder chain rotation during poling, resulting in poor piezoelectric performance.

In view of these observations, we can propose a set of complementary design strategies to enhance PVDF piezoelectric performance, by jointly controlling crystal morphology and orientation, the local electric-field distribution during poling, and interfacial interactions with blend components. These strategies are presented briefly below.

<u>Incorporation of high-modulus, high-permittivity nucleating agents (piezoelectric or not):</u>

To reduce crystal size, nucleating agents can be added to the PVDF matrix. These fillers should strike a balance: they must not interact too strongly with PVDF or be present in excessive amounts, which would increase the polymer-filler interface and hinder chain rotation during poling. At the same time, they should interact enough to prevent cavitation during stretching and avoid incorporating air bubbles that could disrupt the electric field.

The fillers should have a higher modulus than PVDF to focus deformation within the polymer during stretching, enhancing the α-to-β phase transformation. They should also have a higher permittivity than PVDF to concentrate the poling electric field within the polymer and

improve poling efficiency. Hydrophobized ZrO_2 fulfills these criteria and could be suitable for this purpose.

If further enhancement of piezoelectric properties is required, piezoelectric fillers can be incorporated to meet these requirements while additionally contributing to the overall piezoelectric response.

Keeping the PVDF/PLA blend system

It is inevitable that incorporating PLA will reduce the electric field in PVDF during poling, thereby decreasing PVDF's piezoelectric properties. However, this reduction can be mitigated by preventing cavitation during stretching, which can be achieved through the use of a compatibilizer. The compatibilizer should be flexible and only weakly interactive with PVDF to reduce cavitation without hindering chain rotation during poling.

In addition to limiting air incorporation and preserving PVDF's piezoelectric performance, the compatibilizer can enhance elongation and chain alignment within PLA domains, enabling PLA to exhibit its shear piezoelectricity. Indeed, for PLA to display shear piezoelectric behavior, two conditions must be met: sufficient chain alignment and crystallinity.

In conclusion, when designing a multimodal piezoelectric material, a slight reduction in PVDF's piezoelectric response may be acceptable if it allows the material to also harness the piezoelectric contribution of PLA.

Stretching vs electrospinning of pure PVDF

Although electrospinning has been shown to enhance the piezoelectric properties of PVDF compared to conventional film processing at the poling field of 100 V/μm used in this study, several limitations must be considered.

If the sole objective is to obtain a piezoelectric material, stretching and poling remain a more practical approach, particularly for industrial applications. Indeed, electrospinning still has a low throughput despite ongoing efforts to improve it.

Moreover, poling of electrospun membranes is challenging and often leads to electrical breakdown. While optimizing the morphology can slightly reduce the risk, larger electrode surfaces inherently increase the likelihood of breakdown. Moreover, the electric field applied for poling the membranes cannot be increased as freely as for films. For instance, as shown in Figure 3.7, the PVDF film achieved a d_{33} of 18 pC/N at a poling field of 160 V/µm, a value unattainable for the electrospun membrane due to the limitations in applied field.

Therefore, if a porous structure is not required, electrospinning is not the preferred method.

ANNEX I

LITERATURE REVIEW ON PVDF ANNEALING

Table-A I-1 Literature review on PVDF annealing

Fabrication Method	Initial predominant phase	Annealing parameters	Effect on F(β)	Effect on crystal size	Effect on Xc	Piezoelectric properties	Reference
15% PVDF (Sigma Aldrich) dissolved in DMSO at 90°C; The 90°C solution casted on glass plate at RT for 1h and dried at 60°C then immersion in water; Annealing	γ	70, 90, 130, 160°C for 5 hours; Heating and cooling rate of 2°C/min	T > 160°C 100 % α; T < 160°C Mixture of α, β and γ; $F(\beta)_{max}$ at annealing at 90°C but no value specified			P_r = 4.9 µC/cm^2 at 1400 kV/cm at 1 Hz for the film with the highest F(β)	(Satapathy *et al.*, 2011 ; Satapathy *et al.*, 2008)
PVDF (Kynar 761) was hot pressed to form films of 0.5 mm and 100 µm; Annealing or annealing then mechanically rolled or mechanically rolled then annealed	α	100°C for 3h	$F(\beta)_{neatPVDF}$ = 0 %; $F(\beta)_{Annealed}$ = 60 %; $F(\beta)_{Rolled+Annealed}$ = 72 %; $F(\beta)_{Annealed+Rolled}$ = 78 %				(Sharma, Madras et Bose, 2014)

Fabrication Method	**Initial predominant phase**	**Annealing parameters**	**Effect on F(β)**	**Effect on crystal size**	**Effect on Xc**	**Piezoelectric properties**	**Reference**
2g of PVDF (Sigma Aldrich) were dissolved in 100 mL of DMF at 60°C and 400 rpm; Casted on a petri dish with a blade and dried at 60°C in oven; Annealing	No information on the film without annealing	50, 70, 90, 110, 130°C for 5h; "cooled down naturally"	By FTIR: $F(\beta)_{50°C}$ = 40 %; $F(\beta)_{70°C}$ = 55 %; $F(\beta)_{90°C}$ = 57 %; $F(\beta)_{110°C}$ = 66 %; $F(\beta)_{130°C}$ = 47 %; F(β) was also calculated with XRD and Raman; No information on the non-annealed film	Crystal size L: $L_{50°C}$ = 2.87 nm; $L_{70°C}$ = 3.42 nm; $L_{90°C}$ = 3.95 nm; $L_{110°C}$ = 4.25 nm; $L_{130°C}$ = 5.07 nm;	$X_{c50°C}$ = 32 %; $X_{c70°C}$ = 41 %; $X_{c90°C}$ = 46 %; $X_{c110°C}$ = 54 %; $X_{c130°C}$ = 53 %;	d33 measured after poling at 800 kV/cm for 30 min at RT; $d_{33,50°C}$ = 3 pC/N; $d_{33,70°C}$ = 8 pC/N; $d_{33,90°C}$ = 12 pC/N; $d_{33,110°C}$ = 24 pC/N; $d_{33,130°C}$ = 3 pC/N;	(Jaglan et Uniyal, 2022)
0.5 g of PVDF (Shanghai 3F Co.) was dissolved in 10 mL of DMAc at 60°C for 30 min; Ultrasonicated for 20 min; Casted on glass substrate and dried; Annealing	α, β	60, 100, 140, 160°C for 2h; Cooled down with the oven to RT	$F(\beta)_{neatPVDF}$ = 50 %; $F(\beta)_{60°C}$ = 60 %; $F(\beta)_{100°C}$ = 60 %; $F(\beta)_{140°C}$ = 78 %; $F(\beta)_{160°C}$ = 72 %;		$X_{cneatPVDF}$ = 38 %; $X_{c60°C}$ = 39 %; $X_{c100°C}$ = 41 %; $X_{c140°C}$ = 46 %; $X_{c160°C}$ = 43 %		(Zhu *et al.*, 2016)

Fabrication Method	Initial predominant phase	Annealing parameters	Effect on F(β)	Effect on crystal size	Effect on Xc	Piezoelectric properties	Reference
15% wt.% PVDF (Sigma-Aldrich) dissolved in DMSO with 1x10-6 M of red nile added to it; Solution was heated to 90°C and spin coated on ITO glass for 45 s at 700 rpm; Non annealed films left at RT for 1h and dried in oven at 60°C for around 1.5 h; Anneling of spin coated film in parallel;	γ	Spin coated films placed into oven at RT; Oven went to 90°C at 2°C/min; Annealing time of 0.625 h, 1.25 h, 1.825 h, 2.5 h, 5h; No information on cooling rate	After annealing the film presents a mixture of α and β; No quantitative analysis			Poling the film at 1000 kV/cm resulted in Pr = 6.6 μC/cm^2	(Hess, Rudolph et Reid, 2015)

Fabrication Method	**Initial predominant phase**	**Annealing parameters**	**Effect on F(β)**	**Effect on crystal size**	**Effect on Xc**	**Piezoelectric properties**	**Reference**
2 g of PVDF (Sigma-Aldrich) was dissolved in 100 mL of DMF at 50°C; Casted onto a petri dish; Dried in a vacuum oven at 160°C; Annealing	No information on film without annealing	50, 90, 100, 110 and 130°C for 5h	F(β) increases up to annealing at 100°C where almost only β is present; Above 100°C F(β) starts decreasing No quantitative analysis	Increases from 50 to 90°C	Said to probably increased but not characterized	$P_{r,50°C}$ = 0.106 μC/cm^2; $P_{r,90°C}$ = 0.194 μC/cm^2; $P_{r,100°C}$ = 0.386 μC/cm^2; $P_{r,110°C}$ = 0.062 μC/cm^2; $P_{r,130°C}$ = 0.217 μC/cm^2	(Kaur *et al.*, 2017)
10, 15, 20, 30 % PVDF (Sigma-Aldrich) dissolved in DMF for 4h at 60°C; Spin coated at 1000, 3000, 6000, 8000 and 9000 rpm on Silicon wafer; Annealing	β	60, 80 and 100°C	Annealing at 100°C gives the highest F(β) for every rpm; At 1000 rpm and for 15% solution: $F(\beta)_{25°C}$ = 75%; Same for 60 and 80°C; $F(\beta)_{100°C}$ = 80 %				(Shaik *et al.*, 2017)

Fabrication Method	**Initial predominant phase**	**Annealing parameters**	**Effect on F(β)**	**Effect on crystal size**	**Effect on Xc**	**Piezoelectric properties**	**Reference**
20 wt.% PVDF (Sigma-Aldrich) dissolved in a mixture of DMF and Acetone (3:2), then electrospun and annealed	No information on the initial electrospun membrane;	40, 70, 100, 130°C for 4h at heating rate of 2 °C/min; No information on cooling rate	$F(\beta)_{40°C}$ = 59 %; $F(\beta)_{70°C}$ = 63 %; $F(\beta)_{100°C}$ = 87 %; $F(\beta)_{130°C}$ = 70 %	The size of the β crystallites seems to increase with increasing annealing temperature	$X_{c40°C}$ = 41 %; Same for 70 and 130 °C; $X_{c100°C}$ = 45 %	$Pr_{40°C}$ = 0.086 μC/cm^2; $P_{r70°C}$ = 0.181 μC/cm^2; $P_{r100°C}$ = 0.42 μC/cm^2; $P_{r130°C}$ = 0.247 μC/cm^2; $d_{33as\text{-}spun}$ = 10.5 pC/N $d_{33,40°C}$ = 11 pC/N; $d_{33,70°C}$ = 10.5 pC/N; $d_{33,100°C}$ = 15 pC/N; $d_{33,130°C}$ = 12.5 pC/N	(Satthiyaraju et Ramesh, 2019)

ANNEX II

CRYSTALLIZATION TEMPERATURE OF PVDF

Figure A-II-1 shows the crystallization profile of a pressed PVDF sample obtained by DSC at a heating rate of 10 °C/min.

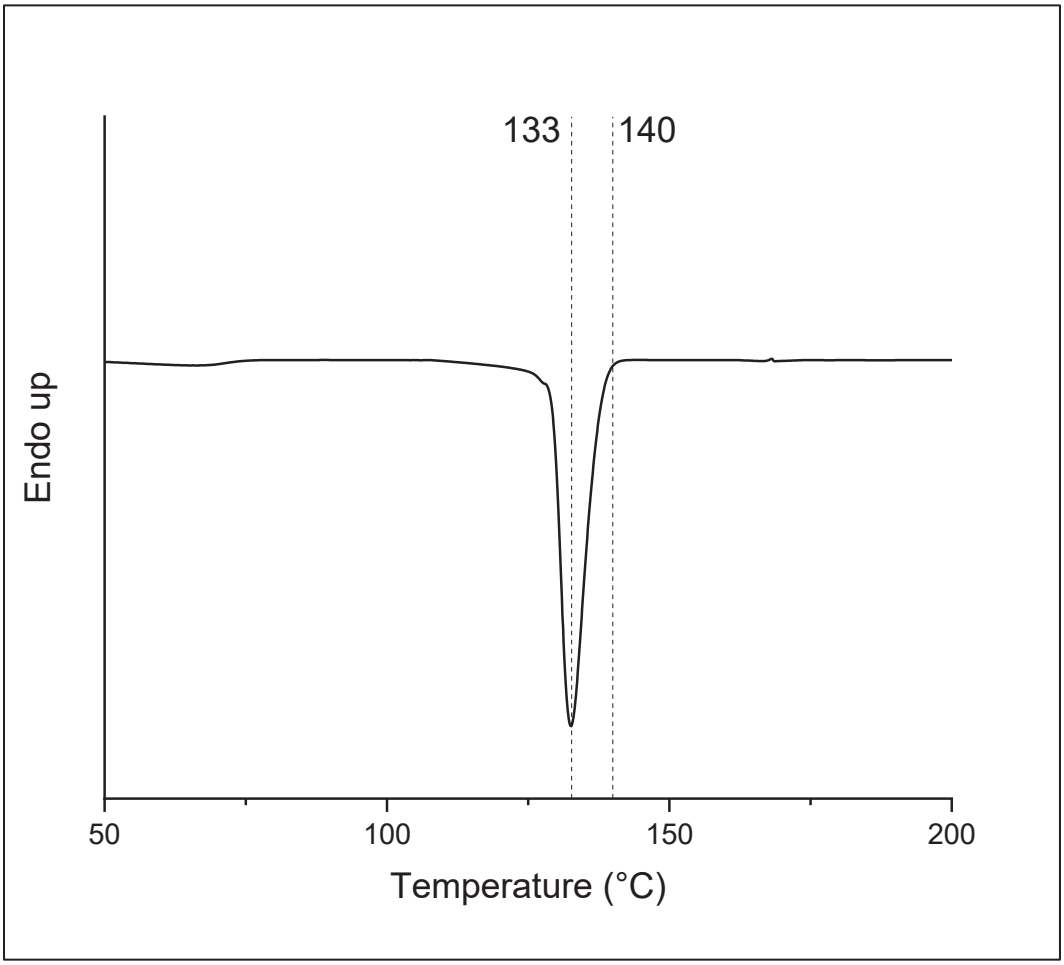

Figure-A II-1 Crystallization temperature of pressed PVDF

ANNEX III

LITERATURE REVIEW ON PVDF/PLA BLENDS

Table A.III-1 summarizes the results from all the articles reviewed regarding the effect of PLA incorporation on the β-phase fraction of PVDF and, when available, on its piezoelectric properties.

Table-A III-1 PVDF/PLA blends literature review

Materials	**PVDF/PLA composition**	**Fabrication method**	**Stretching parameters**	**F(β) or F(EA)**	**Piezoelectric properties**	**Reference**
PVDF KF850 from Kureha (Mw 209,000 and PDI 2); **PLLA** Ingeo 3001D from NatureWorks	70/30 50/50 30/70	**Solvent casting:** 3wt.% PLA dissolved in DMF at 120°C and 3wt.% PVDF dissolved in DMF at 80°C then cooled down to 60°C casted and dried at 60°C overnight	No stretching	XRD and FTIR qualitative: F(β) increases upon addition of PLA (no stretching)	Not characterized	(Rasanani *et al.*, 2022)

Materials	PVDF/PLA composition	Fabrication method	Stretching parameters	F(β) or F(EA)	Piezoelectric properties	Reference
PVDF KF-850 from Kureha; **PLLA** from GoodFellow	100/0 70/30 0/100	**Solvent casting** Separate solutions of 5wt.% PVDF in DMF and 5wt.% PLA in DMF Casted and annealed on a hot plate at 80°C	R = 1 to 5 T = 80°C for pristine PVDF and PLA T = 100°C for PVDFPLA7030 (+annealing at 80°C)	Results are extremely unclear but it seems that: Unstretched samples $F_{PVDF}(\beta)$ = 30 % $F_{PVDFPLA7030}(\beta)$ = 20 % At R = 2 $F_{PVDF}(\beta)$ = 60 % $F_{PVDFPLA7030}(\beta)$ = 20 % At R = 3 $F_{PVDF}(\beta)$ = 80 % $F_{PVDFPLA7030}(\beta)$ = 25 % At R = 4 $F_{PVDF}(\beta)$ = 82 % $F_{PVDFPLA7030}(\beta)$ = 50 % At R = 5 $F_{PVDF}(\beta)$ = 82 % $F_{PVDFPLA7030}(\beta)$ = 40 %	At R = 2 E_{cPVDF} = 130 MV/m P_{rPVDF} = 75 mC/m^2; $E_{cPVDFPLA7030}$= 100 MV/m $P_{rPVDFPLA7030}$ =15 mC/m^2; At R = 4: E_{cPVDF} = 62 mV/m P_{rPVDF} = 55 mC/m^2 d_{31} = 3.2 pC/N $E_{cPVDFPLA7030}$ = 270 MV/m $P_{rPVDFPLA7030}$ = 110 mC/m^2 d_{31} = 2.6 pC/N	(Mukri *et al.*, 2024)

Materials	PVDF/PLA composition	Fabrication method	Stretching parameters	F(β) or F(EA)	Piezoelectric properties	Reference
PVDF FR901 from 3F (Mw 285,500, PDI 1.9); **PLA** Revode101 from Zhejiang Hisun Biomaterials (Mw 81,900, PDI 2.92), crystallin	100/0 95/5 90/10 85/15 80/20	**Melt** Mixed in a torque rheometer at 190°C and 50rpm for 6min Compression molded at 190°C and 7 MPa	R = 4 T = 60, 80, 100°C v = 5 mm/min	Quantitative analysis by FTIR Unstretched samples (PVDF and blends) : F(β) = 0 Stretched at 60 °C: $F_{PVDF}(\beta)$ = 90 % $F_{PVDFPLA9505}(\beta)$ = 92.5 % $F_{PVDFPLA9010}(\beta)$ = 95 % $F_{PVDFPLA8515}(\beta)$ = 92.5 % $F_{PVDFPLA8020}(\beta)$ = 85 % Stretched at 80 °C: $F_{PVDF}(\beta)$ = 85 % $F_{PVDFPLA9505}(\beta)$ = 86 % $F_{PVDFPLA9010}(\beta)$ = 87 % $F_{PVDFPLA8515}(\beta)$ = 88 % $F_{PVDFPLA8020}(\beta)$ = 80 % Stretched at 100 °C: $F_{PVDF}(\beta)$ = 62.5 % $F_{PVDFPLA9505}(\beta)$ = 62.5 % $F_{PVDFPLA9010}(\beta)$ = 70 % $F_{PVDFPLA8515}(\beta)$ = 65 % $F_{PVDFPLA8020}(\beta)$ = 62.5 % Qualitative confirmation by XRD	Not characterized	(Xie *et al.*, 2013)

Materials	**PVDF/PLA composition**	**Fabrication method**	**Stretching parameters**	**F(β) or F(EA)**	**Piezoelectric properties**	**Reference**
PVDF (Mw 534,000) from Sigma Aldrich; **PLA** Poly-MQB 4D from M/s Nature Tech (crystallin)	100/0 30/70 50/50 70/30	**Solvent casting** 5mg of PVDF+ 5mg of PLA dissolved in DMAc at 60°C for 6h Casted on petri dish and dried in oven at 80°C	R = 1 to 3 T = 80°C v = 4 mm/min	All quantitative by FTIR: Unstretched samples: $F_{PVDF}(EA) = 61$ % $F_{PVDF}(\beta) = 45$ % $F_{PVDFPLA3070}(EA) = 49$ % $F_{PVDFPLA3070}(\beta) = 31$ % $F_{PVDFPLA5050}(EA) = 60$ % $F_{PVDFPLA5050}(\beta) = 46$ % $F_{PVDFPLA7030}(EA) = 69$ % $F_{PVDFPLA7030}(\beta) = 50$ % Stretched R = 1 $F_{PVDFPLA7030}(EA) = 70$ % $F_{PVDFPLA7030}(\beta) = 63$ % Stretched R = 2 $F_{PVDFPLA7030}(EA) = 71$ % $F_{PVDFPLA7030}(\beta) = 67$ % Stretched R = 3 $F_{PVDFPLA7030}(EA) = 75$ % $F_{PVDFPLA7030}(\beta) = 70$ % Qualitatively confirmed by XRD The result for stretched neat PVDF are not provided	Not characterized	(Mishra *et al.*, 2021)

Materials	PVDF/PLA composition	Fabrication method	Stretching parameters	F(β) or F(EA)	Piezoelectric properties	Reference
PVDF Alpha-Aesar; **PLA** 4043D (crystallin)	0/100 20/80 40/60 60/40 80/20 100/0	**Melt:** Blended in Filmaq 3D extruder at 6rpm and 220°C for 100/0 and 80/20, 6rpm and 200°C for 60/40 and 40/60, 4rpm and 185°C for 20/80 and 0/100	No stretching	Quantitative by FTIR: 100/0=81% 80/20 = 75% 60/40 = 64% 40/60 = 59% 20/80 = 55%	Not characterized	(de Oliveira *et al.*, 2023)

ANNEX IV

EFFECT OF THE ELECTROSPINNING PARAMETERS ON FIBER DIAMETER AND β-PHASE FRACTION

Table-A IV-1 summarizes the effect of electrospinning parameters on fiber diameter and the resulting β-phase content. Electrospinning of PVDF is always carried out in a solvent system, since PVDF typically dissolves in solvents with low evaporation rates. To ensure process feasibility, a fraction of volatile solvent must therefore be added, which explains the presence of the "volatile solvent content" parameter in the table.

Table-A IV-1 Effect of the electrospinning parameter on fiber diameter and beta phase fraction

	Parameter	Too low	Suitable range	Too high	Reference
Solution parameters	**Volatile solvent content**	Incomplete evaporation; Beaded Fibers; Weak stretching; Less β	Reduction of the solution surface tension; Smooth fibers; Proper stretching; Good amount of β	Fast crystallization unfavorable for β as stated above; Fast evaporation; Less stretching; Thicker fibers, lower β	(Costa, Bretas et Gregorio, 2010 ; Kalimuldina *et al.*, 2020 ; Ghafari, Jiang et Lu, 2018 ; Lei *et al.*, 2015 ; He *et al.*, 2021)
	Entanglement (concentration)	Spray or beaded fibers; Poor stretching; Low β	Higher entanglement; Better stretching; Thinner fibers, higher β	High viscoelastic forces; Difficult stretching; Thicker fibers, lower β	(Shao *et al.*, 2015 ; He *et al.*, 2021)
	Electrical properties (conductivity, dielectric constant)	No electrospinning or very poor stretching; No or thick fibers, low β	Higher electrical properties; More bending instabilities; Better stretching; Thinner fibers, higher β	Possible breaking of the fibers; Thicker fibers, less β	No literature found; Supposition made on my knowledge

	Parameter	Too low	Suitable range	Too high	Reference
Process parameters	**Electric field**	Not enough force to stretch; Thick fibers, low β	Increased voltage; More stretching; Thinner fibers, higher β	Beads or jet breaking; High jet velocity; Less stretching Higher β	(He *et al.*, 2021 ; Damaraju *et al.*, 2013 ; Abolhasani, Azimi et Fashandi, 2015 ; Jiyong *et al.*, 2017)
	Distance	Wet fibers; No time for stretching; Low β	Increased distance; More time for stretching; Thinner fibers and higher β	Weakening of the electric field; Less stretching; Thicker fibers and less β	(He *et al.*, 2021)
	Flow rate	Not enough material to be stretched; No fibers	Increased flow rate; More shearing in the needle; More β; OR Lower flow rate; More stretching; Thinner fibers and higher β	Thicker or wet fibers; Less stretching; Thicker fibers, less β	(Singh, Lye et Miao, 2019 ; Zheng *et al.*, 2007 ; Jiyong *et al.*, 2017)
Ambiant parameters	**Temperature**		Increased temperature; Decrease in viscosity; Better stretching; Thinner fibers and higher β	Faster evaporation; Less stretching; Thicker fibers and less β	(Huang *et al.*, 2008)
	Humidity		Increased humidity; Slower evaporation; Better stretching; Thinner fibers and higher β		(Zheng *et al.*, 2007)

ANNEX V

DETERMINATION OF THE ENTANGLEMENT CONCENTRATION FOR THE PVDF SOLUTION

Shear viscosity measurements were performed on a Anton Paar MCR 302 rotational rheometer using a bob-and-cup geometry. Time sweep tests were conducted for solutions at different concentrations. A constant shear rate of 5 s^{-1} was applied for 30 min. Prior to each measurement, a pre-shear at the same shear rate was applied for 3 min to remove bubbles. The results of these measurements are provided in Figure-A V-1.

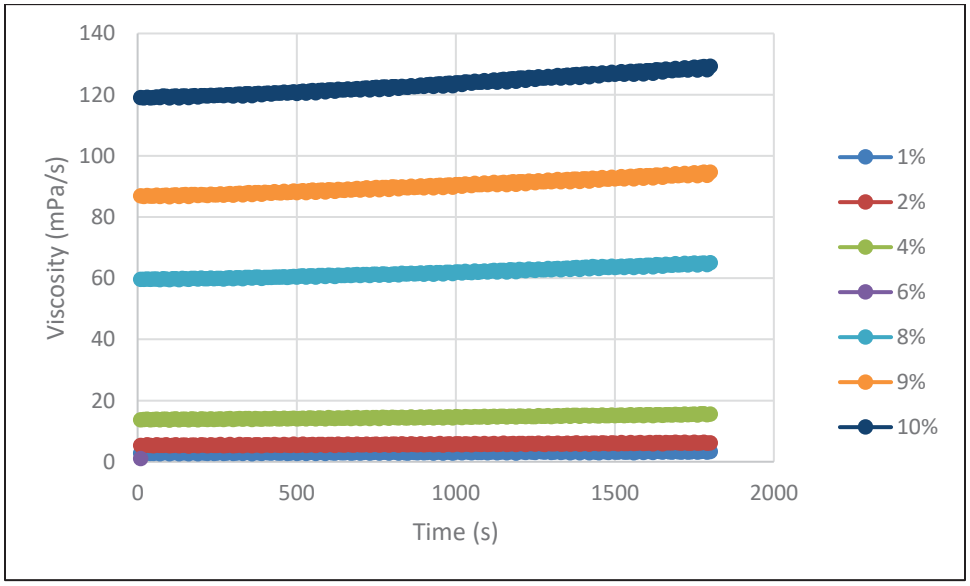

Figure-A V-1 Viscosity of PVDF solutions for determination of the entanglement concentration

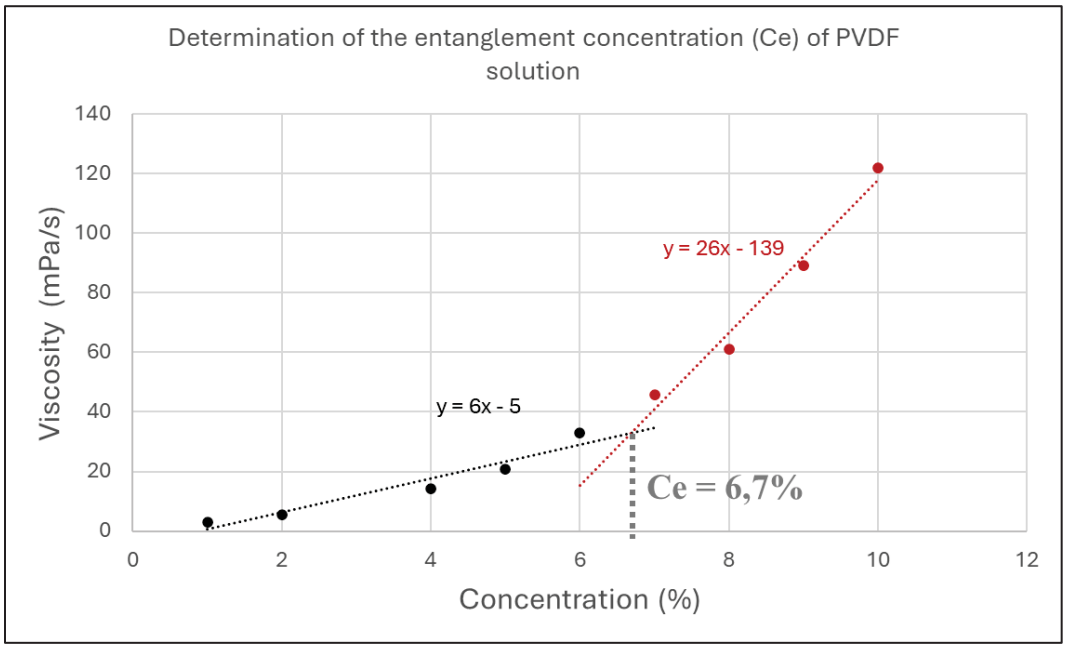

Figure-A V-2 Entanglement concentration

ANNEX VI

DMA OF PVDF AND PLA

The DMA results presented in Figure A-VI-1 help to elucidate why certain PVDF/PLA blends could not be stretched at specific temperatures.

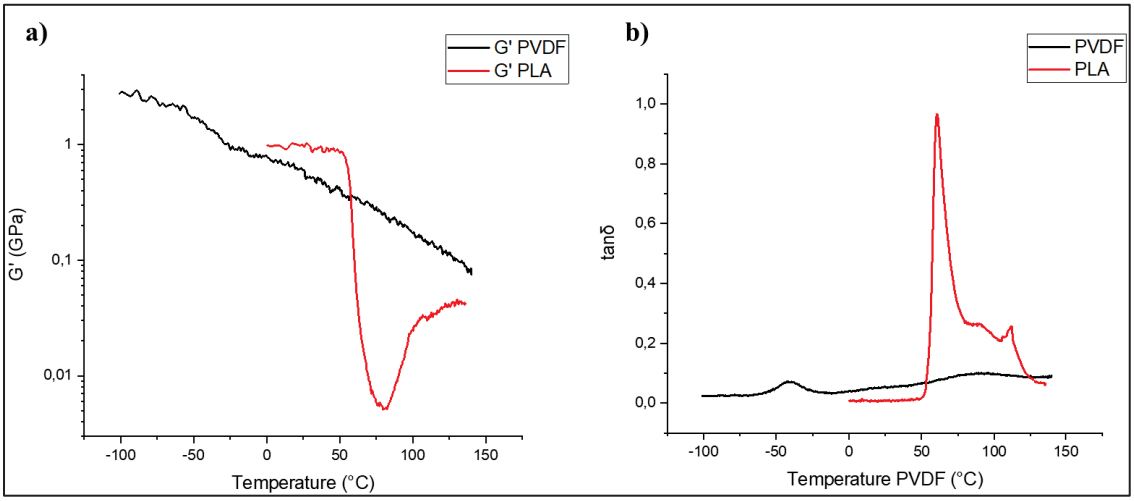

Figure-A VI-1 DMA results for PVDF (black) and PLA (red)

Indeed, the co-continuous blend could not be stretched at 80 °C and 100 °C. At these temperatures, PLA crystallization (Figure-A VI-1) increases the material's brittleness, restricting deformation and leading to fracture.

In contrast, the beaded morphology could not be stretched because PVDF chains were unable to relax properly, resulting in rupture at the interfaces between the two polymers.

ANNEX VII

CALCULATION OF PLA SURFACE-TO-VOLUME RATIO IN BEADED AND CO-CONTINUOUS MORPHOLOGIES

Figure-A VII-1 presents the SEM micrographs of the beaded and co-continuous morphologies along with their binary image generated by ImageJ for the calculation of the PLA surface-to-volume ratio.

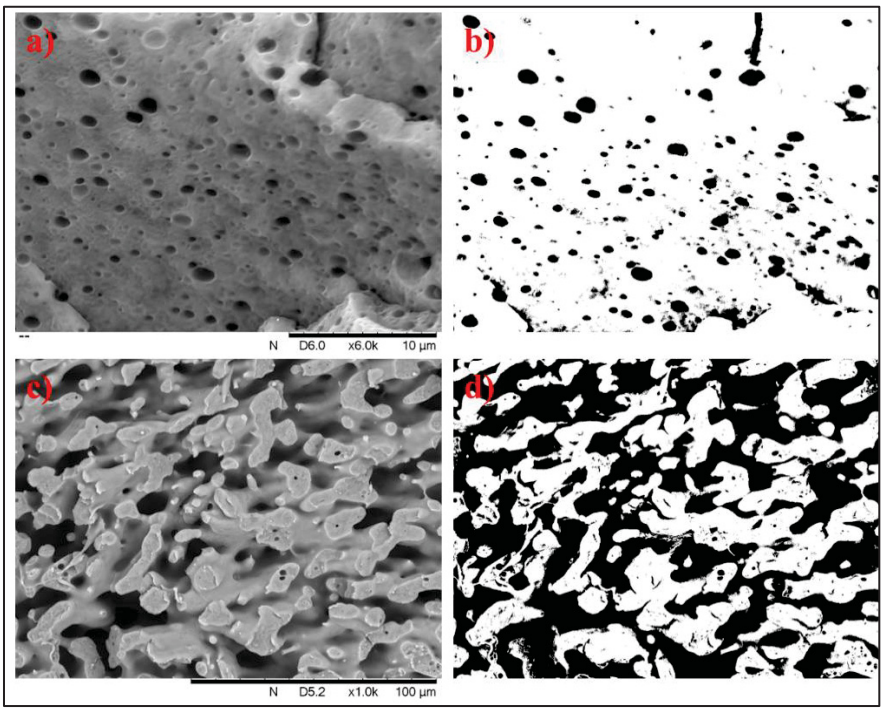

Figure-A VII-1 Original micrographs of a) beaded morphology and c) co-continuous morphology and their binary images generated by ImageJ (b and d) for the PLA surface-to-volume ratio measurement (PLA is in black)

The data presented in Table-A VII-1 gives the area of the black parts in Figure-A VII-1 b and c, their surface fraction, the calculated weight fraction from the surface fraction and the perimeter separating black and white domains.

Table-A VII-1 Data for PLA surface-to-volume ratio calculation extracted from ImageJ

Morphology	**Area (µm^2)**	**Surface fraction (%)**	**Weight fraction (%)**	**Perimeter (µm)**
Beads (PVDFPLA9505)	663	8.2	6	4640
Co-continuous (PVDFPLA6040)	24309	47.6	38	4640

LIST OF BIBLIOGRAPHICAL REFERENCES

Abolhasani, Mohammad Mahdi, Sara Azimi et Hossein Fashandi. 2015. « Enhanced ferroelectric properties of electrospun poly(vinylidene fluoride) nanofibers by adjusting processing parameters ». *RSC Advances*, vol. 5, nº 75, p. 61277-61283. <https://doi.org/10.1039/c5ra11441a>.

Bansal, Narottam P, Eleanor A Gamble -, Rinaldo Gregorio Jr et Nadia Chaves Pereira de Souza Nociti. 1995. *Effect of PMMA addition on the solution crystallization of the alpha and beta phases of poly(vinylidene fluoride) (PVDF) You may also like Crystallization Kinetics of a Solid Oxide Fuel Cell Seal Glass I Effect of PMMA addition on the solution I crystallization of the a and p phases of I poly(viny1idene fluoride) (PVDF)*.

Bodkhe, Sampada, P. S.M. Rajesh, Frederick P. Gosselin et Daniel Therriault. 2018. « Simultaneous 3D printing and poling of PVDF and its nanocomposites ». *ACS Applied Energy Materials*, vol. 1, nº 6, p. 2474-2482. <https://doi.org/10.1021/acsaem.7b00337>.

Cai, Xiaomei, Tingping Lei, Daoheng Sun et Liwei Lin. 2017. « A critical analysis of the α, β and γ phases in poly(vinylidene fluoride) using FTIR ». *RSC Advances*, vol. 7, nº 25, p. 15382-15389. <https://doi.org/10.1039/c7ra01267e>.

Chen, Zuolong, Dipak Rana, Takeshi Matsuura, Derek Meng et Christopher Q. Lan. 2015. « Study on structure and vacuum membrane distillation performance of pvdf membranes: II. influence of molecular weight ». *Chemical Engineering Journal*, vol. 276, p. 174-184. <https://doi.org/10.1016/j.cej.2015.04.030>.

Cheng, Jing, Shichao Wang, Shuangjun Chen, Jun Zhang et Xiaolin Wang. 2011. « Properties and crystallization behavior of poly(vinylidene fluoride) (PVDF)/thermoplastic polyurethane elastomer (TPU) blends ». *Desalination and Water Treatment*, vol. 34, p. 184-189. <https://doi.org/10/5004/dwt.2011.2791>.

Costa, Lígia Maria Manzine, Rosário Elida Suman Bretas et Rinaldo Gregorio. 2010. « Effect of Solution Concentration on the Electrospray/Electrospinning Transition and on the Crystalline Phase of PVDF ». *Materials Sciences and Applications*, vol. 01, nº 04, p. 247-252. <https://doi.org/10.4236/msa.2010.14036>.

Damaraju, Sita M., Siliang Wu, Michael Jaffe et Treena Livingston Arinzeh. 2013. « Structural changes in PVDF fibers due to electrospinning and its effect on biological function ». *Biomedical Materials (Bristol)*, vol. 8, nº 4. <https://doi.org/10.1088/1748-6041/8/4/045007>.

Dani, Sanskruti Smaranika, Bibekananda Sundaray, Sanjay kumar Nayak et Smita Mohanty. 2024. « Electrospun PVDF and composite nanofiber: current status and future prescription towards hybrid piezoelectric nanogenerators ». *Materials Today Communications*, vol. 38. <https://doi.org/10.1016/j.mtcomm.2023.107661>.

Doll, W. W. et J. B. Lando. 1970. « The Polymorphism of Poly(vinylidene fluoride) V. the Effect of Hydrostatic Pressure on the Melting Behavior of Copolymers of Vinylidene Fluoride ». *Journal of Macromolecular Science, Part B*, vol. 4, nº 4, p. 897-913. <https://doi.org/10.1080/00222347008217131>.

Furukawa, T., M. Date et G. E. Johnson. 1983. « Polarization reversal associated with rotation of chain molecules in β-phase polyvinylidene fluoride ». *Journal of Applied Physics*, vol. 54, p. 1540-1546. <https://doi.org/10.1063/1.332182>.

Gao, Qiong et Jerry I. Scheinbeim. 2000. « Dipolar intermolecular interactions, structural development, and electromechanical properties in ferroelectric polymer blends of nylon-11 and poly(vinylidene fluoride) ». *Macromolecules*, vol. 33, nº 20, p. 7564-7572. <https://doi.org/10.1021/ma000111i>.

Ghafari, Ehsan, Xiaodong Jiang et Na Lu. 2018. « Surface morphology and beta-phase formation of single polyvinylidene fluoride (PVDF) composite nanofibers ». *Advanced Composites and Hybrid Materials*, vol. 1, nº 2, p. 332-340. <https://doi.org/10.1007/s42114-017-0016-z>.

Gheibi, Ali, Masoud Latifi, Ali Akbar Merati et Roohollah Bagherzadeh. 2014. « Piezoelectric electrospun nanofibrous materials for self-powering wearable electronic textiles applications ». *Journal of Polymer Research*, vol. 21, nº 7. <https://doi.org/10.1007/s10965-014-0469-5>.

Gomes, J., J. Serrado Nunes, V. Sencadas et S. Lanceros-Mendez. 2010. « Influence of the β-phase content and degree of crystallinity on the piezo-and ferroelectric properties of

poly(vinylidene fluoride) ». *Smart Materials and Structures*, vol. 19, nº 6. <https://doi.org/10.1088/0964-1726/19/6/065010>.

Gomez, Ernesto Suaste. 2010. *Piezoelectric ceramics*. Rijeka : Sciyo.

Gregorio, R. et E. M. Ueno. 1999. « Effect of crystalline phase, orientation and temperature on the dielectric properties of poly (vinylidene fluoride) (PVDF) ». *Journal of Materials Science*, vol. 34, nº 18, p. 4489-4500. <https://doi.org/10.1023/A:1004689205706>.

Gregorio, Rinaldo et Daniel Sousa Borges. 2008. « Effect of crystallization rate on the formation of the polymorphs of solution cast poly(vinylidene fluoride) ». *Polymer*, vol. 49, nº 18, p. 4009-4016. <https://doi.org/10.1016/j.polymer.2008.07.010>.

Han, Ruixuan, Jiezhu Jin, Paisan Khanchaitit, Jingkang Wang et Qing Wang. 2012. « Effect of crystal structure on polarization reversal and energy storage of ferroelectric poly(vinylidene fluoride-co-chlorotrifluoroethylene) thin films ». *Polymer*, vol. 53, nº 6, p. 1277-1281. <https://doi.org/10.1016/j.polymer.2012.02.004>.

Hasegawa, Ryozo, Masamichi Kobayashi et Hiroyuki Tadokoro. 1972. *Molecular Conformation and Packing of Poly(vinylidene fluoride). Stability of Three Crystalline Forms and the Effect of High Pressure*.

He, Zhongchen, François Rault, Maryline Lewandowski, Elham Mohsenzadeh et Fabien Salaün. 2021. *Electrospun PVDF nanofibers for piezoelectric applications: A review of the influence of electrospinning parameters on the β phase and crystallinity enhancement*. *Polymers (Basel)*. <https://doi.org/10.3390/polym13020174>.

Hess, Chelsea M., Angela R. Rudolph et Philip J. Reid. 2015. « Imaging the effects of annealing on the polymorphic phases of poly(vinylidene fluoride) ». *Journal of Physical Chemistry B*, vol. 119, nº 10, p. 4127-4132. <https://doi.org/10.1021/jp512486n>.

Hsiao, Mingyin et Kazukiyo Nagai. 2024. « Degradation phenomenon of compostable poly(lactic acid) films induced by pure halogenated liquid chemicals and mixtures with water ». *Polymer Degradation and Stability*, vol. 229. <https://doi.org/10.1016/j.polymdegradstab.2024.110997>.

Huang, Fenglin, Qufu Wei, Jiaxi Wang, Yibing Cai et Yubo Huang. 2008. « Effect of temperature on structure, morphology and crystallinity of PVDF nanofibers via electrospinning ». nº 152. <http://www.e-polymers.org>.

Ian M. Smallwood. 1996. *Handbook of Organic Solvent Properties*. Elsevier. <https://doi.org/10.1016/C2009-0-23646-4>.

Jaglan, Nitin et Poonam Uniyal. 2022. « On the structural, dielectric, piezoelectric, and energy storage behavior of polyvinylidene fluoride (PVDF) thick film: Role of annealing temperature ». *Journal of Applied Physics*, vol. 132, nº 22. <https://doi.org/10.1063/5.0123674>.

Jiyong, Hu, Zhu Yinda, Zhang Hele, Gu Yuanyuan et Yang Xudong. 2017. « Mixed effect of main electrospinning parameters on the β-phase crystallinity of electrospun PVDF nanofibers ». *Smart Materials and Structures*, vol. 26, nº 8. <https://doi.org/10.1088/1361-665X/aa7245>.

Joseph, Jose, Manish Kumar, Suryasnata Tripathy, G D V Santhosh Kumar, Shiv Govind Singh et Siva Rama Krishna Vanjari. 2018. « A highly flexible tactile sensor with self-poled electrospun PVDF nanofiber ». In *IEEE Sensors*. (28 octobre 2018). IEEE.

Kalimuldina, Gulnur, Nursultan Turdakyn, Ingkar Abay, Alisher Medeubayev, Arailym Nurpeissova, Desmond Adair et Zhumabay Bakenov. 2020. *A review of piezoelectric pvdf film by electrospinning and its applications*. *Sensors (Switzerland)*. <https://doi.org/10.3390/s20185214>.

Kasap, S O. 2006. *Electronic Materials & Devices*.

Kaur, Shobhneek, Ashok Kumar, Amit L. Sharma et Dwijendra P. Singh. 2017. « Influence of annealing on dielectric and polarization behavior of PVDF thick films ». *Journal of Materials Science: Materials in Electronics*, vol. 28, nº 12, p. 8391-8396. <https://doi.org/10.1007/s10854-017-6556-8>.

Kepler, R. G. et R. A. Anderson. 1992. « Ferroelectric polymers ». *Advances in Physics*, vol. 41, nº 1, p. 1-57. <https://doi.org/10.1080/00018739200101463>.

Lei, Tingping, Lingke Yu, Gaofeng Zheng, Lingyun Wang, Dezhi Wu et Daoheng Sun. 2015. « Electrospinning-induced preferred dipole orientation in PVDF fibers ». *Journal of Materials Science*, vol. 50, nº 12, p. 4342-4347. <https://doi.org/10.1007/s10853-015-8986-0>.

Li, Xiongjie, Yiping Wang, Tingrui He, Querui Hu et Ying Yang. 2019. « Preparation of PVDF flexible piezoelectric film with high β-phase content by matching solvent dipole moment

and crystallization temperature ». *Journal of Materials Science: Materials in Electronics*, vol. 30, nº 22, p. 20174-20180. <https://doi.org/10.1007/s10854-019-02400-y>.

Liparoti, Sara, Valentina Iozzino, Vito Speranza et Roberto Pantani. 2024. « Modulating poly(lactic acid) degradation rate for environmentally sustainable applications ». *Waste Management*, vol. 175, p. 215-224. <https://doi.org/10.1016/j.wasman.2024.01.004>.

Litauszki, Katalin, Dániel Gere, Tibor Czigany et Ákos Kmetty. 2023. « Environmentally friendly packaging foams: Investigation of the compostability of poly(lactic acid)-based syntactic foams ». *Sustainable Materials and Technologies*, vol. 35. <https://doi.org/10.1016/j.susmat.2022.e00527>.

Lu, Lijun, Wenqing Ding, Jingquan Liu et Bin Yang. 2020. *Flexible PVDF based piezoelectric nanogenerators*. *Nano Energy*. <https://doi.org/10.1016/j.nanoen.2020.105251>.

Martins, P., A. C. Lopes et S. Lanceros-Mendez. 2014. « Electroactive phases of poly(vinylidene fluoride): determination, processing and applications ». *Progress in Polymer Science*, vol. 39, nº 4, p. 683-706. <https://doi.org/10.1016/j.progpolymsci.2013.07.006>.

Matsushige, Kazumi. 1978. « Melting and Crystallization of Poly(vinylidene Fluoride) under High Pressure ». *Journal of Polymer Science: Polymer Physics*, vol. 16, p. 921-934.

Matsushige, Kazumi et Tetuo Takemura. 1978. « Melting and Crystallization of Poly(vinylidene Fluoride) under High Pressure ». *Journal of Polymer Science*, vol. 16, p. 921-934.

Mendes, S. F., C. M. Costa, C. Caparros, V. Sencadas et S. Lanceros-Méndez. 2012. « Effect of filler size and concentration on the structure and properties of poly(vinylidene fluoride)/BaTiO 3 nanocomposites ». *Journal of Materials Science*, vol. 47, nº 3, p. 1378-1388. <https://doi.org/10.1007/s10853-011-5916-7>.

Mishra, Suvrajyoti, Rajesh Sahoo, Lakshmi Unnikrishnan, Ananthakumar Ramadoss, Smita Mohanty et Sanjay Kumar Nayak. 2021. « Enhanced structural and dielectric behaviour of PVDF-PLA binary polymeric blend system ». *Materials Today Communications*, vol. 26. <https://doi.org/10.1016/j.mtcomm.2020.101958>.

Mohammadi, Mojtaba, Yingjie Li, Jed Randall, Mohammadreza Nofar, Marie Claude Heuzey et Pierre J. Carreau. 2023. « Effects of molecular weight, stereo configuration of PLA,

and processing on the dispersion of multiwalled carbon nanotubes and properties of corresponding nanocomposites ». *Canadian Journal of Chemical Engineering*, vol. 101, nº 10, p. 5729-5742. <https://doi.org/10.1002/cjce.24853>.

Mokhtari, Fatemeh, Akbar Samadi, Ahmed O. Rashed, Xue Li, Joselito M. Razal, Lingxue Kong, Russell J. Varley et Shuaifei Zhao. 2025. « Recent progress in electrospun polyvinylidene fluoride (PVDF)-based nanofibers for sustainable energy and environmental applications ». *Progress in Materials Science*, vol. 148. <https://doi.org/10.1016/j.pmatsci.2024.101376>.

Mukri, N. I., T. S. Velayutham, W. H. Abd Majid et S. H. Mat Zin. 2024. « Uniaxially drawn poly (L-lactic acid)/ poly (vinylidene fluoride) polymer blend as a promising piezoelectric material: Hysteresis and resonance spectroscopy study ». *Journal of Molecular Structure*, vol. 1311. <https://doi.org/10.1016/j.molstruc.2024.138253>.

De Neef, Alexandre, Cédric Samuel, Grégory Stoclet, Mohamed Rguiti, Christian Courtois, Philippe Dubois, Jérémie Soulestin et Jean Marie Raquez. 2018. « Processing of PVDF-based electroactive/ferroelectric films: Importance of PMMA and cooling rate from the melt state on the crystallization of PVDF beta-crystals ». *Soft Matter*, vol. 14, nº 22, p. 4591-4602. <https://doi.org/10.1039/c8sm00268a>.

Nishiyama, Takashi, Takayuki Sumihara, Eriko Sato et Hideo Horibe. 2017. « Effect of solvents on the crystal formation of poly (vinylidene fluoride) film prepared by a spin-coating process ». *Polymer Journal*, vol. 49, nº 3, p. 319-325. <https://doi.org/10.1038/pj.2016.116>.

Oka, Yoshio et Naokazu Koizumi. 1985. *Formation of Unoriented Form I Poly (vinylidene fluoride) by High-Rate Quenching and its Electrical Properties*.

Oka, Yoshio, Yukinobu Murata et Naokazu Koizumi. 1986. *Structure and Spontaneous Polarization in Fast-Quenched Copolymers of Vinylidene Fluoride and Trifluoroethylene*.

de Oliveira, Patrícia Camargo, Rafael Marangoni, Valdirlei Fernandes Freitas, Tania Toyomi Tominaga, Ricardo Yoshimitsu Miyahara, Jarciele Márcia Rosso, Gabriel Batista César, Wilson Ricardo Weinand, Ivair Aparecido dos Santos et Taiana Gabriela Moretti Bonadio. 2023. « Fused filaments of PVDF/PLA blends for biomedical applications ».

Ferroelectrics, vol. 611, nº 1, p. 60-66. <https://doi.org/10.1080/00150193.2023.2201769>.

Rasanani, Ali Hadian, Babak Kaffashi, Shervin Ahmadi et Javad Seyfi. 2022. « Assessment of surface, structural, and viscoelastic properties of immiscible polylactic acid/polyvinylidene fluoride blends ». *Macromolecular Research*, vol. 30, nº 5, p. 285-294. <https://doi.org/10.1007/s13233-022-0040-x>.

Ruan, Liuxia, Xiannian Yao, Yufang Chang, Lianqun Zhou, Gaowu Qin et Xianmin Zhang. 2018. « Properties and applications of the β phase poly(vinylidene fluoride) ». *Polymers*, vol. 10. <https://doi.org/10.3390/polym10030228>.

Sajkiewicz, P, A Wasiak et Z Gocl. 1999. « Phase transitions during stretching of poly(vinylidene fluoride) ». *European Polymer Journal*, nº 35, p. 423-429.

Satapathy, S, P K Gupta, Santosh Pawar et K B R Varma. 2008. *Crystallization of β-phase Poly (vinylidene fluoride) films using dimethyl sulfoxide (DMSO) solvent and at suitable annealing condition*.

Satapathy, S, Santosh Pawar, P K Gupta et B R Varma. 2011. *Effect of annealing on phase transition in poly(vinylidene fluoride) films prepared using polar solvent*.

Satthiyaraju, M. et T. Ramesh. 2019. « Effect of annealing treatment on PVDF nanofibers for mechanical energy harvesting applications ». *Materials Research Express*, vol. 6, nº 10. <https://doi.org/10.1088/2053-1591/ab4037>.

Sencadas, V., S. Lanceros-Méndez, R. Sabater I Serra, A. Andrio Balado et J. L. Gómez Ribelles. 2012. « Relaxation dynamics of poly(vinylidene fluoride) studied by dynamical mechanical measurements and dielectric spectroscopy ». *European Physical Journal E*, vol. 35, nº 5. <https://doi.org/10.1140/epje/i2012-12041-x>.

Sencadas, V., V. M. Moreira, S. Lanceros-Mendéz, A. S. Pouzada et R. Gregório. 2006. « α - To - β transformation on PVDF films obtained by uniaxial stretch ». In *Materials Science Forum*. (2006), p. 872-876. Trans Tech Publications Ltd. <https://doi.org/10.4028/www.scientific.net/msf.514-516.872>.

Sessler, G. M. 1981. « Piezoelectricity in polyvinylidenefluoride ». *The Journal of the Acoustical Society of America*, vol. 70, nº 6, p. 1596-1608. <https://doi.org/10.1121/1.387225>.

Shaik, Habibuddin, S. N. Rachith, K. J. Rudresh, Abdul Sattar Sheik, K. H. Thulasi Raman, P. Kondaiah et G. Mohan Rao. 2017. « Towards β-phase formation probability in spin coated PVDF thin films ». *Journal of Polymer Research*, vol. 24, nº 3. <https://doi.org/10.1007/s10965-017-1191-x>.

Shaliutina-Kolešová, Anna. 2018. *A fundamental study of Morphology Prediction for Nano and Microstructure of PVDF for Membrane Fabrication and Film Formation Applications*. <https://www.researchgate.net/publication/342121695>.

Shao, Hao, Jian Fang, Hongxia Wang et Tong Lin. 2015. « Effect of electrospinning parameters and polymer concentrations on mechanical-to-electrical energy conversion of randomly-oriented electrospun poly(vinylidene fluoride) nanofiber mats ». *RSC Advances*, vol. 5, nº 19, p. 14345-14350. <https://doi.org/10.1039/c4ra16360e>.

Sharma, Maya, Giridhar Madras et Suryasarathi Bose. 2014. « Process induced electroactive β-polymorph in PVDF: Effect on dielectric and ferroelectric properties ». *Physical Chemistry Chemical Physics*, vol. 16, nº 28, p. 14792-14799. <https://doi.org/10.1039/c4cp01004c>.

Singh, Rahul Kumar, Sun Woh Lye et Jianmin Miao. 2019. « PVDF nanofiber sensor for vibration measurement in a string ». *Sensors (Switzerland)*, vol. 19, nº 17. <https://doi.org/10.3390/s19173739>.

Song, Dandan, Yang * Decal et Zhiliu Feng. 1990. « Formation of β-phase microcrystals from the melt of PVF2-PMMA blends induced by quenching ». *JOURNAL OF MATERIALS SCIENCE*, vol. 25, p. 57-64.

Sukumaran, Sunija, Samir Chatbouri, Didier Rouxel, Etienne Tisserand, Frédéric Thiebaud et Tarak Ben Zineb. 2021. « Recent advances in flexible PVDF based piezoelectric polymer devices for energy harvesting applications ». *Journal of Intelligent Material Systems and Structures*, vol. 32, nº 7, p. 746-780. <https://doi.org/10.1177/1045389X20966058>.

Szewczyk, Piotr K., Arkadiusz Gradys, Sung Kyun Kim, Luana Persano, Mateusz Marzec, Aleksandr Kryshtal, Tommaso Busolo, Alessandra Toncelli, Dario Pisignano, Andrzej Bernasik, Sohini Kar-Narayan, Paweł Sajkiewicz et Urszula Stachewicz. 2020. « Enhanced piezoelectricity of electrospun polyvinylidene fluoride fibers for energy

harvesting ». *ACS Applied Materials and Interfaces*, vol. 12, nº 11, p. 13575-13583. <https://doi.org/10.1021/acsami.0c02578>.

Takahashi, N. et A. Odajima. 1981. « Ferroelectric reorientation of crystallites in polyvinylidene fluoride ». *Ferroelectrics*, vol. 32, nº 1, p. 49-59. <https://doi.org/10.1080/00150198108238673>.

Tredwell, M. 2012. *1.5 Fluorine in Medicinal Chemistry: Importance of Chirality. In Comprehensive Chirality*. Elsevier, 70-85 p.

Wu, Chang Mou et Min Hui Chou. 2016. « Sound absorption of electrospun polyvinylidene fluoride/graphene membranes ». *European Polymer Journal*, vol. 82, p. 35-45. <https://doi.org/10.1016/j.eurpolymj.2016.07.001>.

Xie, Qi, Kai Ke, Wen Rou Jiang, Wei Yang, Zheng Ying Liu, Bang Hu Xie et Ming Bo Yang. 2013. « Role of poly(lactic acid) in the phase transition of poly(vinylidene fluoride) under uniaxial stretching ». *Journal of Applied Polymer Science*, vol. 129, nº 4, p. 1686-1696. <https://doi.org/10.1002/app.38873>.

Yang, Decal et Y E Chen. 1987. « β-phase formation of poly(vinylidene fluoride) from the melt induced by quenching ». *JOURNAL OF MATERIALS SCIENCE LETTERS*, vol. 6, p. 599-603.

Yee, Wu Aik, Junhua Kong, Chao Zhang, Tianxi Liu, Masaya Kotaki et Xuehong Lu. 2012. « Polymorphism of electrospun polyvinylidene difluoride/carbon nanotube (CNT) nanocomposites: Synergistic effects of CNT surface chemistry, extensional force and supercritical carbon dioxide treatment ». *Polymer*, vol. 53, nº 22, p. 5097-5102. <https://doi.org/10.1016/j.polymer.2012.08.044>.

Yin, Lu, Jiayao Wang, Taotao Lin et Jichun You. 2022. « Inclusion/Exclusion Behaviors of Small Molecules during Crystallization of Polymers in Miscible PLLA/TAIC Blend ». *Polymers*, vol. 14, nº 13. <https://doi.org/10.3390/polym14132737>.

Yu, Hao, Tao Huang, Mingxia Lu, Mengye Mao, Qinghong Zhang et Hongzhi Wang. 2013. « Enhanced power output of an electrospun PVDF/MWCNTs-based nanogenerator by tuning its conductivity ». *Nanotechnology*, vol. 24, nº 40. <https://doi.org/10.1088/0957-4484/24/40/405401>.

Zhang, Chunmei, Qiaofeng Lan, Tianliang Zhai, Shengqiang Nie, Jun Luo et Wei Yan. 2018. « Melt crystallization behavior and crystalline morphology of polylactide/poly(ε-caprolactone) blends compatibilized by lactide-caprolactone copolymer ». *Polymers*, vol. 10, nº 11. <https://doi.org/10.3390/polym10111181>.

Zhang, Qiming M et Jianzhong Zhao. 1999. « Electromechanical properties of lead zirconate titanate piezoceramics under the influence of mechanical stresses ». *IEEE Transactions on Ultrasonics, Ferroelectrics, and Frequency Control*, vol. 46, nº 6, p. 1518-1526. <https://doi.org/10.1109/58.808876>.

Zhang, Qiuping, Weimin Xia, Zhigang Zhu et Zhicheng Zhang. 2013. « Crystal phase of poly(vinylidene fluoride-co-trifluoroethylene) synthesized via hydrogenation of poly(vinylidene fluoride-co-chlorotrifluoroethylene) ». *Journal of Applied Polymer Science*, vol. 127, nº 4, p. 3002-3008. <https://doi.org/10.1002/app.37975>.

Zhao, Xuanchen, Junhao Xie, Jing Hu, Yan Liu, Shulin Sun et Shixin Song. 2021. « Enhanced energy storage performance of poly(vinylidene fluoride) by water-environmental annealing induced smaller crystallite size ». *Materials Today Communications*, vol. 29. <https://doi.org/10.1016/j.mtcomm.2021.102845>.

Zheng, Jianfen, Aihua He, Junxing Li et Charles C. Han. 2007. « Polymorphism control of poly(vinylidene fluoride) through electrospinning ». *Macromolecular Rapid Communications*, vol. 28, nº 22, p. 2159-2162. <https://doi.org/10.1002/marc.200700544>.

Zhong, Ganji, Lifeng Zhang, Run Su, Ke Wang, Hao Fong et Lei Zhu. 2011. « Understanding polymorphism formation in electrospun fibers of immiscible poly(vinylidene fluoride) blends ». *Polymer*, vol. 52, nº 10, p. 2228-2237. <https://doi.org/10.1016/j.polymer.2011.03.024>.

Zhu, Yunfei, Huijian Ye, Li Yang, Lixiang Jiang, Liang Zhen, Jianguo Huang, Zilong Jiao et Jipeng Sun. 2016. *Effect of Annealing Temperatures and Time on Structural Evolution and Dielectric Properties of PVDF Films*.